DESIGN AND ANALYSIS OF LEAKY WAVE ANTENNAS FOR NOVEL FUNCTIONALITIES

Thesis

Submitted in partial fulfillment of the requirements for the degree of

DOCTOR OF PHILOSOPHY

by

KARTHIK R

DEPARTMENT OF ELECTRONICS & COMMUNICATION ENGINEERING

NATIONAL INSTITUTE OF TECHNOLOGY KARNATAKA

SURATHKAL, MANGALORE - 575025, INDIA

October 2021

DECLARATION

I hereby *declare* that the Research Thesis entitled **DESIGN AND ANALYSIS OF LEAKY WAVE ANTENNAS FOR NOVEL FUNCTIONALITIES** which is being submitted to the **National Institute of Technology Karnataka, Surathkal** in partial fulfillment of the requirements for the award of the Degree of **Doctor of Philosophy** in **Department of Electronics and Communication** is a *bonafide report of the research work carried out by me.* The material contained in this thesis has not been submitted to any University or Institution for the award of any degree.

Karthik R
Register No.: 165080EC16F03
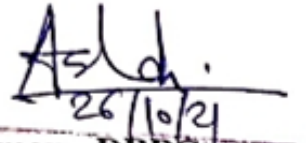Department of Electronics and Communication Engineering

Place: NITK Surathkal

Date: 25/10/2021

CERTIFICATE

This is to *certify* that the Research Thesis entitled **DESIGN AND ANALYSIS OF LEAKY WAVE ANTENNAS FOR NOVEL FUNCTIONALITIES**, submitted by Karthik R (Reg. No.: 165080EC16F03) as the record of the research work carried out by him, is *accepted as a Research Thesis submission* in partial fulfillment of the requirements for the award of degree of **Doctor of Philosophy**.

Dr.Krishnamoorthy K.
Research Guide
Assistant Professor
Department Electronics and Communication Engg.
NITK Surathkal - 575025

Chairman - DRPC
(Signature with Date and Seal)

This thesis is dedicated to my beloved Sister

ACKNOWLEDGEMENTS

ABSTRACT

This thesis deals with the effective design of planar leaky wave antennas (LWA) for novel functionalities. The work describes a methodology based on single-layer transmission based Goubau line and investigation of asymmetry in Half-mode substrate integrated waveguide (HMSIW) periodic LWAs to address very different antenna configurations. Four novel LWAs are proposed to achieve wide angle beam scanning, single layer based End-Fire radiation, dual-band and simultaneous dual-beam scanning functionalities.

Wide beam scanning is designed using Goubau line. In contrast to the conventional LWA with a small scanning angle range and low efficiency, this work employed a periodically bending Goubau line, which not only brings in a periodic perturbation for leaky wave radiation, but also enhances the scanning range due to the increased delay for each line element. The proposed antenna features good radiation performance and has a compact and low profile configuration. Also, a simple and low-profile Planar Goubau line based Endfire antenna is designed. Endfire radiation is achieved by modifying the Goubau line into inverted periodic arrangement of V-shaped unit cells. The proposed endfire antenna has a single metallic layer with a simple configuration which is easy to fabricate and also easy to integrate with other electronics circuits.

Most of the existing LWAs are generally designed for a single band application. In this work, by etching simple spiral type slots on the HMSIW cavity, a novel dual-band dual-polarized LWA is designed. The antenna radiates the linearly polarized (LP) wave in the lower band and circularly polarized wave in the higher operating band. In the higher operating band antenna exhibits both right-hand circular polarization (RHCP) as well as the left hand (LHCP) circular polarization in the near main beam direction. Also, asymmetry is investigated in HMSIW LWA. Based on asymmetry, two different configurations of dual-band LWAs are designed. The first configuration radiates LP

waves in the lower band and CP waves in the upper band when the unit cells are cascaded sequentially. The second configuration, where the sidewall via of the HMSIW unit cells are connected alternatingly, provides simultaneous dual-beams with different polarization in the upper operational band in addition to the LP beam in the lower operational band. These novel functionalities of LWA can be effectively used for multi-objective tracking applications and for enhancing the channel capacity of automotive and satellite-based wireless communication systems. Since both antenna configurations had dual frequency bands with different pointing directions in scanning, it can also be useful for vehicular applications to track different objects in its nearby locations

Proposed designs are fabricated using LPKF protomat machine S103 and experimentally verified using radiation pattern measurement set-up. Impedance bandwidth, peak gain, axial ratio bandwidth and radiation efficiency are measured and compared with the simulated results. The performance of the proposed works are compared with the previous literature.

Keywords: Leaky Wave Antenna, Goubau Line, Circular Polarization, Half Mode Substrate Integrated Waveguide.

TABLE OF CONTENTS

LIST OF FIGURES

LIST OF TABLES

ABBREVIATIONS

LWA   Leaky Wave Antenna

SPP   Surface Plasmon Polaritons

CPW   Co-Planar Waveguide

CP   Circular Polarization

PGL   Planar Goubau Line

HMSIW   Hal-Mode Substrate Integrated Waveguide

LP   Linear Polarization

RHCP   Right Hand Circular Polarization

LHCP   Left Hand Circular Polarization

LP   Linear Polarization

CRLH   Composite Right Left-Handed

CHAPTER 1

INTRODUCTION

This chapter briefly describes the LWA and its classification. Many periodic LWAs are developed but achieving efficient wide-angle beam scanning and dual-beam LWAs is still a challenging task. These research gaps are discussed in the work motivation followed by problem definition and formulation of objectives. Methodology to achieve desired objectives is discussed and the organization of the thesis is outlined at the end of this chapter.

1.1   Leaky Wave Antennas

Leaky Wave Antenna (LWA) is a type of travelling wave antenna which leaks energy continuously as it propagates through the guided medium (Jackson and Oliner (2008)). This type of antenna usually developed using waveguiding structures such as microstrip or closed waveguides. These antennas possess unique properties such as narrow-beam, high directvity, wide bandwidth and beam direction that can be steered with the change in excitation frequency. Also, these are simple to realize since there is no complex feed network is required. Due to this simplicity, they are often attractive for applications in the microwave and millimeter-wave systems. The main applications of LWAs include satellite links, sensor systems, such as automotive radars etc. These unique properties make LWAs attractive.

LWAs have been investigated and known for more than 70 years. Early LWAs are based on the closed waveguide structure. The first known LWA is the slitted rectangular waveguide was developed by W. W. Hansen in 1940 (Hansen (1940)) is shown in Figure 1.1. Here, energy leakage was generated by cutting a uniform slit along the side of a waveguide. These slits cut across the current line which results in the disturbance on

the fields. To overcome this difficulty 'Holey Waveguide' was developed (Hines and Upson (1957)), in which uniform slit was replaced by an array of closely spaced holes. Later, many LWAs were developed which includes asymmetric trough open waveguide (Rotman and Oliner (1959)), dielectric waveguide LWA (Itoh and Adelseck (1980)), metal-strips over a metallic waveguide (Guglielmi and Boccalone (1991)), microstrip LWA (Metzler (1981))and metamaterial (Caloz and Itoh (2003)) based LWA .
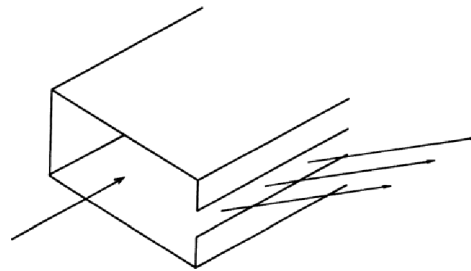
Figure 1.1: Slitted rectangular waveguide LWA (example of uniform LWA).

LWAs are basically categorized into two types, depending on whether the guiding structure is uniform or periodically modulated. In uniform LWA, modulation is uniform along the length of the guiding medium. This type of antenna radiates only in the forward quadrant, which limits the beam scanning range. Periodic LWA is basically periodic modulation of the guiding structure.This periodic modulation produces infinite space harmonics, in which fast space harmonics are radiating to free space. A typical example of a periodic LWA is a dielectric rectangular waveguide on which periodic metal strips are placed, as shown in Figure 1.2
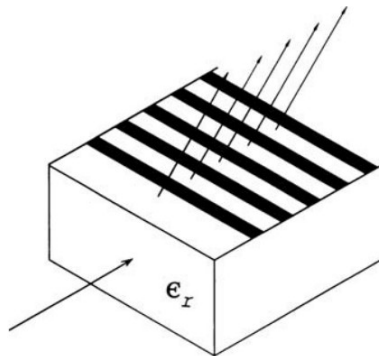
Figure 1.2: Dielectric waveguide with metallic strips (example of periodic LWA).

Periodic LWA scans from backward quadrant to end-fire through broadside whereas uniform LWA scans only in the forward quadrant. Due to this advantage, many periodic LWAs are developed over the decades, which includes microstrip, substrate integrated waveguide (SIW) and composite right/left-handed (CRLH) LWA antennas. Existing LWAs provide limited beam scanning. But, the new technologies requires wide angle beam scanning and dual-beam LWAs.

1.2   Motivation

The number of wireless communication user grown drastically. Today there are more than seven billion cell-phone users. Wireless devices are expected to reach 17 billion by 2030 in the world. Hence, the growth of wireless technology demands for compact and miniaturized antennas for multiple applications. Non-resonant antenna such as microstrip antennas offer interesting features e.g., low profile, light weight, or low production cost and can be integrated with the feeding network on the same substrate. Resulting structures are compact and, hence, very useful in practical applications. But the main drawbacks of the microstrip antennas are low gain, radiation efficiency, narrow-bandwidth. Array of microstrip elements are used to increase the gain. But it uses the complex feed network to feed the elements. Also, phase shifters are used along with the feed network in order to steer the beam in a particular direction which leads to huge losses. In contrast, Non-resonant antennas such as LWA do not resonate but rather leak energy along the length, thereby producing high gain and more bandwidth. In LWA, beam steering can be achieved by simply varying the frequency. Hence, it does not need any complex phase shifters to steer the beam. It has widely used for beam scanning applications due to its advantages.

Many microstrip LWA are developed in the past few years. But their efficiencies are low due to dielectric and conductor losses. If the ground plane is eliminated, the confinement of the field in the dielectric substrate is reduced and, hence, a large reduction of both dielectric and ohmic losses is achieved. Hence, efficiency will be increased. The

resulting transmission line is known as the planar Goubau line (PGL). Due to its advantages, LWA based Goubau line are recently investigated. Generally, to date, very few works were reported to enhance the scanning range of the Goubau line LWA. Another important drawback of microstrip antenna is low power handling with high losses as the operating frequency increases. Substrate Integrated Waveguide (SIW) technology is planar version of conventional rectangular waveguide that can overcome these drawbacks. Half-Mode SIW (HMSIW) is similar to the SIW but its size is reduced by half of the SIW. Eventhough many LWAs are investigated, there is a need for multifunctional LWAs like Dual-band, Dual-polarized and Dual-beams with improved performance.

1.3 Problem Statement

As we discussed in the previous section, the growth of wireless technology demands for compact and miniaturized antennas. Hence there is a need for innovative compact LWA that can produce novel functionalities such as wide angle beam scanning with high efficiency. For ease of use, a single metallic layer endfire antenna is desired. Dual-band with different polarization should be incorporated in an antenna. Simultaneous dual-beams with dual-band is required for multifunctional applications. These research gaps need to be filled, we try to use the current state-of-art technology for optimization and fabrication of various designs that can meet these demands appropriately. The existing literature presents various designs inline with these demands, but our extensive survey shows that certain gaps need to be filled.

Thus, in order to fill the research gaps, the following objectives have been formulated and listed in the next section.

1.4   Objectives

Formulated objectives are:

- To design a single metallic layer based LWA to achieve wide-angle beam scanning from backfire to endfire through broadside with stable efficiency and gain over the operating band.

- To design a simple and low profile single metallic layer planar Goubau line based LWA to produce radiation towards endfire direction.

- To develop a dual-band dual-polarized LWA that can produce LP in the lower band and CP in the upper band and also to obtain both RHCP and LHCP in the upper band for polarization diversity applications.

- To design and study of asymmetry in periodic LWA that offer dualband with simultaneous dual-beams of different polarization in the upper band along with the LP beam in the lower band for multifunctional applications.

1.5   Methodology

For achieving above mentioned objectives, Goubau-line and HMSIW technologies are used. Periodic and asymmetric properties are also incorporated to design the proposed models. Methodology to adopted for the same is described below:

- To design planar Goubau line based LWA for large angle beam scanning, the unit cell is designed by periodically bending Goubau line, which brings in a periodic perturbation for leaky wave radiation, and also enhances the scanning range due to the increased delay for each line element. Dispersion diagram is obtained by simulating unit cell using Eigen-Mode solver. The scanning range and radiation characteristics of the unit cell is analysed using the dispersion diagram. The dimensions LWA is optimized to obtain large beam scanning.

- To design single metallic layer Goubau line LWA for endfire radiation, Goubau line is modified into an inverted periodic arrangement of V-shaped unit cells. The dispersion diagram of the proposed unit cell is analyzed to predict the behavior of its fundamental mode. The Hanson-Woodyard criteria for the endfire radiation with increased directivity is applied to design. The antenna is further optimized to get better results.

- To design dual-band HMSIW LWA, spiral loaded periodic unit cells are etched on a HMSIW line. The dispersion diagram of the spiral shaped unit cell is analyzed. The LWA is configured based on the unit cell, its Bloch impedance and

leakage constant are analysed for better matching. A four port LWA is designed, which produces dual-bands of different polarization states. The combination of the etched spiral slot, the central vias along with the HMSIW vias form the required bands. Four-port overall LWA antenna exhibits RHCP as well as LHCP at upper band based on the excitation port.

- Asymmetry is investigated in the HMSIW technology. A series of vias are placed on one side of the unit cell which forms longitudinal asymmetry. This type of asymmetry produces LP waves in the lower band and CP waves in the upper band. Similarly, the sidewall vias of the HMSIW unit cells are connected alternatingly, provides simultaneous dual-beams with different polarization in the upper operational band in addition to the LP beam in the lower operational band. The unit cells of two antennas are analysed in terms of their dispersion behaviors. The position of the short-circuits will alter the mode propagation behavior inside the structure.

1.6   Organization of the Thesis

The goal of thesis is to design and implement dual-beam, dual-band and wide-angle beam scanning LWAs using the Goubau and asymmetric HMSIW transmission lines. This thesis is organized into several chapters based on the various designs proposed and obtained results. The introduction section of the thesis describes LWA, their classification. Motivation to design innovative antennas is presented, followed by problem formulation. The objectives, work methodology and thesis organization are provided in separate sections.

The second chapter discusses a brief literature of LWAs. The upcoming sections describe the literature works and their limitations on LWAs A brief theory of LWAs and Transmission lines are included in the next section.

In the third chapter, planar Goubau transmission line based antennas are discussed. In the first section, Goubau line LWA is presented which provides wide-angle beam scanning. Conventional Goubau LWAs exhibit a limited scanning angle, this work employed a periodically bending Goubau line, which not only brings in a periodic perturbation for leaky wave radiation, but also enhances the scanning range due to the increased delay for each line element. The second section explains Goubau endfire antenna. Endfire radiation is achieved by modifying the Goubau line into an inverted

periodic arrangement of V-shaped unit cells. The unit cell, dispersion analysis, working principle, fabricated prototypes, simulated and measured results are presented.

The fourth chapter provides a novel dual band dual polarized LWA with polarization diversity is proposed using half-mode substrate integrated waveguide (HMSIW) based technology. HMSIW LWAs are generally single band. In this work, by etching simple spiral type slots on the HMSIW cavity, a novel dual band dual polarized leaky wave antenna is designed.

In the fifth chapter, two configurations of novel dual-band HMSIW LWAs are presented. The first proposed antenna radiates LP waves in the lower band and CP waves in the upper band when the unit cells are cascaded sequentially. The second antenna, where the sidewall via of the HMSIW unit cells are connected alternatingly, provides simultaneous dual beams with different polarization in the upper operational band in addition to the beam in the lower operational band. The unit cells of the two antennas are analysed in terms of their dispersion behaviors. Finally, the performance of both the antennas are experimentally verified.

The sixth chapter gives conclusions about the contributions provided through different designs in the thesis. Also, it discusses the future scope to develop antennas with improved performances for new applications.

CHAPTER 2

LITERATURE SURVEY AND BACKGROUND

This chapter presents a brief literature review on the Leaky Wave Antennas and its limitations. Also, Fundamental design principles of periodic LWAs such as Floquet theorem and radiation characteristics of periodic structure are discussed in the Background Section. Finally, a brief introduction of Goubau Line and HMSIW transmission line is presented which are used to design LWAs in this thesis.

2.1 Literature Survey

LWAs are widely investigated due its unique properties such as beam direction that can be steered with the change in excitation frequency (Jackson and Oliner (2008)). Also, these are simple to realize since there is no complex feed network is required. LWAs are basically categorized into two types, depending on whether the guiding structure is uniform or periodically modulated. In uniform LWA, modulation is uniform along the length of the guiding medium (Hines and Upson (1957)). This type of antenna radiates only in the forward quadrant, which limits the beam scanning range. Periodic LWA is basically periodic modulation of the guiding structure. This periodic modulation produces infinite space harmonics, in which fast space harmonics are radiating to free space.(Guglielmi and Boccalone (1991)).

Early periodic LWAs are based on the closed metallic waveguide structure (Hines and Upson (1957)). These are bulky and hence their applications are limited. Later, microstrip and dielectric waveguide based LWAs are developed (Metzler (1981)) which are compact and small in size. But, these LWAs are suffering from open stop-band problem. This is due to reflections at the broadside which leads to gain reduction of an antenna at broadside. Hence, it limits the performance and scanning range of an

LWA. Metamaterial based CRLH LWA was designed ((Caloz and Itoh (2003))). In this work fundamental mode is used for radiation and open stop band is eliminated using metamaterial CRLH technique. Later, many LWAs are designed to eliminate openstop problem. Recently, asymmetric LWA (Otto et al. (2014a)) was designed to suppress the open-stop band problem. Many technologies are developed to increase the scanning range of LWAs and to develop circular polarized LWAs. Most of the early LWAs are working in single band, dual-band LWAs are also developed in these days. However, there is limited research work on efficient wide angle beam scanning and dual-beam dual-polarized LWAs. Some of the works related to above problems are discussed in the below sections.

2.1.1   Goubau Line Leaky Wave Antennas

A group at the Valencia Polytechnic University has investigated the possibilities of constructing Goubau line based LWAs (Sánchez-Escuderos et al. (2013)). High losses in the dielectric and ground conductor of the microstrip technology offer a challenge at millimeter-wave frequency range. Hence, other types of transmission lines are required to overcome this problem. At submillimeter wavelengths, single-wire waveguides have been investigated and validated for low-loss transmission. The leaky-wave configuration that is based on the Goubau line is shown in Figure 2.1.
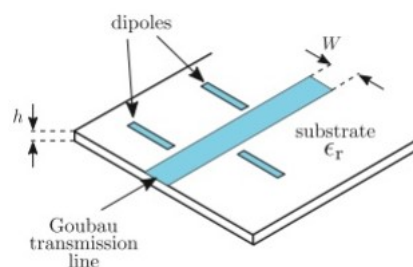
Figure 2.1: Goubau line LWA (Sánchez-Escuderos et al. (2013)).

The fundamental mode of the Goubau line is bounded. It can therefore be used as a LWA by adding dipole radiators along the transmission line. The transverse planar dipole sources are periodically perturbed along the line and they excites an infinite

number of space harmonics. If a any one of these harmonics is fast, it leads the structure to radiate. It was later observed that the absence of a ground conductor resulted in two main beams, as opposed to the intended single-beam radiation. To realize the single-beam, a metallic conductor was added to the LWA at an optimized distance from the antenna. This optimization was required so that the power radiated towards the metallic conductor would be completely reflected and added in-phase to the generated beam. Adding the two beams in-phase resulted in a maximum directivity. Furthermore, reduced losses could be obtained if the metallic conductor and the antenna were separated by an air gap.
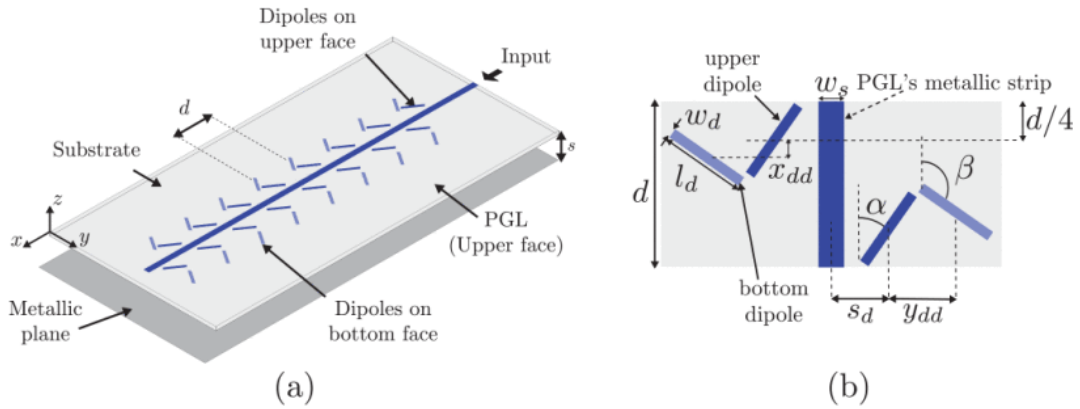
Figure 2.2: Circularly polarized Goubau LWA (Sánchez-Escuderos et al. (2016)).

A later modification to the Goubau line is presented (Sánchez-Escuderos et al. (2016)) is shown in Figure 2.2, involved the design of arrays that produces CP beam. This was obtained by etching crossed dipoles on the substrate with an electric contact between the dipoles. The above discussed methods suffer from open stop-band problem.
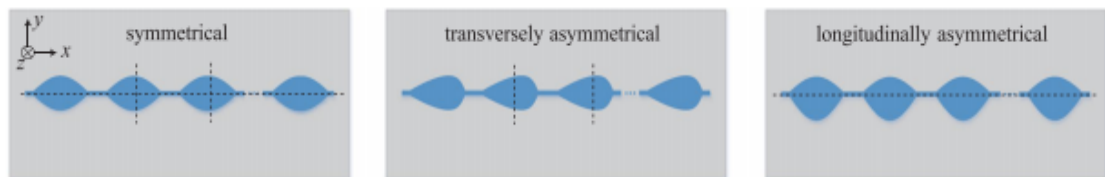
Figure 2.3: Asymmetrically modulated Goubau line (L.Tang et al. (2017)).

To overcome this drawback, asymmetrically modified Goubau line is presented by (L.Tang et al. (2017)). Transversely asymmetrical modulated Goubau line is shown in Figure 2.3. The measured results obtained from the prototype shows that radiation efficiency and gain is very good at broadside and scanning range is around $30°$ degrees.

We can conclude from the above literature review that scanning range in the above designs is limited to 30 degrees. The LWA proposed in Chapter 3 of the thesis overcomes this limited scanning range. The work employed a periodically bending Goubau line, which not only brings in a periodic perturbation for leaky wave radiation, but also increases the scanning range due to the increased delay for each line element. 155^0 wide-angle beam scanning is achieved.

2.1.2 Endfire Leaky Wave Antennas

Recently, leaky-wave endfire antennas have been developed and compared with the geometries of the typical Yagi–Uda antenna and the log-periodic antenna. Periodic leaky wave endfire antenna arrays are attractive substitutes for traditional endfire antenna. Also, Hansen–Woodyard (H–W) antenna arrays can achieve the maximum directivity at endfire (Hansen and Woodyard (1938)), the modified H–W condition has been applied for the design of the periodic LWA arrays (Liu et al. (2014)), and the relevant theories have been acutely researched (Fuscaldo et al. (2017)). There are many conventional endfire antennas exhibit good performance. But, there is a limited research work reported on the single metallic-layer based endfire antennas. Spoof surface plasmon polariton (sSPP) is also a type of single layer transmission line, which does not have any ground plane. A few endfire antennas were reported using sSSP transmission line. SSP fed dipole antenna is used to achieve endfire radiation (Yin et al. (2017)) and broadband endfire traveling wave antenna is designed based on the sSPP (Kandwal et al. (2018)). In these sSPP antennas, SPP is used for only transmission purpose and dipoles as a radiators. There is limited research on single layer LWAs which radiates towards endfire direction. There is need to design single layer based LWA to achieve endfire radaition using Goubau line. The work proposed in the section 3.3 of chapter 3 is a simple and low profile planar novel Goubau line based endfire antenna.

2.1.3 Dual-Band Dual-Polarized Leaky Wave Antennas

Dual-Band and Dual-Polarized LWAs are widely investigated in recent days. A millimeter-wave frequency scanning antenna was designed (Cheng et al. (2010)), which is capable of dynamically changing the state of polarization thereby providing four modes of operation. It is able to operate in either LP or CP, depending on the requirements of its specific application. A new method to achieve dual-band operation from an HW-MLWA by periodically loading the antenna with U-shaped slots (Karmokar and Esselle (2015)). These dual-band MLWAs are able to steer the beam in forward directions in one band and in backward directions in the other band. HW-MLWA loaded with periodic L-shaped slots (Karmokar et al. (2017)). The antenna exhibits tri-band operation, and the main beam can be steered in the forward direction in one band, and in the backward direction in the other two bands. But, LP wave is radiated i all these bands. There is need for dual-band LWA with different polarization in each band. There is scope to design dual-band and dual-polarized LWA.

The fourth chapter of the thesis proposes the dual-band dual-polarized LWA with polarization diversity is proposed using HMSIW based technology. LWAs are generally single band. In this work, by etching simple spiral type slots on the HMSIW cavity, a novel dual-band dual-polarized LWA is designed. The antenna radiates the LP wave in the lower band and CP wave in the upper band. Also, in the higher operating band he proposed overall antenna exhibits both RHCP as well as the LHCP.

2.1.4 Dual-Beam and Asymmetric Leaky Wave Antennas

Dual-beam LWAs are able to detect multiple targets and hence they play important roles in automotive radar and vehicular communication. There were a few dual-beam periodic LWAs that were reported in the previous literatures. A long rectangular patch was excited using CPW to work in its first higher-order mode (Luxey and M. Laheurte (1997)). The triple periodic LWA antenna is designed to excite two modes simultaneously for dual-beam scanning (Ma and Jiang (2015)). Configuration and radiation

pattern of the triple perioidc LWA at 5.8 GHz is shown in Figure 2.4.
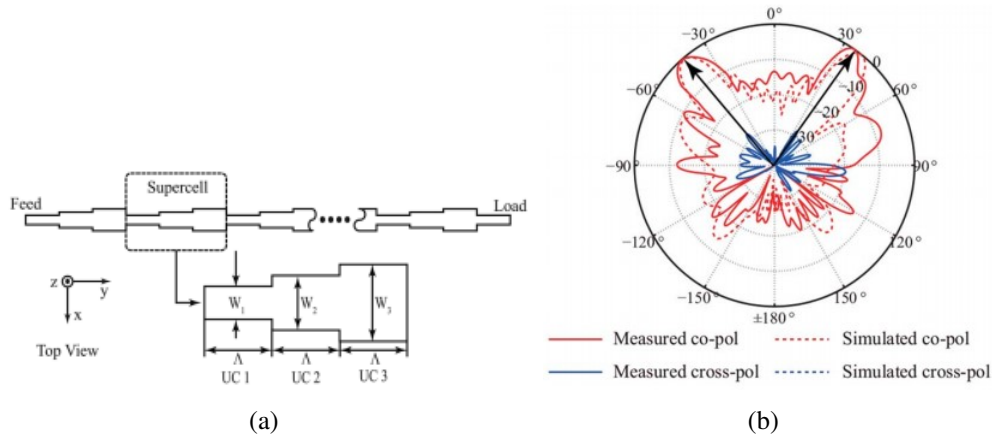
Figure 2.4: Tripple periodic dual-beam LWA (a) Configuration (b) Simulated and Measured radiation pattern at 5.8 GHz (Ma and Jiang (2015)).

In (Karmokar et al. (2016)), both the edges of the microstrip line was used to obtain symmetrical side beams. Characterizations of multi-period structures were analyzed, and were used to obtain multi-beams (Ma et al. (2015)). A super-cell dielectric LWA was used to produce dual-beams (Ma et al. (2016)). Substrate integrated ridge-gap waveguide was used to excite two space harmonics, leading to simultaneous dual-beam scanning (Rahimi and Kishk (2018)). However, these dual-beam LWAs are limited to single polarization.
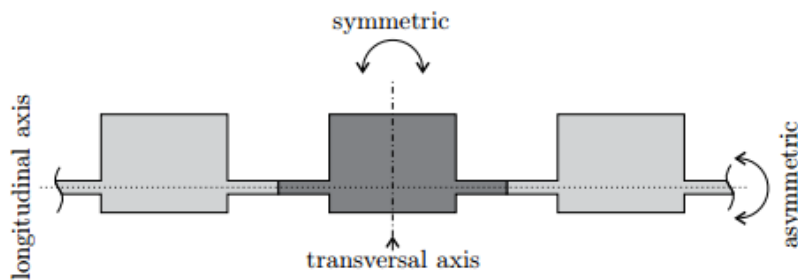
Figure 2.5: Longitudinally asymmetric series-fed LWA (Li et al. (2010)).

Recently, asymmetry in periodic LWA was studied to overcome the open-stop band problem (Otto et al. (2014a)). Asymmetry (longitudinal or transversal) in periodic LWA antennas results in simultaneous frequency balance, quality-factor balance, and polarization control. In (Otto et al. (2014b)), asymmetry was introduced for CRLH and

series-fed LWA to investigate the open-stop band problem. The geometry of the longitudinally asymmetric series-fed LWA is shown in Figure 2.5. In (Sarkar et al. (2019)), double asymmetry is investigated to obtain high gain with wide full-space scanning in LWA. Here, tilted double asymmetric radiating Eighth-Mode SIW is incorporated with interdigital capacitive (IDC) slots enables the unit cell to hold the CRLH property. These above LWAs are limited to single-beam radiation. In (Al-Bassam et al. (2017)), double asymmetric periodic LWA is further studied, asymmetry with respect to both longitudinal and transversal axis of the structure allows for simultaneous radiation of two orthogonal modes excited at the two ports of an antenna. Here, two separate ports are required to excite orthogonal beams. Hence, there is a requirement to design LWA to produce simultaneous dual-beams with different polarization using single port.

The fifth chapter of the thesis presents two configurations of novel dual-band HM-SIW LWAs. The theory of asymmetry is investigated in HMSIW. The first proposed antenna radiates LP waves in the lower band and CP waves in the upper band when the unit cells are cascaded sequentially. The second antenna, where the sidewall via of the HMSIW unit cells are connected alternatingly, provides simultaneous dual-beams with different polarization in the upper operational band in addition to the LP beam in the lower operational band.

2.1.5 Research Gap Analysis

Efficient Wide-Angle Beam Scanning LWA : There lies a need for the design of highly efficient wide-angle beam-scanning LWA. Single layer Goubau LWAs are highly efficient when compared to microstrip LWA. But, scanning range in Goubau LWA is limited. The LWA requires miniaturized designs that can scan from backfire to endfire with good efficiency.

Endfire LWA based on Goubau Line : On investigation of existent designs, it is found that there is a scope for single layer Goubau line Endfire LWA. There is limited research on Goubau line endfire LWA. There lies a need for developing new kind of single layer LWA.

15

Dual-Band Dual-Polarized LWAs : There are many Dual Band LWAs. But, all the bands radiates LP wave. There is need for antenna that radiates LP wave in the lower band and CP wave in the upper band. The research gap analysis points out the requirement for the design of LWA that can provide two different bands with different polarization in each band.

Dual-Beam LWAs : As we discussed in the above section, most of the existing dual-beam LWAs are single polarized. It is required to obtain a compact design that offers dual-band dual-polarized with simultaneous dual-beam LWA for different functionalities.

2.2   Theory of periodic leaky wave antenna

Periodic LWA is composed of a transmission line with periodic unit cells. The wave propagation in the periodic LWAs is analyzed by using the Floquet theorem and their radiation characters are obtained by using dispersion diagram of a unit cell. Therefore, a brief theory of Floquet theorem and dispersion diagram of a periodic structure is discussed in this section.

2.2.1   Floquet Theorem

A French mathematician Floquet discovered the solution for periodic differential equations (Collin (1991)) and analysed the wave transmission through periodic structures. It decomposes the electric field along the wave transmission direction into spatial harmonics. To understand this electric field decomposition, let us take an example of series fed periodic LWA as shown in Figure 2.6. The wave propagation direction on this antenna is along the x-direction. The unit cell shown in the figure with length p is called one period. The infinite repetition of these unit cells forms the periodic structure.

From the Floquet theorem, electric field of a wave along infinite periodic structure
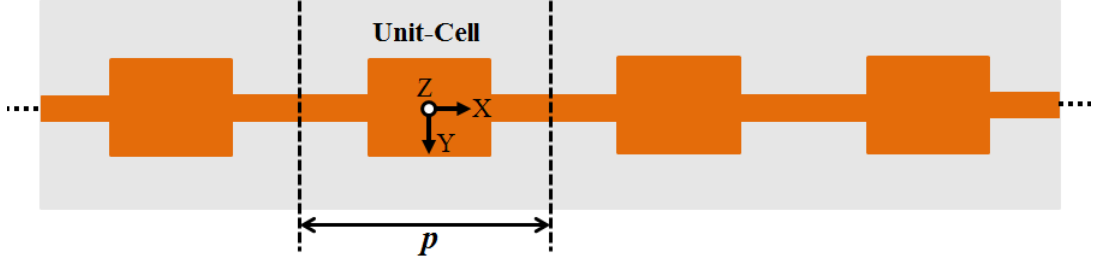
Figure 2.6: Series-fed LWA as an example of periodic LWA.

in the positive x-direction is

$$\vec{E}(x + mp, y, z) = \vec{E}(x, y, z)e^{-\gamma mp} \tag{2.1}$$

where $\vec{E}$ is the vector electric field, γ is complex propagation constant and m is integer number. From the above equation, it is noticed that electric field at the point x and $x + p$ are only differentiable by complex propagation term $e^{\gamma p}$. The complex propagation constant is given by $\gamma = \alpha + j\beta$ where α is the leakage constant and β is the phase constant. A periodic vector function $\vec{F}$ with period p along the propagation direction is

$$\vec{F}(x + mp, y, z) = \vec{F}(x, y, z) \tag{2.2}$$

Next, the electric field is expressed as a product of periodic function and the complex propagation term

$$\vec{E}(x, y, z) = \vec{F}(x, y, z)e^{-\gamma x} \tag{2.3}$$

upon substation of equation 2.3 into equation 2.1, then

$$\vec{E}(x + mp, y, z) = \vec{F}(x + mp, y, z)e^{-\gamma(x+mp)} \tag{2.4}$$

Applying periodicity principle from equation 2.2 to $\vec{F}$ of equation 2.4 becomes

$$\vec{E}(x + mp, y, z) = \vec{F}(x, y, z)e^{-\gamma x}e^{-\gamma mp)} \tag{2.5}$$

by back substituting equation 2.3 into 2.5 simplfies to

$$\vec{E}(x + mp, y, z) = \vec{E}(x, y, z)e^{-\gamma mp} \tag{2.6}$$

which is same as equation 2.1. The key observations from these equations are the electric field from location x to $x + p$ is only differentiable by complex prorogation term and electric field in the periodic structure is the product of periodic function and propagation term. The fourier series for the periodic function in the equation 2.2 is

$$\vec{F}(x, y, z) = \sum_{n=-\infty}^{+\infty} \vec{E}_n(y, z)exp\left(-jn\frac{2\pi}{p}x\right) \tag{2.7}$$

where n is an integer number referring to the order of the space harmonic, $\vec{E}_n(y, z)$ is the cross-sectional field distribution of the nth space harmonic. As we know that, electric field in the periodic structure is the product of periodic function and propagation term. By substituting equation 2.3 in 2.7 one obtains expression for electric field

$$\vec{E}(x, y, z) = \left[\sum_{n=-\infty}^{+\infty} \vec{E}_n(y, z)exp\left(-jn\frac{2\pi}{p}x\right)\right]exp(-\gamma x) \tag{2.8}$$

After simplification, final electric field of periodic structure becomes

$$\vec{E}(x, y, z) = \sum_{n=-\infty}^{+\infty} \vec{E}_n(y, z)exp\left[-j\left(\gamma + n\frac{2\pi}{p}\right)x\right] \tag{2.9}$$

From the above equation, propagation constant n^{th} space harmonics is given by

$$\gamma_n = \gamma + jn\frac{2\pi}{p} = \alpha + j\left(\beta_0 + \frac{2n\pi}{p}\right) \tag{2.10}$$

Finally, field along the periodic structure is

$$\vec{E}(x, y, z) = \sum_{n=-\infty}^{+\infty} \vec{E}_n(y, z)e^{-\gamma_n x} \tag{2.11}$$

It is important to note that the cross sectional field distribution $\vec{E}_n(y, z)$ is independent

of x. The only x-dependency is found in the propagation term, so that the total field is decomposed into sinusoidal waves of different phase constants (or wavenumbers), traveling along an effective homogeneous transmission line. These waves are referred to as space harmonics. All space harmonic experience the same leakage α and the phase constant differs by integer multiples of $2\pi/2$.

2.2.2 Dispersion Diagram

Dispersion diagram is a graphical representation of phase constant (β_n) versus angular frequency (ω) (Volakis (1991)). The phase constant from equation 2.10.

$$\beta_n(\omega) = \beta_0(\omega) + \frac{2n\pi}{p} \tag{2.12}$$

where $\beta_0(\omega)$ is the phase constant of the fundamental mode and $\beta_n(\omega)$ phase constant of the nth space harmonic. Figure 2.7 shows the dispersion diagram which is constituted by shifting β_0 with 2π. The horizontal axis is the normalized phase constant β_n and the vertical axis is angular frequency ω. The blue lines shows the wave propagation of different space harmonics along the positive x-direction. periodic structures generally show passband and stopband behaviors over frequency.
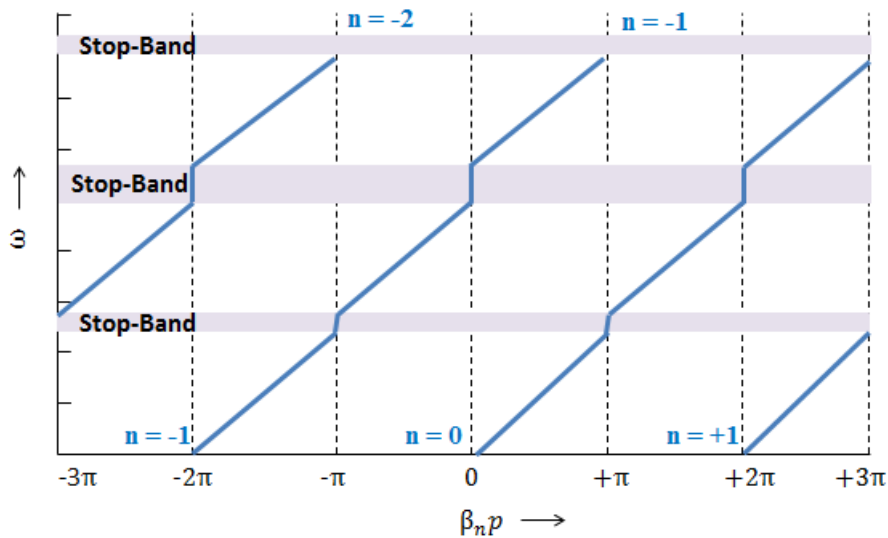
Figure 2.7: Dispersion diagram of a periodic structure.

Dispersion diagram helps us to analyze the radiation properties of the periodic LWA. It also helps us to understand about beam scanning behaviour of the LWA. Space harmonics shown in Figure 2.7 are just shifted curves of fundamental space harmonic ($n = 0$). Therefore, it is sufficient to limit the dispersion diagram to a range of $-\pi < \beta_n p > +\pi$ which is shown in Figure 2.3. The air line ($k_0 p$) shown in the Figure 2.8 divides the dispersion diagram into two different regions, guided wave region and radiation wave region. The shaded cone represents the radiation region. If the space harmonics falls into the shaded cone then it is fast wave propagation and it radiates into free space. If the space harmonic is out the radiation cone then its slow wave propagation. The fundamental space harmonics ($n = 0$) is below the air line and it is located in the guided wave region. Therefore, the fundamental space harmonic is bounded and does not radiate.
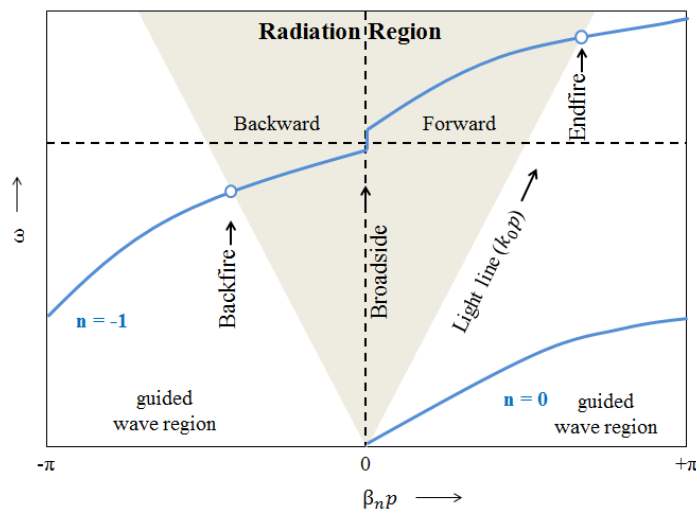
Figure 2.8: Simplified Dispersion diagram of a periodic structure.

The direction of the main beam in a periodic LWA is steered with the frequency. At lower frequencies the LWA radiates into the backward direction, as β_n is negative. At the broadside frequency, the LWA radiates into the broadside direction (x-direction), as $\beta_n = 0$. At frequencies higher than the broadside frequency, the LWA radiates into the forward direction, as β_n is positive. This beam steering property is described by the

main beam scanning law of periodic LWAs

$$\theta(\omega) = arcsin\left[\frac{\beta_n \omega}{k_0}\right] \qquad (2.13)$$

where θ is the angle measured in the XZ-plane from the Z-axis and k_0 is the free-space wavenumber. It is clear from the above discussion, dispersion diagram is the key parameter to analyse the behaviour of the periodic LWAs.

2.3 Goubau Transmssion Line

Goubau line is a type of high frequency transmission line which is formed by single metallic wire coated with dielectric layer (Goubau (1951)). In 1898, Sommerfeld theoretically proved the propagation of surface wave on single metallic wire. Few years later, Goubau experimentally verified the Sommerfeld theory of single wire transmission. A typical Goubau transmission line is shown in Figure 2.9. It consists of metallic rod coated with dielectric material and horns are used to couple the energy from in and out the Goubau line. The wave propagating through Goubau line slows down the velocity of the wave to less than the free space velocity which results in the transmission of wave on the metallic wire.
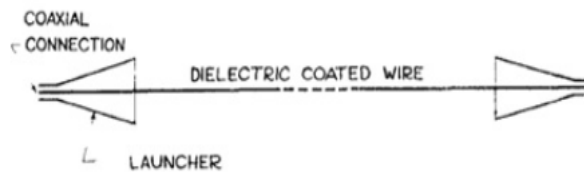
Figure 2.9: Goubau Transmission line [Goubau (1956)].

Conventional high frequency transmission lines like parallel-line and coaxial-cables have high losses hence these are not preferred for long distance transmission. The main advantage of the Goubau line is low attenuation level. Therefore, Goubau lines can serve as low loss antenna feed-lines at high frequencies is shown in Figure 2.10. It was also used for long distance high frequency transmission as shown in Figure 2.11.
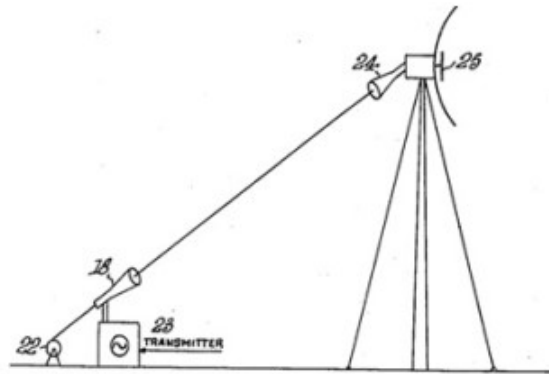
Figure 2.10: Goubau line as a feed-line for an antenna [Goubau (1950)].

Recently, planar version of Goubau line is proposed (Treizebre et al. (2005)). The excitation is based on electromagnetic transition between a co-planar waveguide (CPW) and the desired Goubau line in a planar configuration is shown in Figure 2.12. CPW line is used for the excitation which plays the role of an horn antenna used for the excitation of the mode and tapered CPW is used for smooth mode transition.
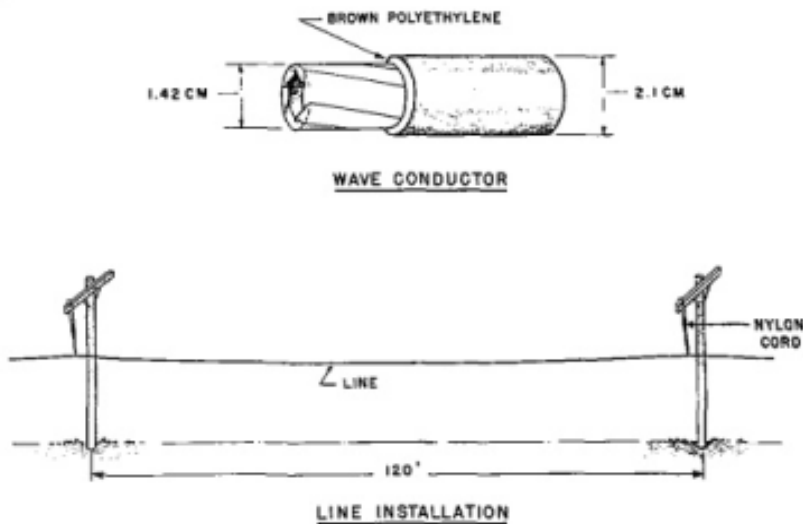
Figure 2.11: Goubau line for long distance communication.

The planar Goubau line has very small dielectric loss at millimeter wave frequency, due to the high field confinement around the metal line. Hence planar excitation of Goubau line is opened many applications. Researchers employed planar Goubau line to design low-loss transmission lines (Akalin et al. (2006)), filters (Horestani et al. (2013)),
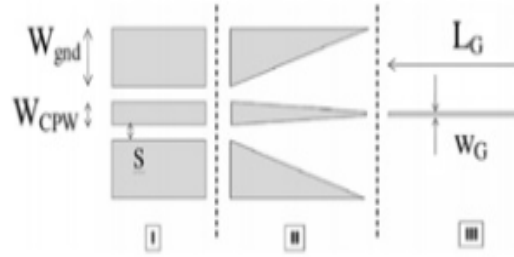
Figure 2.12: CPW to Goubau line transition with three different zones: I is CPW line, II is the tapered transition, and III pure Goubau line Zone [Treizebre et al. (2005)].

LWAs (Tang et al. (2019)) and THz Spectroscopy, Wireless power transfer (Vaughn et al. (2018)) etc. Goubau line is widely used to design LWAs due its low loss behaviour.

2.4 Half-Mode Substrate Integrated Waveguide

HMSIW was first developed in 2006 (Hong et al. (2006)). HMSIW is basically drawn from SIW. It is of great research interest due to its compact nature which preserves nearly all the advantages of SIW like high power handling, easy to integrate, small size and low cost, etc. Substrate Integrated Waveguide (SIW) is a closed structure where as HMSIW has open cavity by its own which is very easy for antenna design. HMSIW geometry is created by cutting SIW in half and extending the substrate from the open aperture side as shown in Figure 2.13. It is fed using tapered microstrip line and TE_{10} is the propagation mode.

Figure 2.13: Fabricated prototype of HMSIW.

For the dominant mode, it is known that the symmetric plane along the transmission direction is equivalent to a magnetic wall (MW), thus half of the SIW will keep the
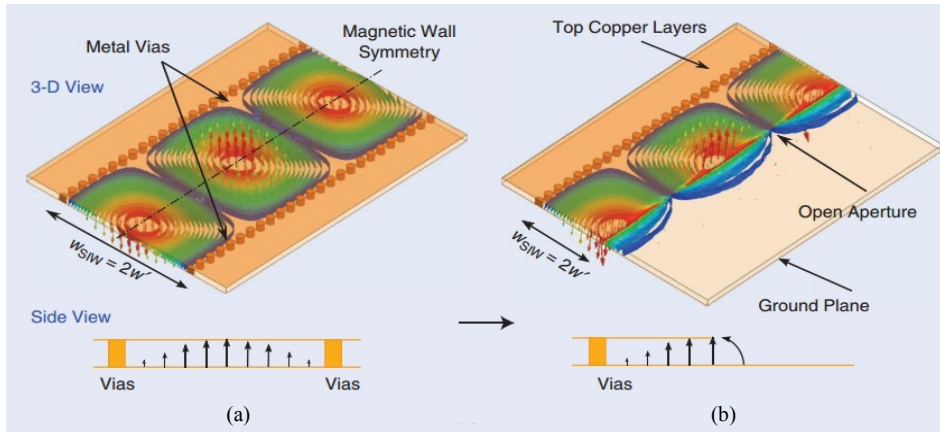
Figure 2.14: Simulated electric field distribution (a) SIW (b) HMSIW (Nguyen-Trong and Fumeaux (2018)).

half field distribution unchanged if cutting plane is a magnetic wall. Actually, the open side aperture of the HMSIW is nearly equivalent to a perfect MW due the high ratio of width to height (Nguyen-Trong and Fumeaux (2018)). This is justified by observing that the field distribution inside of the HMSIW is nearly half of that SIW as shown in Figure 2.14. Based on this concept, many scientists developed a number of high quality microwave and millimeter wave passive elements, such as filters (Wang et al. (2007)), couplers (Jie et al. (2019)), power dividers (Zhou et al. (2018)) and antennas (Xu et al. (2008)) etc.

Many LWAs are designed using HMISW line. In (Xu et al. (2008)), HMSIW based LWA is designed for millimeter applications. Later, a CRLH based HMSIW (Dong and Itoh (2011)) leaky wave structure is developed. Fixed-frequency beam steering LWA (Suntives and Hum (2012)) is proposed using HMSIW. In (Pourghorban Saghati et al. (2014)), LWA with CP and backward-broadside-forward radiation is developed. Recently, in (Sarkar et al. (2018)), a combination of spiral-slots has been etched from HMSIW-based structure to produce continuous beam scanning linearly polarized LWA.

In this section, a brief theory to design LWAs is explained. The fundamental tools to design LWAs like Floquet theory and Dispersion diagram are discussed. Also, two different transmsssion line such as Goubau and HMSIW lines which are used to design LWAs are discussed.

CHAPTER 3

WIDE ANGLE BEAM SCANNING AND ENDFIRE LEAKY WAVE ANTENNAS BASED ON GOUBAU LINE

3.1   Introduction

In this chapter, planar Goubau transmission line based antennas are developed. In the first section, A Goubau line LWA with large scanning angle is presented. In contrast to the conventional Goubau line LWA with a small scanning angle range around 30^0, this work employed a periodically bending Goubau line, which not only brings in a periodic perturbation for leaky wave radiation but also enhances the scanning range upto 155^0. The simulation and experimental results show that the proposed leaky wave antenna provides 90% radiation efficiency and 7-10 dBi radiation gain from backfire to endfire through broadside as frequency changes. The proposed antenna features good radiation performance, compact and low-profile configuration. The second section explains proposes a simple and low profile planar Goubau line based end-fire antenna. There are many conventional end-fire antennas exhibit good performance. But, there is a limited research work reported on the single metallic-layer based End-fire antennas. Eventhough single layer sSPP based endfire antennas availabele. But, they are only used to feed dipoles. Single layer based Endfire LWAs are stil a challenge. This work proposes a Goubau line based Endfire antenna. The Endfire radiation is achieved by bending the Goubau line in inverted-V shape. The proposed antenna possesses all the advantages of microstrip line like compact, simple, and easy to fabricate. The unit cell, dispersion analysis, working principle, fabricated prototypes, simulated and measured results are also presented.

3.2 Leaky Wave Antenna for Wide-Angle Beam Scanning From Backfire to Endfire based on Goubau Line

This section presents a wide-angle beam scanning Goubau line LWA. A Goubau line LWA with large scanning angle is presented. In contrast to the conventional Goubau line LWA with a small scanning angle range around 30^0, this work employed a periodically bending Goubau line, which not only brings in a periodic perturbation for leaky wave radiation but also enhances the scanning range upto 155^0. Initially, dispersion diagram of the planar Goubau line is analysed. Based on the analysis, operating principle of the proposed LWA is discussed. Finally, results of the proposed antenna is compared with the previous works.

3.2.1 Dispersion analysis of planar Goubau line

The planar Goubau line is composed of a metallic strip over a dielectric substrate without ground plane, as shown in Figure 3.1, where the parameters w, t, and h denote the line width, the strip thickness, and the substrate thickness, respectively. The fundamental mode of the planar Goubau line is bounded.
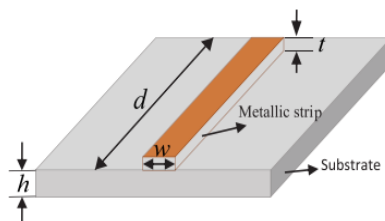
Figure 3.1: Planar Goubau transmission line

The dispersion diagram of the fundamental mode of the planar Goubau line with dimensions w=1 mm, t=18 mm, h=1.52 mm, and d=21.5 mm on Rogers 4003C substrate (ϵ_r=3.38 and tan δ=0.027) is shown in Figure 3.2. It is observed that the fundamental mode of the planar Goubau line is below the air line. Hence, it is a slow-wave mode,

which is strongly bounded to the surface and does not radiate into the free space. According to the dispersion curve in Figure 3.2, the Goubau line with d=21.5 mm length reaches 180^0 phase at 5.5 GHz.
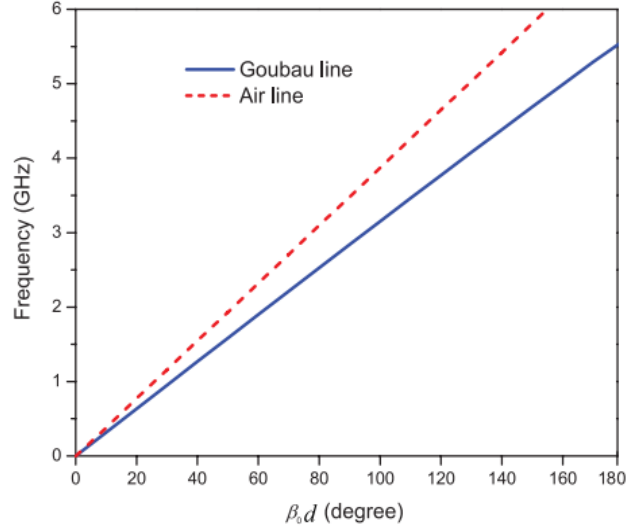
Figure 3.2: Dispersion diagram planar Goubau transmission line.

3.2.2   Operating principle and Antenna configuration

The operation principle of the Goubau line LWA is based on the generation of a radiating space harmonics. Adding periodic perturbations along the planar Goubau line excites an infinite number of space harmonics, whose propagation constant is characterized by

$$\beta_n = \beta_0 + \frac{2n\pi}{p} \tag{3.1}$$

where β_n is the propagation constant of nth space harmonic, β_0 is the propagation constant of the dominant mode, and p is the modulation period. One usually considers $n = -1$ harmonic, whose propagation constant is given by

$$\beta_{-1} = \beta_0 - \frac{2\pi}{p} \tag{3.2}$$

By choosing a proper p, one is able to let n =-1 harmonic enter the fast wave region, i.e., $-k_0 \leq \beta_{-1} \leq k_0$, where k_0 is the propagation constant in the air. The main beam

27

direction of the LWA is calculated by

$$\theta = arcsin\left(\frac{\beta_{-1}}{k_0}\right) \tag{3.3}$$

Therefore, by choosing a different p, one is able to control β_{-1} and hence the beam angle θ. For example, one may choose $p = d = 21.5$mm and then calculate the frequency of broadside radiation. To get radiation at broadside, it requires that $\beta_0 p = 2\pi$. Since $\beta_0 p = \beta_0 d$ reaches π at 5.5 GHz, according to Figure 3.2, it should satisfy $\beta_0 p = 2\pi$ at 11 GHz. Therefore, the antenna radiates into the broadside direction at 11 GHz.
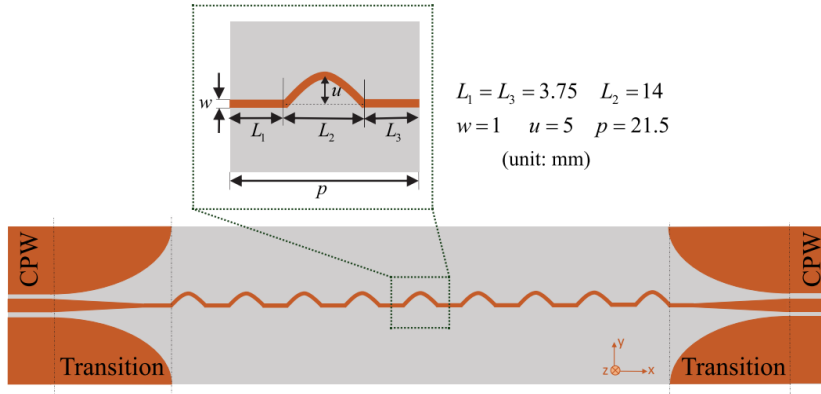
Figure 3.3: Configuration of the Goubau line LWA.

There are various modulation ways to design a LWA. Here, we periodically bend the Goubau line to achieve the radiation, as shown in Figure 3.3. Such a bending offers two benefits in the design of LWAs. First, this smooth bending has a very small reflection, resulting in a very broadband LWA. Second, the bending itself extends the line length and hence increases the group delay, which further enhances the scanning angle range within a specific frequency band. Simulated reflection coefficient for different values of u is shown in Figure 3.4. It is observed that, reflections are more for the values $u = 6$ and 7 mm, optimum for value $u = 5$ mm and minimum for value $u = 4$ mm. But, scanning range is limited for $u = 4$ mm . Hence, Optimised value $u = 5$ mm is selected for the proposed LWA.

In this design, the bending period is set as $p = d = 21.5$ mm. Due to the bending, the effective length (approximated by $L_1 + L_3 + \sqrt{L_2^2 + 4u^2}$) is about 24.7 mm, which is
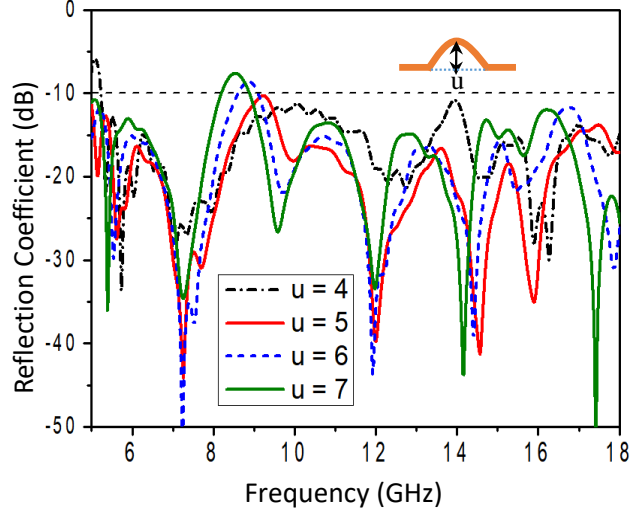
Figure 3.4: Simulated reflection coefficient for different values u.

approximately 15% longer than the modulation period $p = 21.5$ mm. It means that the slope of the effective dispersion curve should be 15% smaller than that of the straight Goubau line in Figure 3.2. Therefore, the expected broadside frequency $f_{broadside}$ is also 15% smaller than the original one (11 GHz), i.e., $f_{broadside} = 9.35$ GHz. In addition to the broadside frequency, one is also able to calculate the cutoff frequency when it enters the fast-wave region. This frequency corresponds to the backfire radiation, which satisfies $\beta_{-1} = \beta_0 - 2\pi/p = -k_0$, where $\beta_0 = 2\pi f/(pf_{broadside})$. After some calculation, one computes the cutoff frequency as $f_{cutoff} = 5.6$ GHz. Accordingly, this antenna starts to radiate only when $f \geq 5.6$ GHz.

The proposed Goubau line LWA employs two transitions connected to 50Ω CPW lines (width 4.5 mm and gap 0.3 mm). At both ends, tapered ground planes are used for smooth transitions between CPW and Goubau lines. This transition structure efficiently converts the transversal electromagnetic mode in CPW to a transversal magnetic surface wave mode in Goubau line. The scattering parameters of the designed antenna are simulated using CST Microwave Studio, as shown in Figure 3.5. As can be seen from the dispersion curve, the cutoff frequency of the fundamental mode is around 5.5 GHz, which is very close to the approximated cutoff frequency 5.6 GHz. Below 5.5 GHz, the transmission loss is below 1 dB and reflection is below 10 dB. Above 5.5 GHz until 20
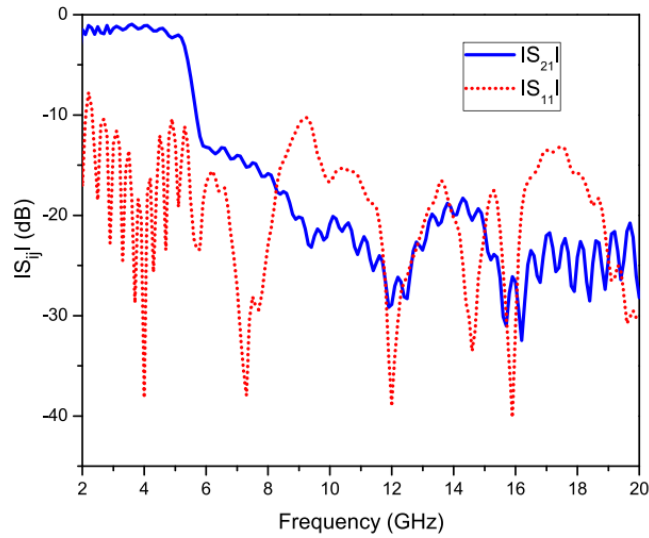
Figure 3.5: Simulated scattering parameters of the LWA in Fig 3.3.

GHz, both transmission and reflection are below 10 dB. The operational bandwidth for radiation ranges from 5.5 to 20 GHz.

3.2.3 Experimental validation of the designed LWA

The designed LWA is fabricated and experimentally verified, as shown in Figure 3.6. The scattering parameters are measured using a vector network analyzer as shown in Figure 3.7. Both simulated and measured results are matched over a wide range of frequency, in spite of a slight frequency shift that probably results from the dielectric tolerance.

Figure 3.6: Fabricated prototype of the proposed Goubau line.

The simulated and measured radiation patterns at different frequencies are shown in Figure 3.8. At 5.5 GHz, the beam is radiated at the backfire direction. As the frequency increases, the beam continues scanning toward the endfire through broadside. At around

30
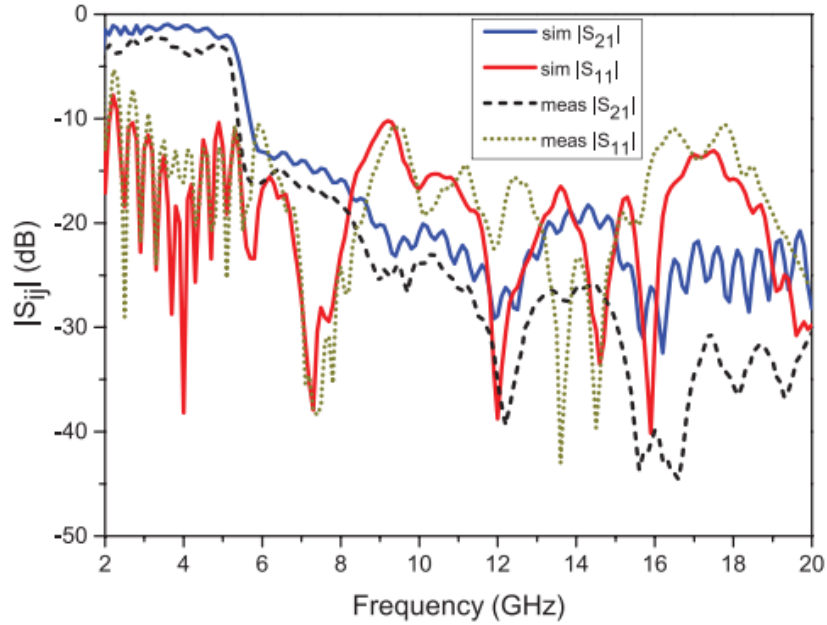
Figure 3.7: Scattering parameters from simulation and measurement.

9.6 GHz, the beam is radiated at the broadside direction. Within the frequency range 5.5-20 GHz, the proposed antenna scans continuously from backfire toward endfire with a large scanning range of about 155^0.

The radiation efficiency and gains of the proposed antenna are shown in Figure 3.9 and 3.10, respectively. The efficiency at the backfire direction (5.5 GHz) is only 50% because it is close to the cutoff frequency. At other frequencies away from the cutoff frequency, e.g., 7-12 GHz, the radiation efficiencies are all above 90%. The simulated and measured gains are shown in Fig 3.10. Note that simulation and measurement have a good agreement. The measured gains within 7-20 GHz are between 9 and 11 dB. Within 6-7 GHz, the gain drops because it is close to the cutoff frequency. Interestingly, the backfire gain at 5.5 GHz reaches 12 dB, featuring the highest among all the frequencies which results from the fact that the two beams merge at the backfire direction. Also, the beam continuously scans through the broadside without gain and efficiency degradation. It is worth mentioning that there are two beams due to the groundless feature, which can be improved by adding a ground plane beneath it.
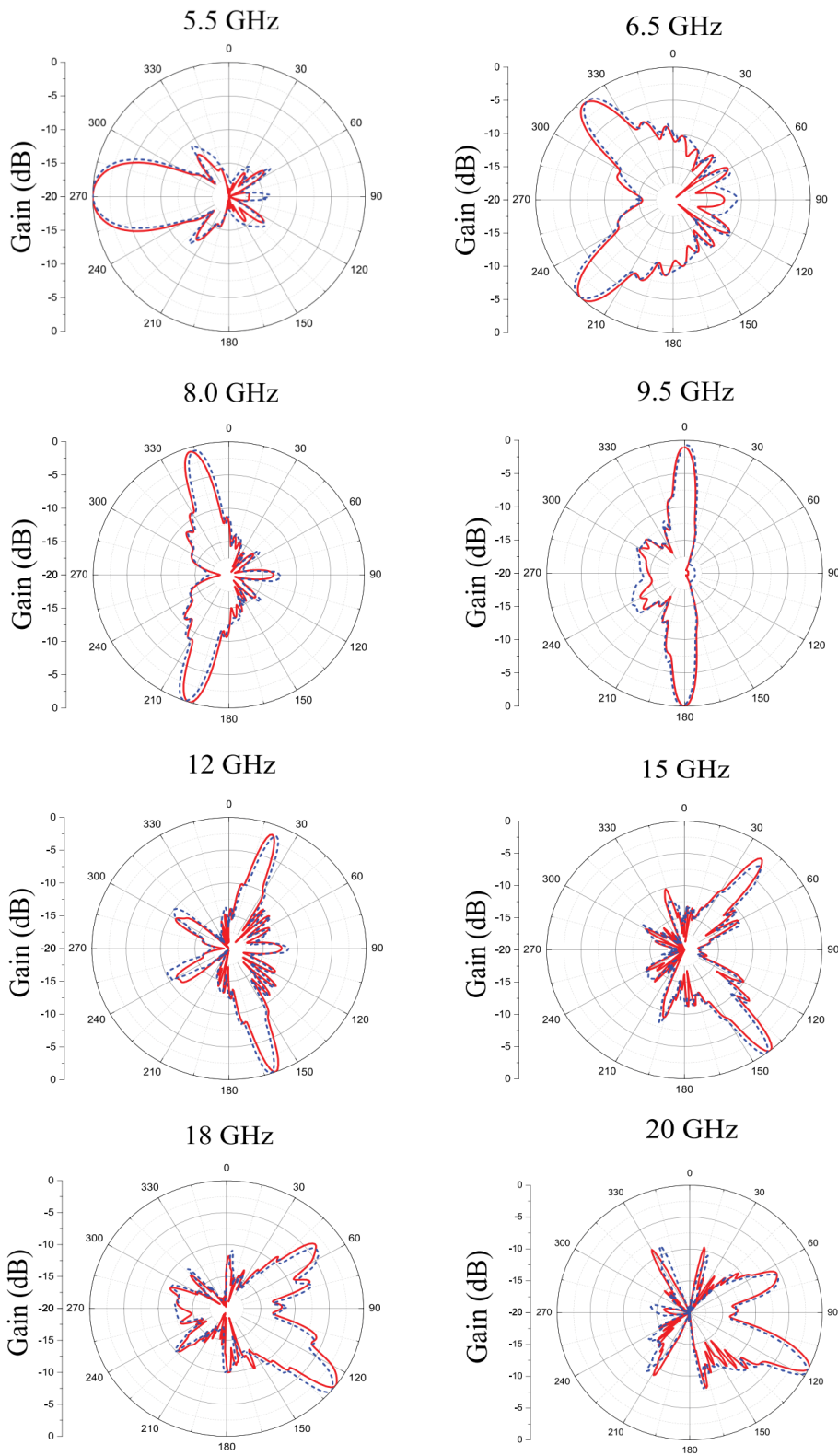
Figure 3.8: Radiation patterns of the Goubau line LWA at different frequencies.
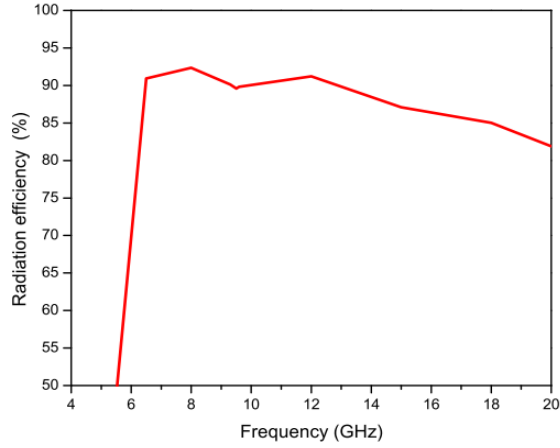
Figure 3.9: Simulated efficiency of the Goubau line LWA.
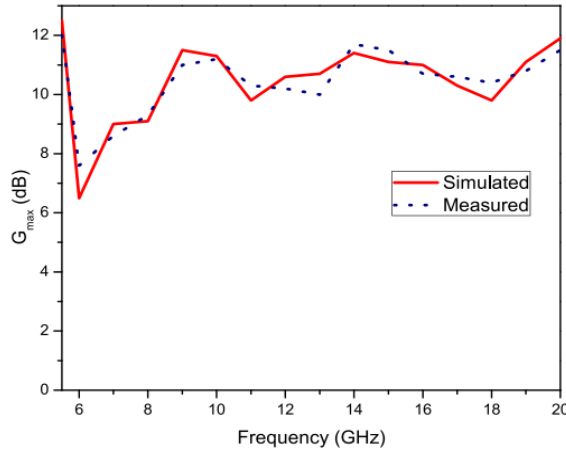
Figure 3.10: Simulated and measured gains of the Goubau line LWA.

To show the benefit of the proposed antenna, we compare it with all the other Goubau line LWAs in Table 3.1. Note that the proposed LWA exhibits the maximum scanning range, which is almost twice the second largest one in (Kianinejad et al. (2017)), although its efficiency is slightly smaller than that of (Sánchez-Escuderos et al. (2016)) and (L.Tang et al. (2017)). Actually, if we do not consider the frequency point 5.5 GHz, which is too close to the cutoff frequency, the average efficiency is around 88%. Therefore, this letter features the best scanning range and a good efficiency. In (L.Tang et al. (2017)), scanning range is around 32^0 and maximum 85^0 in sSPP LWAs ((Kianinejad et al. (2017)). In the proposed work, scanning range is 155^0 which covers the upper plane.

Table 3.1: Comparison of all the Goubau line LWAs

Goubau line leaky wave antennas	Averege Gain (dB)	Averege Efficiency (%)	Scanning Range (^{0})
Sánchez-Escuderos et al. (2013)	11	70	10
Sánchez-Escuderos et al. (2016)	15	93	05
L.Tang et al. (2017)	09	90	32
Kianinejad et al. (2017)	10	80	85
Proposed work	11	83	155

We have proposed a Goubau line LWA and experimentally validated it. The proposed antenna achieves a wide-angle beam scanning range with consistent gain and efficiency through the broadside. The proposed antenna can be potentially applied to radars and communications.

3.3 Goubau Line Endfire Antenna

This section presents a simple and low profile Planar Goubau Line based endfire antenna. Endfire radiation is achieved by modifying the Goubau line into inverted periodic arrangement of V-shaped unit cells. Designed prototype is simulated and verified experimentally. Proposed Endfire antenna has a single metallic layer with simple configuration which is easy to fabricate and also easy to integrate with other electronics circuits.

3.3.1 Antenna Geometry

The geometry of the proposed Goubau line endfire antenna is shown in Figure 3.11. The Goubau line is printed on Rogers RT Duriod substrate RO4003C ($\epsilon = 3.38$, $\delta = 0.0027$) with height h = 1.52 mm. The proposed antenna configuration consists of CPW, CPW to Goubau line transition and five inverted V-shape periodic unit cells. The dimensions of the CPW line are W_s = 5 mm, g = 0.3 mm, W_g = 25 mm, L_{CPW} = 53.5 mm, L_A =

71.5 mm, L_t = 120 mm and the impedance of the CPW line is 50Ω. CPW with tapered ground planes is used for mode conversion from CPW Quasi TEM mode to Goubau TM surface wave mode. CPW with tapered ground planes can efficiently excite surface wave mode along the Goubau line (Zehar et al. (2013)). Dimensions of inverted V-shapes are optimized in such a way that the radiation from all the V-shaped unit cells add in phase along the endfire direction
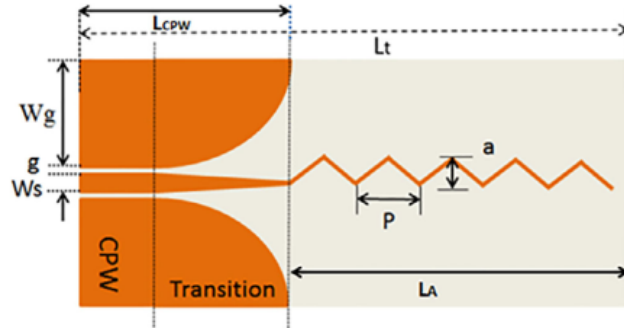
Figure 3.11: Geometry of the Goubau endfire antenna.

3.3.2   Operating Principle

Fundamental mode of a Goubau line is bounded and it does not radiate. So, the radiation is achieved by bending the Goubau line (Chiba (1977)). Goubau line based LWA is achieved by periodically bending the line (Rudramuni et al. (2018)). An array of V-shaped elements is commonly used to design an endfire antenna (Cumming (1955)). This type of periodic V-shaped conductor will carry a travelling wave (Sengupta (1958)). Hence, the proposed endfire antenna is designed by modifying the Goubau line with periodic inverted V-shaped elements.

The dispersion diagram of the proposed unit cell is analyzed to predict the behavior of its fundamental mode. The proposed inverted V-shaped unit cell is printed on a very low loss Rogers RT Duriod 4003C substrate having thickness 1.52 mm and loss tangent 0.0027. Geometry of the unit cell is shown in Figure 3.12. The dimensions of the unit cell are as follows $a = 5.5$ mm, $\theta = 95^0$ degrees and period $P = 13.5$ mm. The dispersion diagram of the proposed unit cell is simulated using Eigen mode solver of
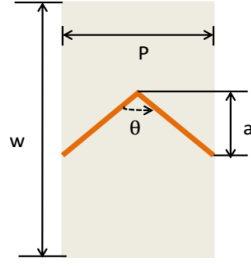
Figure 3.12: Unit cell of the Goubau endfire antenna

CST Microwave studio as shown in Figure 3.13.
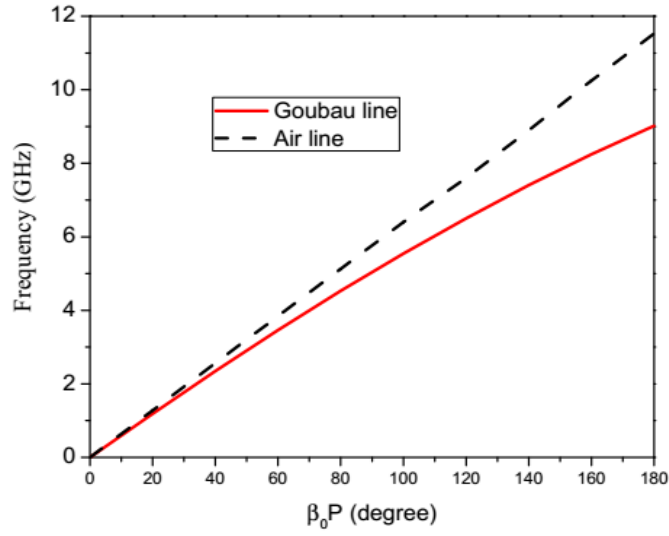
Figure 3.13: Dispersion diagram of the Goubau line endfire antenna.

According to the Hanson-Woodyard criteria for the endfire radiation with increased directivity, optimum guided phase constant should be larger than that in the air (Hansen and Woodyard (1938)) which signifies that dispersion curve should be below the air-line within a short distance (Kandwal et al. (2018)). In the present analysis dominant mode is observed below the airline, and hence it can act as a slow wave structure and it also validates the Hanson-Woodyard condition for endfire radiation with increased directivity. Even though the slow waves are tightly bound to a finite structure still it can produce radiation field (Greiser and Mayes (1964)).

The main beam direction of the travelling wave antenna is given by

$$\theta = arcsin\left(\frac{\beta}{k_0}\right) \qquad (3.4)$$

36

where β is the phase constant and k_0 is the propagation constant in free space. From the dispersion diagram, at frequency 8 GHz, $\beta * P = 160^0$ and $k_0 * P = 130^0$. These values are in degrees but the phase constant (β) is in rad/meter. Hence we converted from degrees to rad/meter. After conversion $\beta = 207$ rad/meter and $k_0 = 168$ rad/meter. Then $(\beta/k_0) = (207/168) = 1.2 \cong$. If we substitute (β/k_0) in equation 3.4 then the main beam direction becomes $\theta_m = 90^0$, which validates that the proposed antenna radiates towards endfire direction.

To verify this, according to the Hanson-Woodyard criteria (Liu et al. (2018)). To obtain maximum directivity in the endfire direction. The phase constant β needs to satisfy the following equation

$$\beta = \left(k_0 + \frac{2.94}{L_A} \right) \tag{3.5}$$

where L_A is the length of the antenna (excluding CPW transition). If we substitute $k_0 = 168$ rad/meter and $L_A = 71.5$ mm are substituted on the above equation (3.5). Then $\beta = 209$ rad/meter and after conversion $\beta * P = 161^0$. It is observed that phase constant from dispersion diagram gives the similar value. This validates our proposed design concept.

3.3.3 Experimental Validation

This section describes the simulation and measurement results of the proposed structure. The simulated and measured reflection coefficient reported in Figure 3.14. It is observed that reflection coefficient is below -10 dB between 7.8-8.3 GHz. By controlling the period P of the unit cell, we can design for any required frequency band.

To better understand this fact, let's take an example, if period becomes $P = 3$ mm, the operating frequency range will be is around 30 GHz and if the period becomes $P = 18$ mm, the operating frequency range will be 3 GHz. So the advantage of the proposed structure is lying on the fact that it can easily be tuned to give endfire radiation for both the microwave and the millimeter wave frequency band.
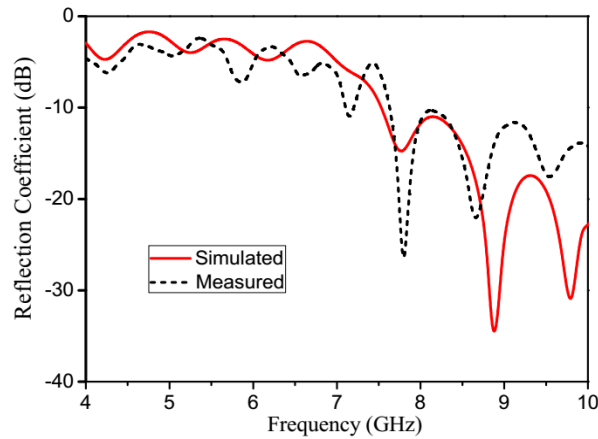
Figure 3.14: Simulated and measured reflection coefficient.
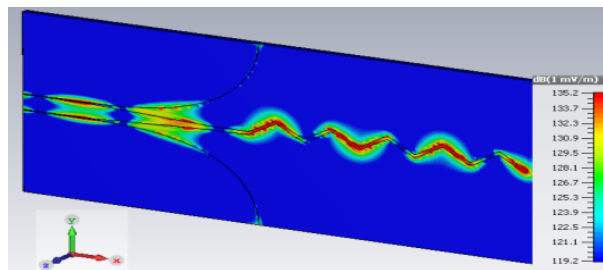
(a)
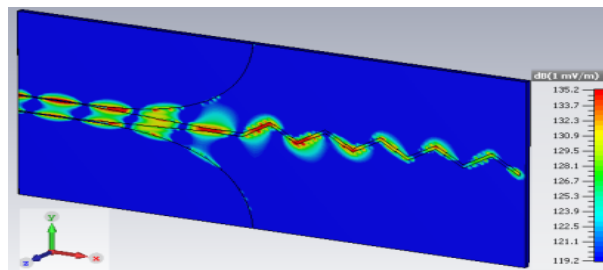
(b)

Figure 3.15: Simulated electric field distribution (a) At 5 GHz (b) At 8 GHz.

Simulated electric field distribution of the entire antenna is reported in Figure 3.15. It is noticed that at 5 GHz most of the energy reaches to the last unit cell, which means fundamental mode is bounded. Hence it is acting as a guided medium at 5 GHz. On the contrary, at 8 GHz, most of the energy radiates into free space and it does not reach the end. Since most of the energy radiates into free space within the five unit cells, if we increase the number of unit cells further, the performance of the antenna remains same with slight increase in the gain as reported in Figure 3.16(a). At 8 GHz, the Gain is 7.2 and 8.1 dB for five and eight unit cells respectively. If we add 3 more unit cells which

means 40.5 mm more to 5 unit cell antenna results in only 1 dB increase in the gain. Hence we have limited number of unit cells to five to make antenna compact.
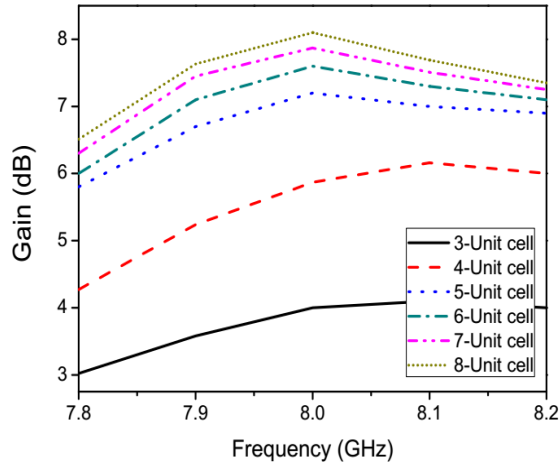
(a)
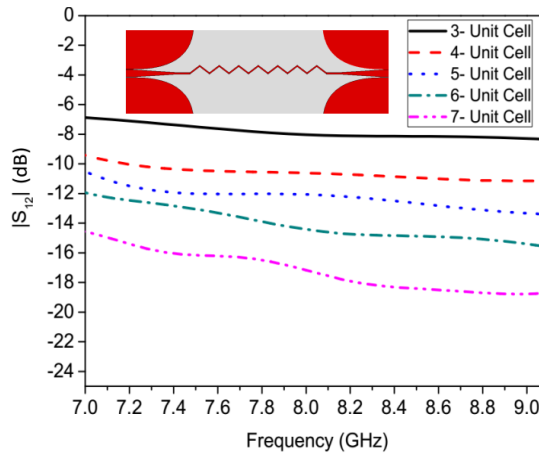
(b)

Figure 3.16: Simulated and measured results (a) Gain variation for different number of unit cells. (b)Transmission coefficient.

To validate this we have simulated transmission coefficient for different number of unit cells is reported in Figure 3.16(b). For five unit cells S_{12} is -11 dB at 8 GHz which means only 20% is transmitting to port 1 to port 2 and remaining 80% energy is radiating to free space. Also the phase constant β is fixed in the equation 3.5 to obtain maximum directivity in the endfire direction. Therefore, the length of the antenna L_A should not be too large. Considering all above factors, the number of unit cells are limited to five.

(a)   (b)   (c)
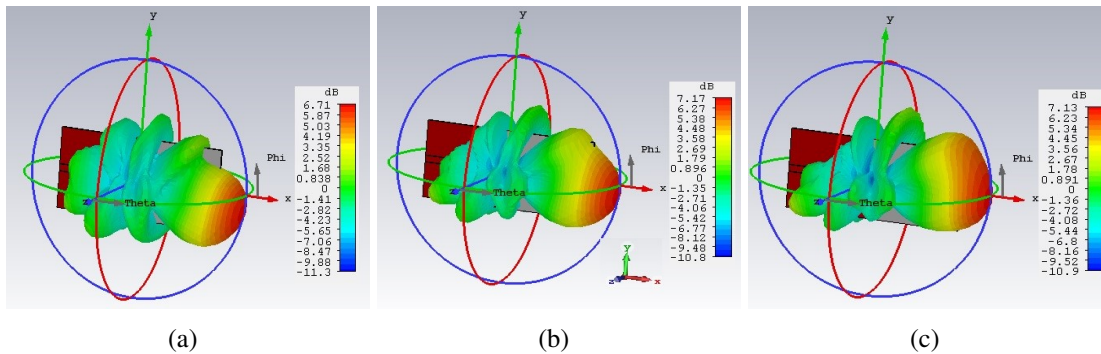
Figure 3.17: Simulated 3D radiation pattern at different frequencies (a)At 7.9 GHz (b)
        At 8 GHz (c) At 8.1 GHz.

Simulated 3D-radiation pattern for proposed endfire antenna is shown in Figure
3.17. At $f = 8$ GHz, antenna radiates towards endfire direction and the maximum gain
over frequency band is around 7.2 dBi.
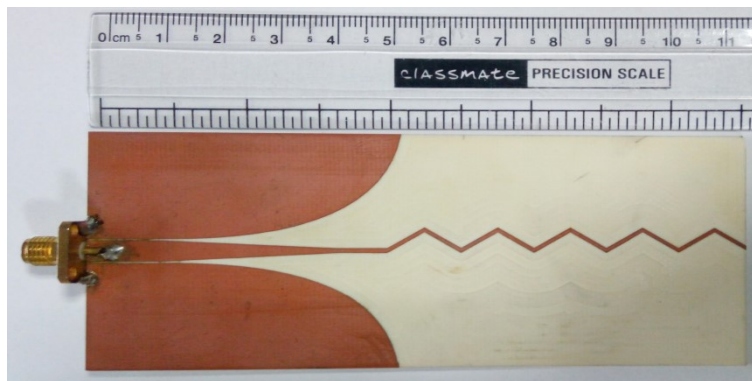
Figure 3.18: Fabricated prototype of the proposed endfire antenna.

Fabricated prototype of Goubau line endfire antenna is reported in Figure 3.18. The
antenna radiation pattern is measured using the in-house Anechoic chamber of the mi-
crowave lab of NIT Surathkal as shown in Figure 3.19.

The simulated and measured radiation patterns at different frequency bands are
shown in Figure 3.20. It can be observed that the antenna is radiating towards the
endfire direction over the entire frequency band. The cross polarization level is below
15 dB over the frequency band.
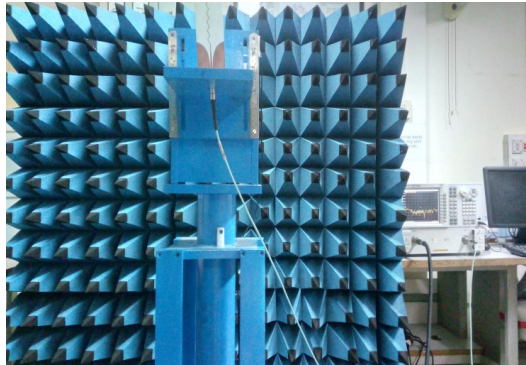
Figure 3.19: Proposed antenna mounted on a chamber in receiving mode for characterization.
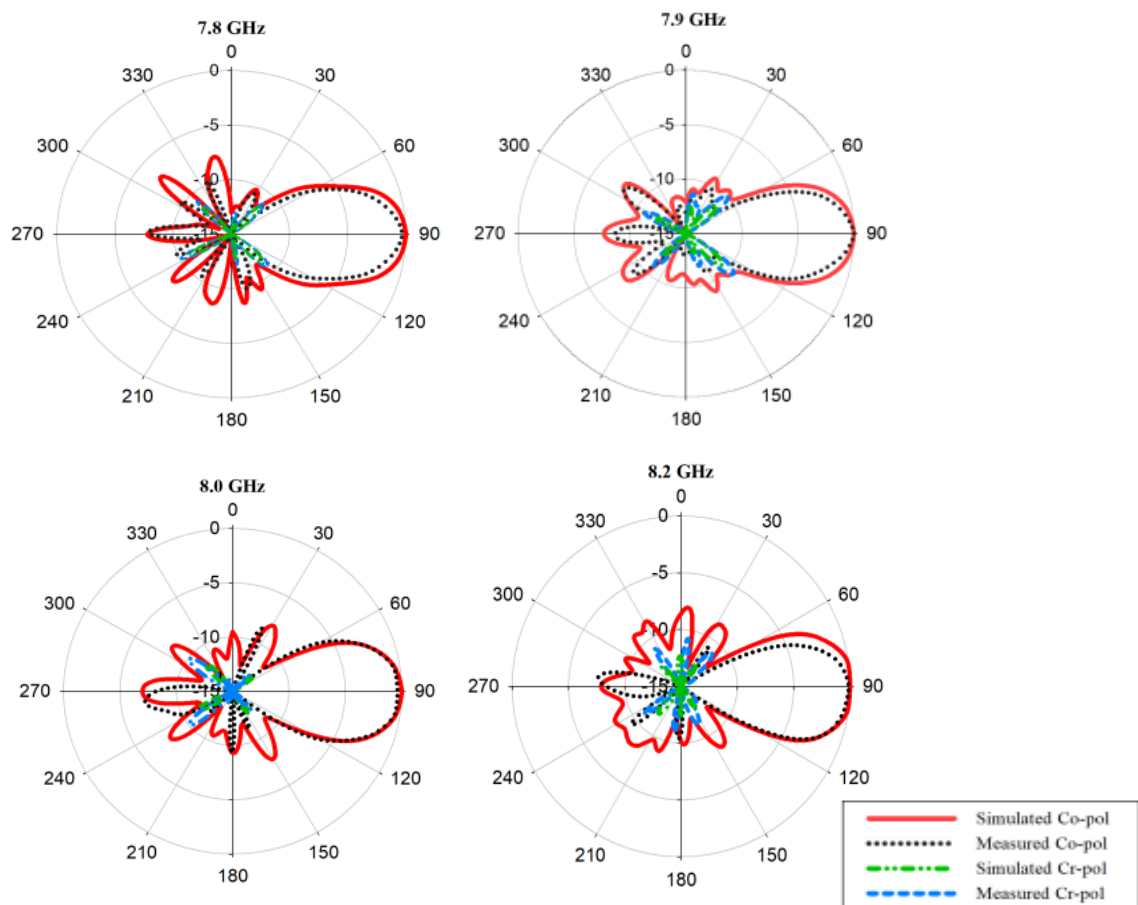
Figure 3.20: Simulated and measured radiation pattern at different frequencies.

Simulated and measured gain is shown in Figure 3.21(a). Average gain is around 7dBi. The simulated efficiency is reported in Figure 3.21(b). The average efficiency is observed to be around 70% over the whole operating band.
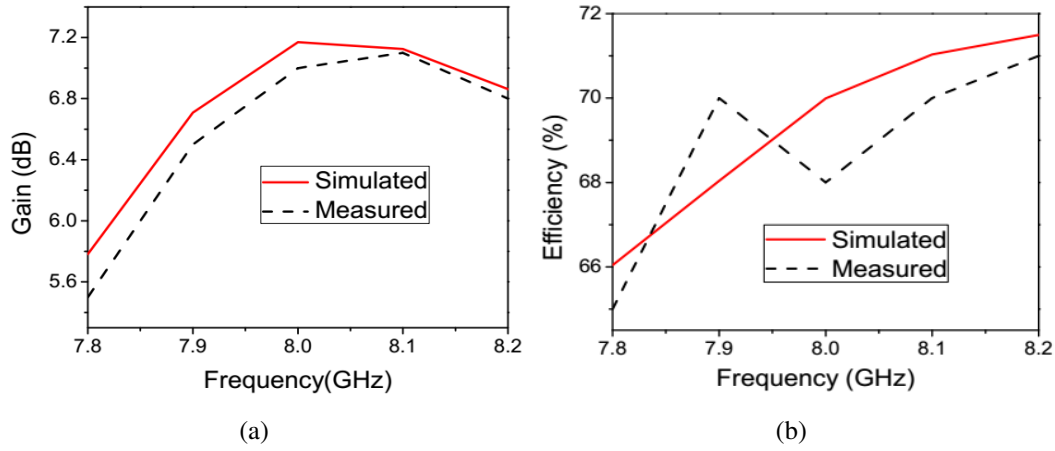
Figure 3.21: Simulated and measured results (a) Variation of gain over frequency band. (b)Variation of efficiency over frequency band.

Table 3.2: Comparison of planar Endfire Antennas

Reference	Methodlogy	Length (λ_0)	Bandwidth (%)	Peak Gain (dBi)	Comments
Liu et al. (2014)	SIW+Slots	14	2.79	13	It uses slots on both the sides of the conductor, it is bulky.
Yin et al. (2017)	SPP+Dipoles	22.6	2.21	7	SPP is used on both the layers.
Liu et al. (2018)	Microstrip+PILA	6	20	11.5	It has MIcrostrip, PILA and Vias, omplex in nature.
Feng et al. (2020)	SPP+Stubs	2.8	36.36	8.65	It is designed on both layers with shorting vias, Complex design.
Proposed work	Goubau Line	3.2	5	7.2	Groundless and easy to design.

To show the advantages of the proposed antenna, we compare it with some of the recent endfire antennas in Table 3.2. All the Goubau line LWAs reported to date only are designed to steer the beam, and very few studies have been dedicated to endfire radiations using single layer devices like in (Feng et al. (2020)) where an SPP-fed dipole like antenna was designed for endfire radiations. However, this endfire antenna used both top and bottom conductor which leads to complex design. Endfire SIW LWA in

(Liu et al. (2014)) is complex due to slots on both the layers of the antenna and its size is more. In (Liu et al. (2018)), PILA and Vias are used to design endfire which are difficult to fabricate. Recently, Composition of SPP and Stubs are used (Feng et al. (2020)) to design endfire antenna. Here, SPP is designed on both layers of the antenna and also shorting vias used. This design is also difficult to fabricate. However, proposed design uses only single conductor with inverted V-Shape to achieve radiation in endfire direction. From the above discussion, we can conclude that the proposed antenna is groundless and compact in size with moderate gain and efficiency when compared above discussed antennas. Goubau line is widely applied THz frequencies due its low losses. Proposed is an outline to design THz endfire antennas using Goubau line.

3.4 Summary

This chapter discusses the Goubau line based antennas for two different functionalities. The first design is a Goubau line LWA that facilitates wide-angle beam scanning upto 155^0. In contrast to the conventional Goubau line LWA with a small scanning angle range, this work employed a periodically bending Goubau line, which not only brings in a periodic perturbation for leaky wave radiation, but also enhances the scanning range due to the increased delay for each line element. The simulation and experimental results show that the proposed LWA provides 90% radiation efficiency and 7–10 dBi radiation gain from backfire to endfire through broadside as frequency changes. The second design discusses a Goubau line based endfire antenna. Endfire radiation is achieved by modifying the Goubau line into inverted periodic arrangement of V-shaped unit cells. Proposed endfire antenna has a single metallic layer with simple configuration which is easy to fabricate and also easy to integrate with other electronics circuits.

CHAPTER 4

DUAL-BAND DUAL-POLARIZED LEAKY WAVE ANTENNA FOR CIRCULAR POLARIZATION FLEXIBLE ANTENNA APPLICATION

4.1 Introduction

In this chapter, a novel dual-band dual-polarized leaky-wave antenna (LWA) with polarization diversity is proposed using HMSIW based technology. HMSIW LWAs are generally single band. In this work, by etching simple spiral type slots on the HMSIW cavity, a novel dual band dual polarized LWA is designed. The proposed antenna resonates at 5.6 and 8.5 GHz. Moreover, the antenna radiates the linearly polarized wave in the lower band and circularly polarized (CP) wave in the higher operating band. Also, in the higher operating band between 8.7 and 9.3 GHz, the proposed overall antenna exhibits both right hand circular polarization as well as the left hand circular polarization in the near main beam direction. The -10 dB impedance bandwidth of the proposed antenna at the lower and the higher operating bands are 27% (4.86 to 6.4 GHz) and 25% (7.4 to 9.6 GHz), respectively. In the higher band, the 3 dB axial ratio bandwidth of 6.6% (8.7 to 9.3 GHz) is achieved. The main beam of the antenna can be steered from 19^0 to 69^0 in the forward direction in the lower operating band. In the higher operating band, the antenna can steer the CP beam between In the first section, the unit cell is designed by etching spiral slots on HMSIW and its dispersion diagram is analysed. The LWA is configured based on the unit cell, Its Bloch impedance and leakage constant is discussed. A four port LWA is designed which produces two bands but in the higher operating band between 8.7 GHz and 9.3 GHz the proposed four port overall LWA antenna exhibits both RHCP as well as LHCP waves. The antenna performance

parameters including the S-parameters, gain and efficiency values are experimentally verified. Good agreement is obtained between simulated and measured results.

4.2 Antenna Geometry

The geometry of the overall LWA along with its basic unit cell and the fabricated prototype is shown in Figure 4.1. It can be seen from Figure 4.1 that the antenna is a four-port passive device where the left side two ports (port 1 and port 3) are used for feeding purposes while the other two ports (port 2 and port 4) are terminated with a matched load. When the antenna is fed at port 1, LP wave generates at the lower band, whereas a LHCP wave generates at the upper band. But when it is fed at port 3, a RHCP wave generates at the upper band along with LP wave in the lower band.
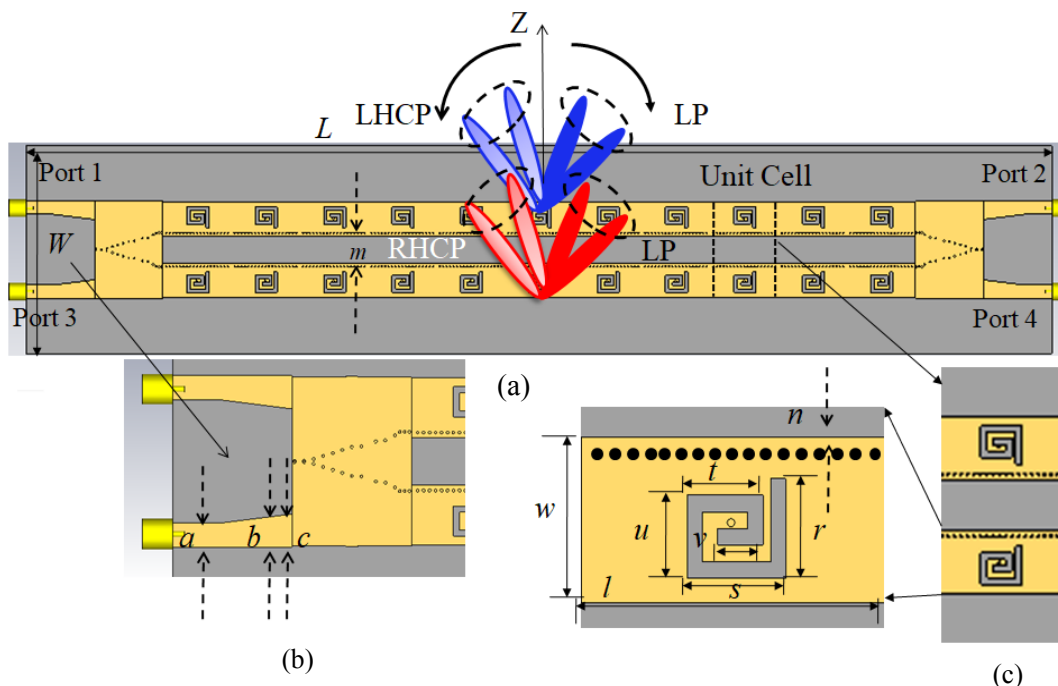
Figure 4.1: Configuration of the proposed LWA antenna (a) Complete LWA structure. (b) Transition. (c) Unit cell.

The optimized dimensions of the proposed overall-antenna are reported in Table 4.1. The unit cell of this antenna is printed on a Rogers substrate having permittivity of 2.2,

loss tangent of 0.001 and the thickness of 1.57 mm and is shown in Figure 4.1(c). The spiral slot is etched at 1 mm distant from the series SIW-vias.

Table 4.1: Optimized dimensions of the proposed LWA

Parameters	L	W	m	a	b	c	n	d	w	l	r	s	t	u	v	g
Value (mm)	292	60	8	4	5.2	14	0.5	0.5	10	20	6	6.5	5	5	3	0.5

4.3   Dispersion Analysis and Operating Principle

The dispersion diagram must be started with the unit cell analysis, where the dispersion diagram and the Bloch mode impedance of the unit cell should be investigated in details to understand the working principle of the LWA. Dispersion Analysis can also be done using the S-parameter results obtained from the unit cell analysis in CST MWS either by using the Eigen mode analysis or by driven mode analysis. Eigen mode analysis is chosen to analyze the unit cell since this method is more accurate than the latter.
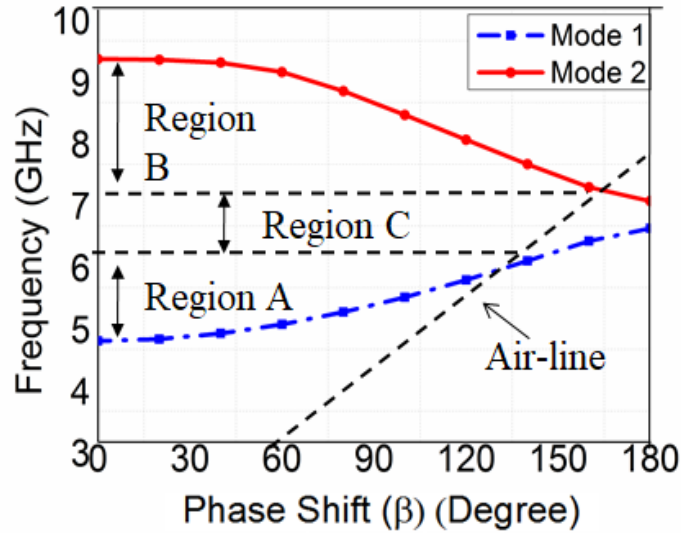
Figure 4.2: Simulated dispersion diagram Dispersion diagram of the unit cell.

Figure 4.2 shows the required dispersion diagram of the proposed spiral slot loaded unit cell. The light line (shown in black dotted line in Figure 4.2) is obtained by plotting the equation $k_0 = \omega\sqrt{\mu_0\epsilon_0)}$ where k_0 is the free space wave number. When $(\beta_0/k_0) <$

1, the electromagnetic wave shows the leaky wave property where β is the propagation constant. From the dispersion diagram, it can be shown that two distinguished leaky wave region exists. When $\beta > 0$ (Region A) the unit cell structure shows right handed (RH) properties (between 4.9 GHz and 6.4 GHz) and the antenna radiates in the forward direction. When $\beta < 0$ (Region B), the structure exhibits Left handed (LH) properties (between 7.4 GHz and 9.6 GHz) and the antenna radiations occur in the backward direction. From the dispersion diagram it can also be seen that in between the RH region and LH region there exists a region (Region C) which is called the non-radiating region or band-gap region. The non-radiating region exists between 6.4 GHz and 7.5 GHz.

For an infinitely long LWA, the direction of the main beam depends on this dispersive behavior of the unit cell and it is a function of frequency as given by

$$\theta(f) = arcsin\left(\frac{\beta(f)}{k_0(f)}\right) \tag{4.1}$$

Where $\theta(f)$ represents the angle of the beam scanning measured from the boresight. The boresight direction in the present case is in the positive Z direction perpendicular from the plane of the antenna substrate. It is depicted in Figure 4.1. As the value of the $\frac{\beta}{k_0}$ changes with the frequency so the scanning angle of the main beam also changes accordingly. But in a finite length LWA structure this scanning angle depends upon the number unit cell that is merged to form the overall antenna. In other words, if the LWA is sufficiently long, the equation reported in 4.1 can predict the beam direction more accurately.

The series SIW vias on one side of the unit cell gives the shunt inductance which alone is capable of giving the lower RH mode. On the other hand the etched spiral slot on the top of the metallic conductor and the central vias connected between the top metal layer and ground below play a crucial role to exploit the higher order LH leaky wave mode. Precisely, the combination of the etched spiral slot, the central vias along with the SIW vias form the required distributed shunt and series inductances and capacitances to form the overall dispersive response of the unit cell (shown in Figure

4.2). The position of the spiral slots and its dimensions have been properly optimized so that the RH mode can start from a lower frequency and can compensate the extra reactance offered by the central vias of the unit cell. For designing a full-length LWA, we should consider a single period (l) to combine the unit cell together. In general for a traveling slot array, the spacing of the etched slot should be less than the half of guide wavelength (λ_g) in order to maintain the homogeneity and also, a matched load must be placed at the second end of the structure. In these situations, a leaky-wave structure can be realized. Periodicity of the unit cell and can influence the dispersive property of the CRLH unit cell. By controlling these dimensions of the unit cell, the slope of the air line in the dispersion diagram of the unit cell (Figure 4.2) can be changed and so the fast/slow-wave regions also can be modified.
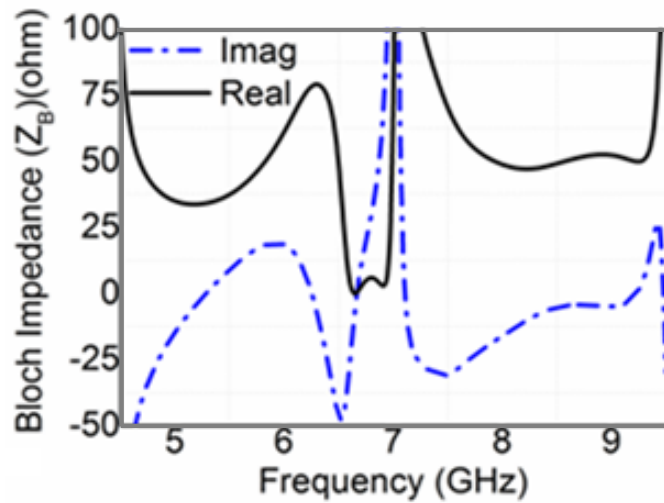
Figure 4.3: Bloch Impedance over the frequency band.

For the impedance matching of the full length LWA, Bloch wave analysis is performed and it is shown in the Figure 4.3. Bloch Impedance can either be calculated by using the s-parameter relation or by the ABCD parameter of the unit cell as shown in equations 4.2 and 4.4 or by using the driven mode simulation in CST MWS. The Bloch wave analysis is performed using CST MWS considering the N number of unit cells. The Bloch impedance after neglecting the radiation resistance can be expressed as follows

$$Z_B = \pm \frac{-2jZ_0 S_{21} sin(\beta l)}{(1 - S_{11})(1 - S_{22}) - S_{21}S_{12}} \tag{4.2}$$

$$Z_B = \pm \frac{-(A - D) \pm \sqrt{(A + D)^2 - 4}}{2C} \tag{4.3}$$

From the Bloch wave analysis shown in Figure 4.3, it can be seen that in the RH region the average value of the real part of the Bloch impedance is 40Ω which could be easily matched by the microstrip based taper line, whereas in the LH region the average value of the real part of the Bloch impedance is around 45Ω. In the RH region the extra inductance is compensated by the capacitance provided by the series spiral shaped radiating slot and the position of the first unit cell and thereby achieving a good reactance matching over the entire RH band. In the LH region the reactance of the Bloch impedance is observed to be around zero which indicates proper impedance matching over both the frequency region of the antenna.

4.4 Results of the proposed dual-band LWA

The complete antenna is simulated using CST MWS software. The simulated and measured reflection and transmission coefficient magnitudes are plotted in Figure 4.4(a) when the antenna is fed at its port 1. It can be seen that they are in well agreement with each other. There are some differences which can be observed, in between the two may arise due to the imperfections in the fabrication or may be because of the change in the material properties. For our present analysis this difference is acceptable and can be tolerated.

It is observed that antenna impedance bandwidth at the lower band is 273 MHz (from 4.86 GHz to 6.4 GHz) and at the upper band is 258 MHz (from 7.4 GHz to 9.6 GHz). In the lower band of the RH region i.e. between 4.9 GHz and 5.5 GHz, the antenna transmission co-efficient is very low and also the reflection coefficient is also observed very low, which suggests that most of the power fed is radiating without reach-
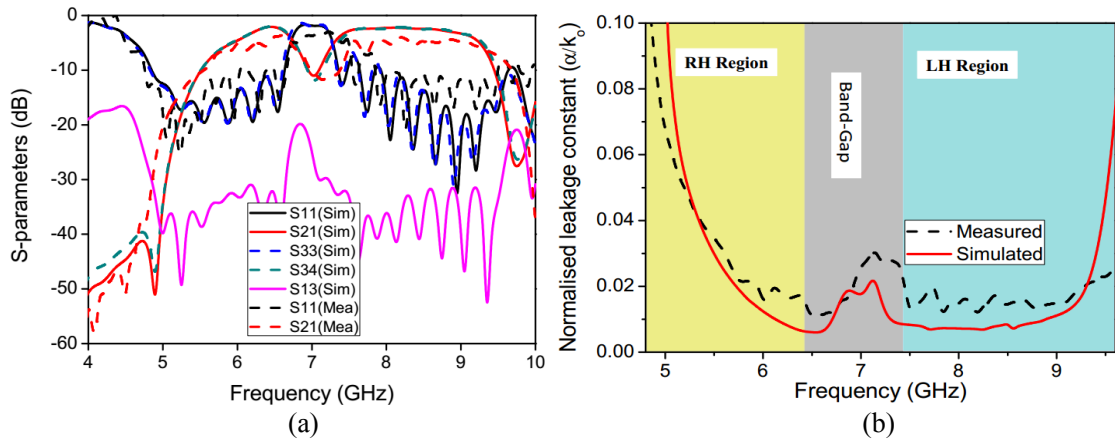
Figure 4.4: Simulated and measured results (a) S-parameters of the proposed antenna. (b) Normalized leakage constant antenna [For simplicity only port-1 results are shown.]

ing to the load located at the other end. When the frequency is further increased and reaches in the non-radiating region, the transmission coefficient is low and reflection is 0 dB indicating that no possible radiation from this zone. In the LH band extending between 7.5 GHz and 9.5 GHz, the reflection coefficient is greater than -10 dB and the transmission coefficient is around -5 dB suggesting that LH leaky wave radiation is possible. From Figure 4.4 (a) it can also be observed that the isolation between port 1 and 3 is very high since they are separated by series SIW vias (Perfect Electric Conductor Wall). Figure 4.4(b) depicts the normalized attenuation constant of the overall antenna, when the antenna is fed at port 1. From this It can be inferred that at the lower end of the RH band and at the higher end of the LH band the leakage is high enough indicating more radiation. The discrepancy between the simulated and the measured normalized attenuation constant is mainly because of the small disagreement between the simulated and measured scattering parameters. Generally, as the frequency increases leakage rate decreases indicating that most of the power radiates from the furthest end of the source port and closure end of the load port, thereby increasing the directivity and gain.

Figure 4.5 shows the simulated normalized far-field radiation patterns at both the RH and the LH region in the X-Z plane when the antenna is fed at port 1. It is observed that antenna scans in the two different frequency bands showing the bidirectional radiation pattern behavior. Fig. 4.6 shows the simulated and the measured normalized radiation
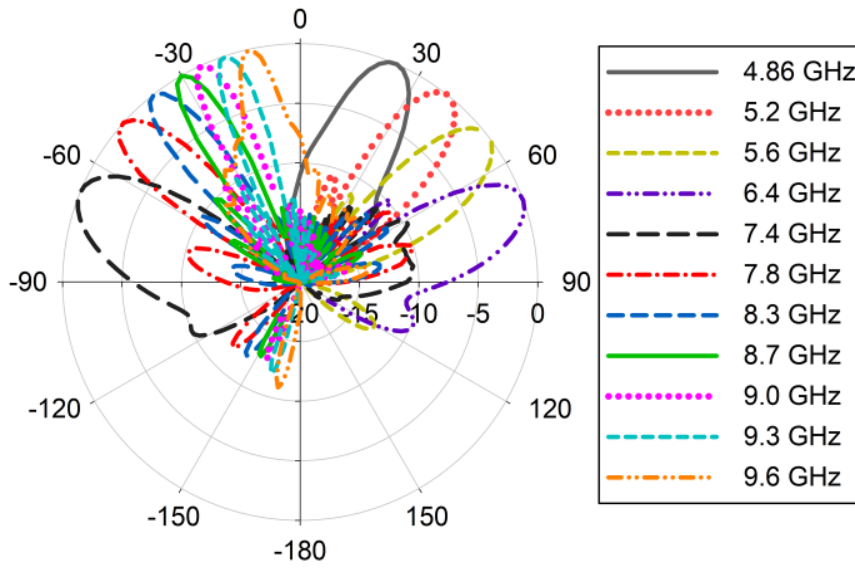
Figure 4.5: Simulated radiation pattern at Port 1.

pattern in the RH region (Lower Band). A good agreement is observed between its simulated and measured results. Also it can be seen that the antenna scans in the forward direction between 19^0 and 69^0 and radiates LP wave. The direction of the forward main beam-scanning can be verified using equation 4.1. The radiation which is closed to the boresight happens at 4.89 GHz and the angle is found to be 20^0. As the frequency increases, the angle also increases and at 6.4 GHz the antenna points away from the boresight at an angle of 69^0. It can be noticed from Figure 4.6 that the cross-pol level is below -10 dB in each of its forward beam scanning points.

Figure 4.7(a) further depicts the radiation pattern between 8.5 GHz and 9.5 GHz at port 1 where axial ratio is obtained less than 6 dB. The antenna exhibits the perfect CP behavior between 8.7 GHz and 9.3 GHz. One of the main feature of the proposed LWA is that the CP behavior in the backward direction while maintaining a good LP wave in the lower band thereby achieving a dual-polarized behavior in the upper half of the radiation space. Good quality of the CP radiation is measured using the axial ratio (AR) of below 3 dB. Figure 4.7(b) depicts the axial ratio variation over the main beam direction in the LH band. It can be observed that the simulated and the measured results are consistent with each other and the CP scan region exists between -17^0 and -32^0. The antenna produces LHCP radiation in this band. The ratio of the orthogonally

52
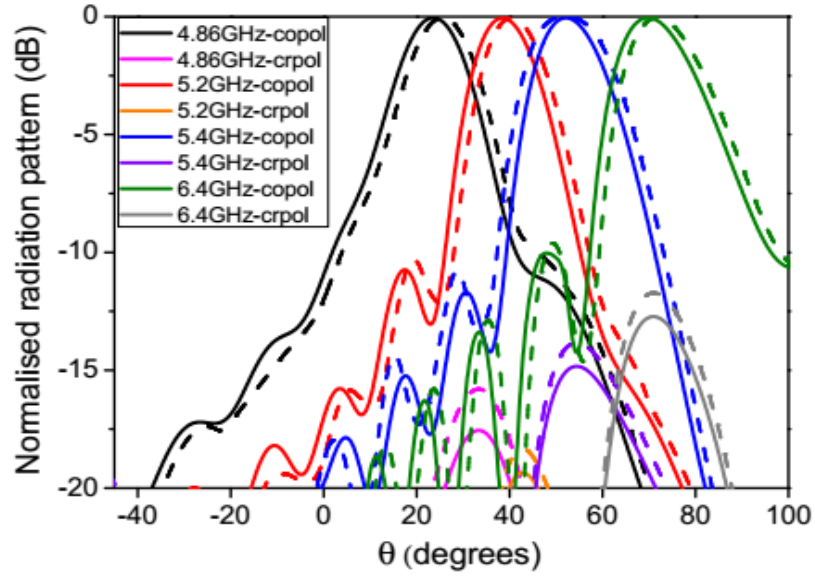
Figure 4.6: Normalized radiation pattern of lower band at port 1 (The solid lines denote simulated results while the dotted lines denotes the measured results).

polarized E field components from the spiral slots constructing the CP radiation is low and below 3 dB to provide perfect CP radiation between 8.7 GHz ad 9.3 GHz. As the angle moves from the backfire to the boresight, the axial ratio becomes more than 3 dB and the CP wave converts into an elliptically polarized wave which is in well agreement with the results reported in (Liu et al. (2012b)). It is noted that considering the 6 dB AR criteria, the backward scan region exists between -16^0 and -40^0.

The above analysis proves that by etching a spiral shaped slot on the top of Microstrip based SIW array, a single radiator based dual-polarized LWA antenna design is possible. The length, width and the distance between SIW-via array and the center of the spiral slot are the very crucial parameter to tune the performance of the CP radiation and the axial ratio bandwidth.

Similarly, the simulated radiation pattern of the LWA in the X-Z plane is reported in Figure 4.8 when it is fed at its port 3 and. It is observed that antenna scans in the two different frequency bands like the case when it was fed at port 1. In the lower frequency band, antenna scans linearly polarized wave in the forward direction which ranges between 19^0 and 69^0. But, it can be noticed that in the upper frequency band (LH band), the antenna scans RHCP wave in the backward direction between 8.7 GHz to 9.3
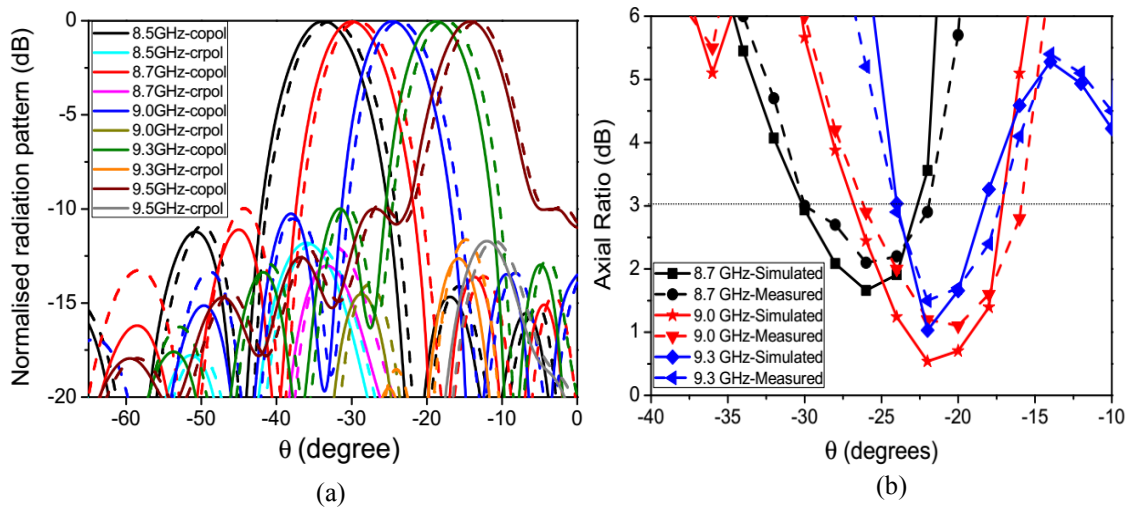
Figure 4.7: Simulated and measures results (a) Normalised radiation pattern of upper band at port 1 (within AR 6 dB) (b) Axial ratio vs. radiation angle when the antenna is fed at port 1. (The solid lines denote simulated results while the dotted lines denotes the measured results).
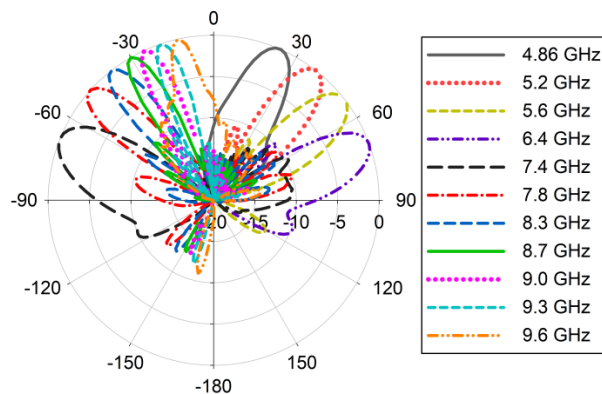
Figure 4.8: Simulated radiation pattern at Port 3.

GHz which was different than the case when it was fed at port 1. Figure 4.9(a) and 4.9(b) represent the backward RHCP beam scanning (from backfire to the boresight) and the axial ratio variation over the angular region. In the LH band also, a good agreement between the simulated and measured results is observed. A good quality of RHCP radiation is also observed between 8.7 GHz and 9.3 GHz. From the results reported in Figure 4.9, it can be seen that the cross-pol component is below -10 dB in the overall CP scanning range and around 30% of the total backward scanning region contributes to the useful CP radiations.

54
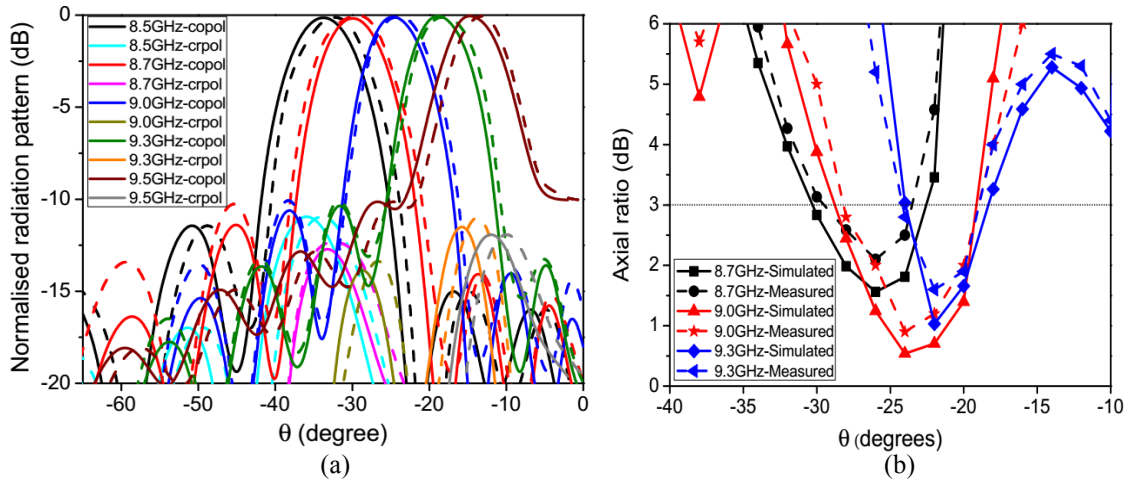
Figure 4.9: Simulated and measures results (a) Normalised radiation pattern of upper band at port 3 (within AR 6 dB) (b) Axial ratio vs. radiation angle when the antenna is fed at port 3. (The solid lines denote simulated results while the dotted lines denotes the measured results).
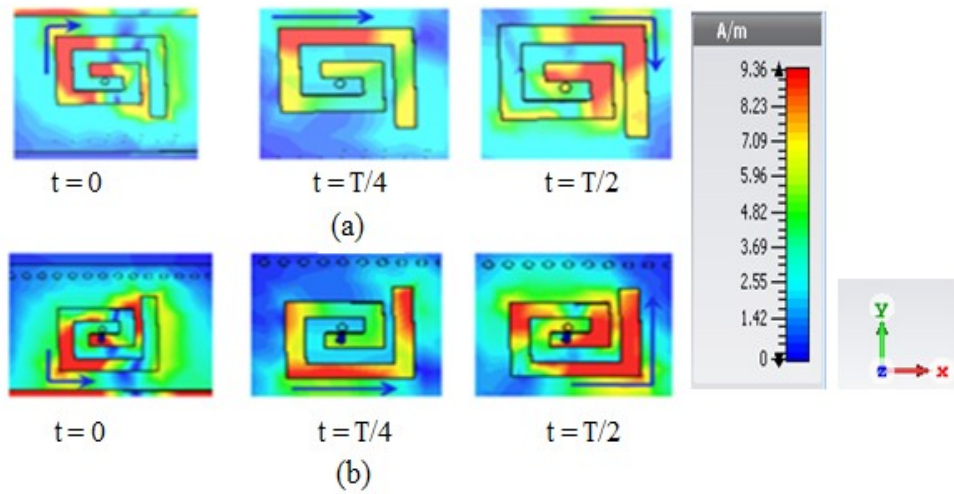
Figure 4.10: Simulated surface current distribution (a) At port 1 (LHCP configuration). (b) At port 2 (RHCP configuration).

To get a better understanding about the sense of the CP behavior, the surface current distribution at 9 GHz inside both the spiral shaped slot is investigated in Figure 4.10 (a) and (b) when it is fed at port 1 and port 3 respectively. The spiral shaped slot produces two orthogonally polarized electric field components (E_θ and E_ϕ) in the horizontal and the vertical arm of the slots. The associated magnetic field with it when making a cross product with its outward normal plane produces the surface current on the slot.

Firstly, it can be seen that the maximum current intensity exists in the spiral shaped etched slots indicating the fact that the spiral slots leak the radiation to generate the CP radiation which is a class of a travelling type slot array in general. This behavior is also in consistent with the work reported in (Liu et al. (2012b)). It can also be observed (arrow direction) from Fig. 4.10 (a) that when the etched spiral slot is made in the clockwise direction (top unit cells of the proposed LWA), the induced surface current also moves along the spiral slot at different time instants and when it is seen from the far-field region a clockwise movement of the CP wave is observed, thereby achieving a LHCP radiation. So, this analysis proves that when the antenna is fed at port 1, it can generate the LHCP radiation. The observed surface current distribution (at 9 GHz), when the antenna is fed at port 3, is reported in Figure 4.10(b). From this figure it can be noted that, since the etched spiral shaped slots are in the anti-clock wise direction, the surface current distributions at different instant of time instant form an anti-clockwise movement when looking toward it from its far-field thereby generating a RHCP wave.
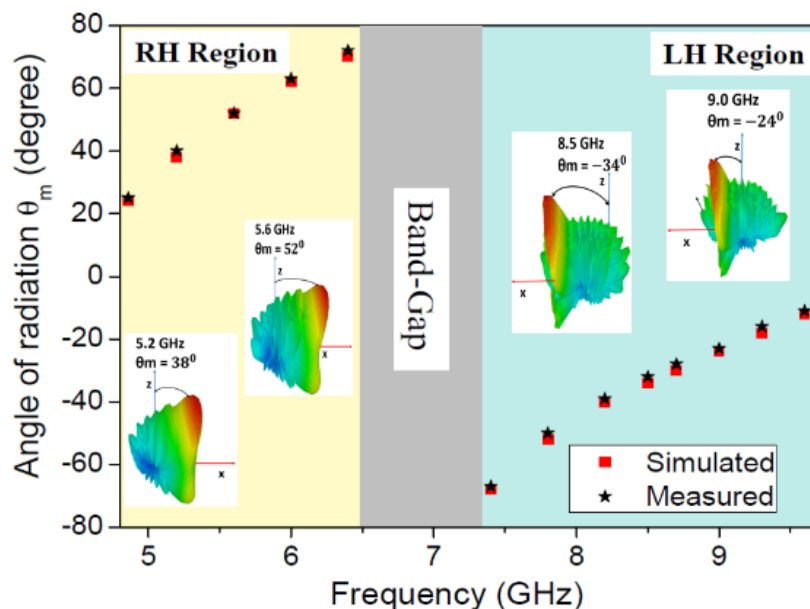
Figure 4.11: Variation of angle of radiation with change in frequency (3D patterns also included for different frequencies.)

The angle of radiation with change in frequency is estimated using equation 4.3. The required phase constant (β) for equation 4.3 is obtained from the dispersion relation as reported in Figure 4.2. Simulated and measured variation of angle of radiation

56

with change in frequency is reported in Figure 4.10. 3D radiation pattern at different frequency is also inset in the Figure 4.10 to get a better understanding of angle of radiation. It can be observed that, RH band scans in the forward direction and LH band scans in the backward direction.
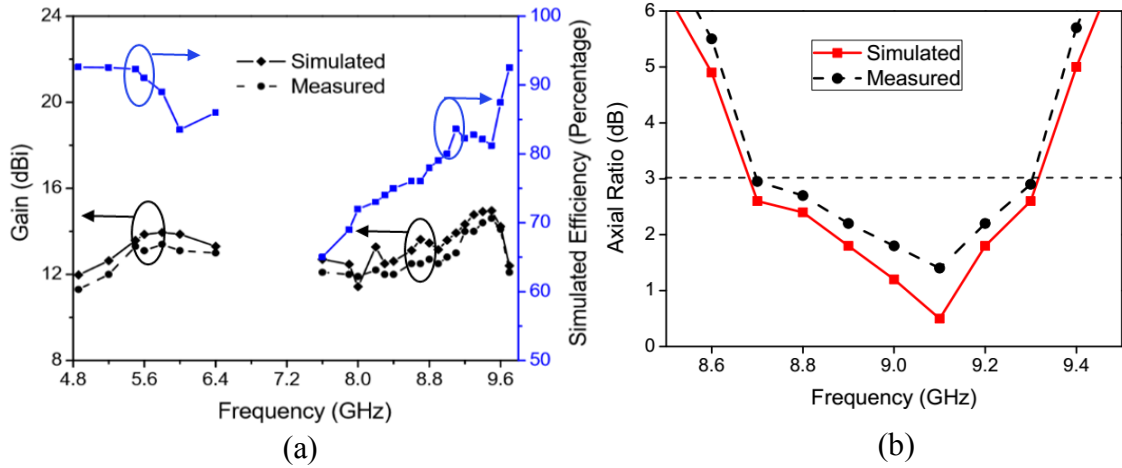
Figure 4.12: (a) Gain and Efficiency variation over Frequency (b) Axial Ratio vs. Frequency

Figure 4.12(a) shows the realized gain in the X-Z plane and simulated radiation efficiency variation over the RH and LH bands. From this figure, it can be observed that in the RH band the peak realized gain is obtained around 13.3 dBi, whereas in the LH band, peak gain found around 14 dBi. Also, it can be noticed that as the frequency increases the gain also increases toward the upper portion of the LH and RH band. The peak gain at the RH band is low as compared to the peak gain in the LH band as expected. From the simulated efficiency plot, it can be seen that at the RH band the efficiency variation is between 85% and 93% from 4.86 to 6.4 GHz, but at the LH band, the simulated efficiency is observed between 76% and 83% from 8.7 to 9.3 GHz (3-dB axial ratio bandwidth). The directivity and the efficiency of the antenna can be improved by combining more number of unit cells while forming the overall antenna. Fig 4.12(b) shows the simulated and measured axial ratio over the frequency band. It can be seen that between 8.7 and 9.3 GHz, the axial ratio is below 3 dB. A slight variation between the simulated and measurement result is observed which may be due to the imperfections while taking the measurement. Finally, the performance

57

Table 4.2: Comparison of all dual-band LWAs

Ref.	Fabrication Technology	Geometry LP/CP	Frequency (GHz) (Scan BW)	Scan Angle (degree)	3-dB CPBW	Peak Gain (dBi)	CP-Scan range (degree)	Polarization
Pourghorban Saghati et al. (2014)	HMSIW +CRLH $(6.25\lambda_0)$	Ramp shaped ID	7.4 -13.5	-70 to +70	7.4-13.5	14.56	-70 to +70	Circular
Liu et al. (2012b)	SIW+RH $(10.37\lambda_0)$	H Shaped 3-Slots	9.9-11.7	+8 to +75	10.3-10.5	12.5	-68 to +60	Circular
Liu et al. (2012a)	SIW+Slots $(10.4\lambda_0)$	Uniform slots	10.2-12	-15 to +70	-	14	-	Linear
Simorangkir and Lee (2015)	Microstrip +MNG $(5\lambda_0)$	Lumped Capacitor Loaded Tx Line	3.7-5.5 6.7-10	-43 to +73 -80 to +83	-	10, 15	-	Linear, Linear
Haghighi et al. (2015)	SIW +CRLH $(9\lambda_0)$	A pair of Meandered slots	7.1-10.75 12.6-13.4 15.1-21.75	-78 to +78 +22 to +54 -40 to +20	-	16, 16, 18	-	Linear, Linear, Linear
Karmokar and Esselle (2015)	Half-Microstrip +slots $(4.2\lambda_0)$	U Shaped slot	5.24–6.37 7.9-9.02	+30 to +65 -46 to -10	-	14, 15	-	Linear, Linear
Li and Wang (2018)	Microstrip +SIW $(7\lambda_0)$	Uniform slots	5.3-8.4 35-41.5	-64 to 0 +11 to 70	-	15	-	Linear, Linear
Chen et al. (2009)	SIW+RH $(13.3\lambda_0)$	45^0 inclined two paired of slots	15.8-16.2	-2 to +2	Very limited	18.98	-	Circular
Suntives and Hum (2012)	HMSIW +CRLH $(3.25\lambda_0)$	Transverse ID slot + open wall of HMSIW	9.9-11.7	+8 to +75	Very limited	9.8	-31 to +35	Circular
[Proposed Work]	HMSIW + CRLH $(6\lambda_0)$	Spiral shaped slot	4.86–6.4 7.4-9.6	19 to 69 - 69 to -13	8.7-9.3	13.5, 15.5	-17 to -32	Linear, Circular

of the antenna is compared in Table 4.2 with some of the already existing literature. It is observed from the table, the works Pourghorban Saghati et al. (2014), Liu et al. (2012b) and Liu et al. (2012a) are operated only in single band either linear or circularly polarized beam. Later, dual-band and triband LWAs (Simorangkir and Lee (2015), Haghighi et al. (2015), Karmokar and Esselle (2015)) are developed. But unfortunately, all of these antennas generally operate in LP mode. The proposed LWAs produces two-bands with different polarization in each band. The first band produces LP beam and second band produces CP beam. Also, in the higher operating band between 8.7 and

9.3 GHz, the proposed overall antenna exhibits both right hand circular polarization as well as the left hand circular polarization in the near main beam direction. The main beam of the antenna can be steered from 19^0 to 69^0 in the forward direction in the lower operating band.

The proposed antenna can be used for both the LHCP and RHCP polarization-flexible operations along with the LP polarization in the lower band with, scan in both the forward and backward direction and produce good realized gain and radiation efficiency over both the operating bands. Proposed LWA can be used for multifunctional applications in radar where both CP and LP scanning is required. These attractive features made these antennas suitable for modern wireless applications such as automotive radar system applications and point to point satellite communications.

4.5   Summary

In this chapter, By etching a combination of spiral-shaped slots on the HMSIW cavity, a novel dual-band dual-polarized LWA is designed. The proposed antenna resonates at 5.6 and 8.5 GHz. Moreover, the antenna radiates the LP wave in the lower band and CP wave in the upper operating band. Also, in the upper operating band between 8.7 and 9.3 GHz, the overall antenna exhibits both RHCP as well as LHCP in the near main beam direction. The main beam of the antenna can be steered from 19^0 to 69^0 in the forward direction (RH band) in the lower operating bandwidth. In the higher operating band, the antenna can steer the CP beam between -17^0 and -32^0. In both the lower band, the peak realized gain is observed around 13.3 dBi whereas in the higher band, the realized peak gain is observed around 14 dBi.

CHAPTER 5

STUDY OF ASYMMETRY IN HMSIW LEAKY WAVE ANTENNA FOR MULTIFUNCTIONAL APPLICATIONS

5.1   Introduction

In this chapter, two configurations of novel dual-band HMSIW LWAs based on the unit cell asymmetry are presented. Dual-beam LWAs are able to detect multiple targets and hence they play important roles in automotive radar and vehicular communication. However, existing dual-beam LWAs were limited to single linear polarization. Hence, two different configurations are designed to achieve dual polarization with simultaneous beam scanning. The first proposed antenna radiates LP waves in the lower band and CP waves in the upper band when the unit cells are cascaded sequentially. The second antenna, where the sidewall via of the HMSIW unit cells are connected alternatingly, provides simultaneous dual-beams with different polarization in the upper operational band in addition to the LP beam in the lower operational band. The unit cells of two antennas are analysed in terms of their dispersion behaviors. Antennas configured and their operating principles are discussed. Finally, both the LWAs are fabricated and the performance parameters are experimentally verified.

5.2   Unit cell design and Dispersion Analysis

The basic unit cell of the proposed LWA is reported in Figure 5.1(a). This unit cell is designed on the substrate Rogers 5880, having permittivity 2.2, loss tangent ($\tan \delta$) 0.0009 and height of 1.6 mm. The unit cell consists of SIW vias on one side of the

patch, two horizontal stubs in the middle of the vertical edges of the patch, and a via located at the center of the patch, as shown in Figure 5.1(a).
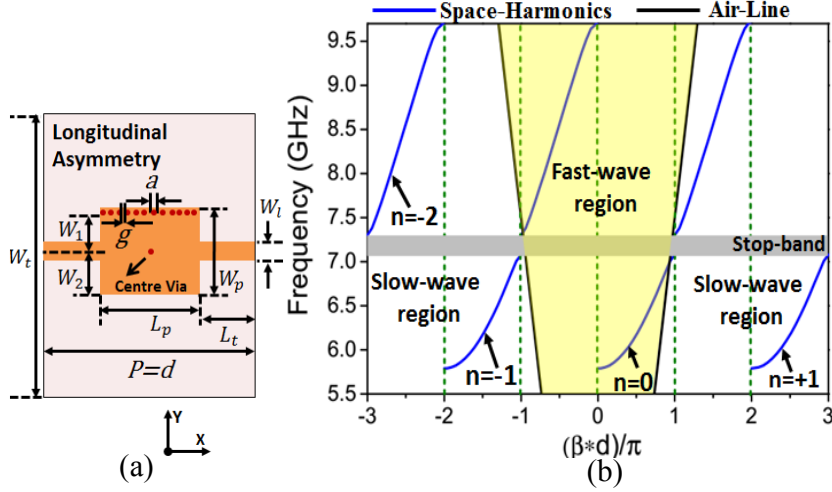
Figure 5.1: (a) Unit cell when P=d. (b) Dispersion diagram analysis when P=d

Table 5.1: Optimized dimensions of the proposed LWA

Parameters	W_t	W_l	W_p	W_1	W_2	L_t	g	a	L_p	D
Value (mm)	80	2	9.5	4.1	4.75	5	0.3	0.5	10	20

The dimensions of the unit cell are reported in Table 5.1 To design the LWA, the dispersion curve of the proposed unit cell should be investigated first. The dispersion characteristic of the unit cell is extracted using the Eigenmode Solver of CST MWS. In general, the shunt capacitances and the series inductances are distributed along with the geometry for a conventional Right Hand (RH) transmission line. By introducing the sidewall vias and step width on the top patch of the unit cell, the distributed capacitances and the inductances have been modified. Their combined effect can be observed in the dispersion behavior in Fig. 5.1(b). The solid black line in Figure 5.1(b) is the air line, i.e., $K_0 = w\sqrt{\mu_0\epsilon_0}$ where k_0 is the free space wavenumber. The electromagnetic wave becomes fast wave when $|\beta/k_0| \leq 1$ where β is the phase constant. Also, when $\beta > 0$, the structure exhibits RH properties and radiates in the forward direction, and when $\beta < 0$, the structure shows Left Hand (LH) properties and it radiates in the backward direction. From this, it can be inferred that, between 5.8 GHz and 7.0 GHz, the unit cell shows RH behavior and radiates in the forward direction. The first higher-order space

harmonic ($n = -1$) occurs between 7.3 GHz and 9.7 GHz, exhibiting LH properties and radiating in the backward direction. There is also a non-radiating region between 7.0 GHz and 7.3 GHz, which does not contribute to any radiation. It is known as the open stop-band or band-gap region. This unit cell configuration reported in Figure 5.1(a) has been arranged periodically along the X-direction to produce dual-band dual-polarized radiation beams. It can be noted from the unit cell geometry that this unit cell possesses a longitudinal asymmetry with respect to the wave propagation direction.
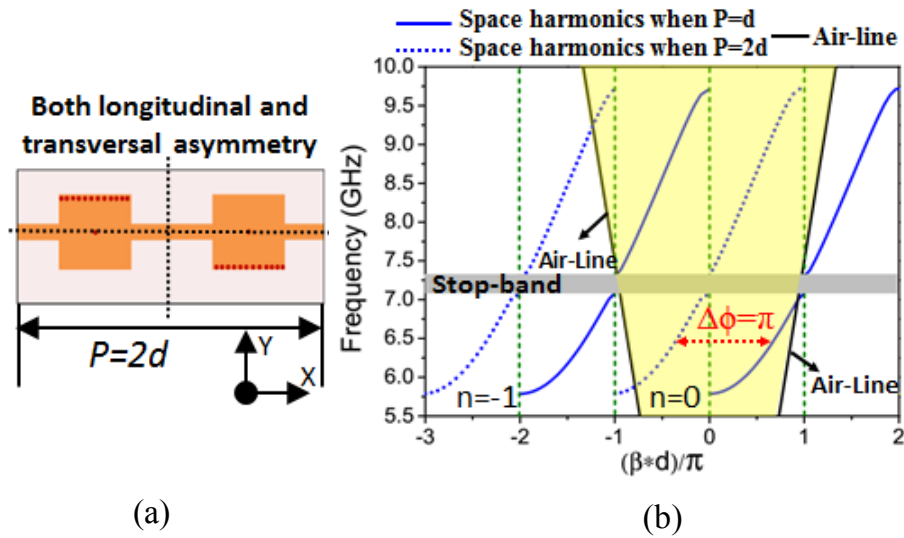
Figure 5.2: (a) Unit-cell when P=2d. (b) Shifting of modes due to change in modulation period from d to 2d.

We subsequently modify the proposed unit cell geometry reported in Figure 5.1(a) to form a new unit cell in Figure 5.2(a). The fundamental difference between them lies in the placement of the sidewall short-circuited vias. The unit cell reported in Figure 5.2(a) consists of alternatingly placed sidewall vias between its adjacent unit cells, thereby making the structure both transversely and longitudinal asymmetric. The position of the short-circuits will alter the mode propagation behavior inside the structure. Hence the dispersion characteristics should be investigated separately. It can be noted that the alternatingly loaded short-circuit vias produce an extra phase shift of π, as a result of which, the fundamental mode is shifted by π with the modulation period of P=2d and this leads to a shift in the dispersion curve by π to the left side, as shown in Figure 5.2(b).

The shift in the dispersion curve is calculated using propagation constant given by

$$\beta_n(w) = \pm \left(\beta_0(w) + \frac{(2n+1)\pi}{P} \right) \tag{5.1}$$

where $\beta_n(w)$ is the propagation constant of nth space harmonics and $\beta_0(w)$ is the propagation constant of the fundamental mode.

The dotted lines in Figure 5.2(b) show the modes when $P = 2d$. It is observed that, after this phase reversal, the fundamental mode (n = 0), is now placed between $-\pi$ and π. It exhibits LH properties between 5.9 and 6.9 GHz, leading to radiation in a backward direction. The stop-band exists between 6.9 GHz and 7.4 GHz. The RH behavior extends between 7.4 to 9.7 GHz which radiates in the forward direction. It is noticed that the local reflection between the adjacent unit cells due to this phase reversal is negligibly less and does not alter the input reflection coefficient of the over-all antenna when it is matched with the external transmission line.

This shift in dispersion diagram has been further verified using the Bloch Floquet theorem (Brillouin (1946)). The periodic modulation of the transmission line excites infinite space harmonics whose propagation constant is given by

$$\beta_n = \beta_0 + \frac{2n\pi}{P} \tag{5.2}$$

where β_n is the propagation constant of the nth space harmonic, β_0 is the propagation constant of the dominant mode and P is the modulation period. For $n = -1$ space harmonics, propagation constant is given by

$$\beta_{-1} = \beta_0 - \frac{2\pi}{P} \tag{5.3}$$

Multiplying "d" on both sides, the equation (5.3) becomes

$$\beta_{-1}d = \beta_0 d - \frac{2\pi d}{P} \tag{5.4}$$

To compensate the mismatched phase $\Delta\phi = \pi$ in Fig. 2(b), the equation (5.4) becomes

$$\beta_{-1}d = \beta_0 d - \frac{2\pi d}{P} = 0 \tag{5.5}$$

Substituting $\beta_0 = \Delta\phi = \pi$ to equation (5.5) leads to $P = 2d$. This verifies the shift in dispersion diagram when P changes from "$d\,to\,2d$" as reported in Figure 5.2(b). The beam scanning angle can be obtained from the dispersion diagram, as expressed in equation (5.6) below. The beam angle (θ) for $n = -1$ space harmonics is

$$\theta = arcsin\left(\frac{\beta_{-1}}{k_0}\right) \tag{5.6}$$

where k_0 is free space propagation constant which is given by $k_0 = \frac{2\pi f}{c}$ and the first-order space harmonics is $\beta_{-1} = \beta_0 - \frac{2\pi}{P}$. Upon substitution of the above equations and $P = 2d$, (5.6) becomes

$$\theta = arcsin\left(\frac{c}{2fd}\left(\frac{\beta_0 d}{\pi} - 1\right)\right) \tag{5.7}$$

If $\beta_0 d = 3\pi/2$ and f=8.5 GHz, the beam scanning angle becomes $\theta = 26^0$, and if $\beta_0 d = \frac{2\pi}{3}$ and f = 6.4 GHz, $\theta = 23^0$. This will be further verified while discussing the radiation pattern of the proposed antenna in section 5.2. The alternatingly loaded short-circuit was previously investigated to form an MLWA with backward radiation in the lower order mode (Nguyen-Trong and Fumeaux (2018)). However, the reported antenna was restricted to LP applications.

5.3   Antenna Geometry

To validate the proposed concepts, two different LWA configurations are formed by placing 10 unit cells periodically along the X-direction. One configuration consists of sequentially placed short-circuits in its consecutive unit cells (Configuration-1) and the other one consists of alternatingly placed short-circuits in its consecutive unit cells

(Configuration-2). The geometry of these two configurations are reported in Figure 5.3. Both configurations are designed on Rogers RT/duroid 5880 substrate having dielectric constant (ϵ_r) of 2.2, loss tangent ($tan\delta$) of 0.0009, and thickness of 1.6 mm. The proposed antenna geometries are planar in nature, with simple microstrip feed line and a linearly tapered microstrip to SIW transition for broadband impedance matching. Optimized parameters of the microstrip transitions in these configurations are reported in Table 5.2.
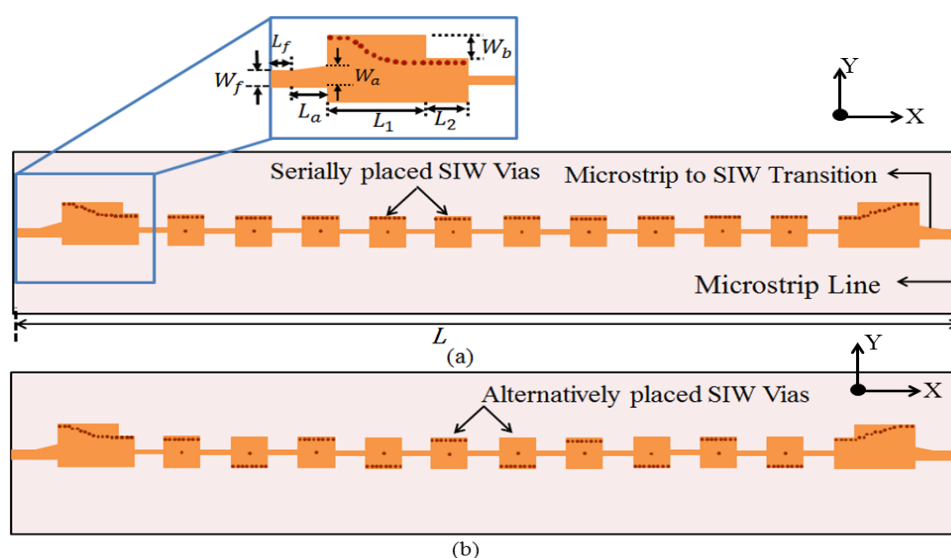
Figure 5.3: Geometry of the proposed LWAs. (a) Configuration-1 (sequentially placed unit cell). (b) Configuration-2 (alternatingly placed unit cell)

.

Table 5.2: Optimized dimensions of the proposed LWA

Parameters	W_f	W_a	W_b	L	L_1	L_2	L_a	L_f
Value (mm)	4	5.5	5	300	20	5	12	8

5.4   Operating Principle

5.4.1   Operating Principle of Sequentially Loaded Case

From the dispersion diagram reported in Figure 5.1(b), it can be seen that the lower mode (fundamental mode) appearing here is similar to the lower mode of a conventional

HMSIW. The radiation properties of this mode are similar to the conventional HMSIW LWAs for forward beam scanning (Nguyen-Trong and Fumeaux (2018)). It has also been verified by our analysis that, in the fundamental mode (lower order mode) the main beam points in the forward direction. It is noted that the E-field vectors at the transverse plane of the propagation direction meet at a point where the sidewall vias are present, indicating that the proposed guided structure mimics the Half-Width (HW) microstrip mode (First Higher-Order Mode, EH1).
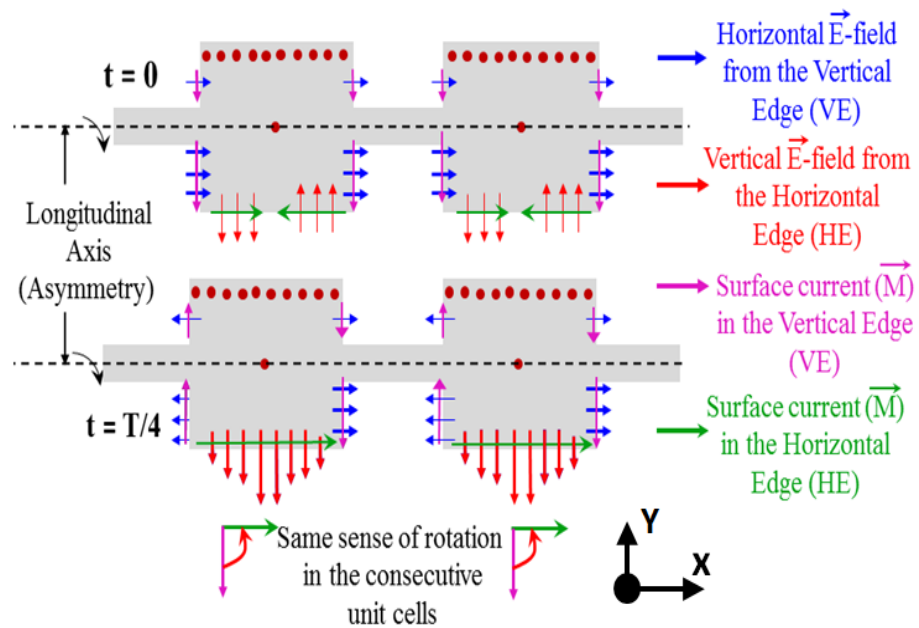
Figure 5.4: Graphical illustration of the vector field distributions at 9 GHz of configuration-1.

To understand the radiation behavior in the upper band, we plot the vector field distribution at 9 GHz in Figure 5.4. In the upper operating band, CP is achieved due to the axial asymmetry (Otto et al. (2014b), Rahmani and Deslandes (2017)) (longitudinal) which was created by placing the series of vias on one side of the transmission line. It can be observed that the radiation occurs mainly from the horizontal and vertical edges of the top patch. It can also be noted that the horizontal E-fields are dominant from the vertical edges of the patch at the zeroth time instant. The field from the horizontal edge of the patch cancels them. On the other hand, at the quadrature time interval the fields from the horizontal edge of the patch becomes dominant and the fields from

the vertical edge of the patch cancel them. The dimension of each unit cell has been optimized so that these two orthogonal fields are in quadrature phase difference and have equal magnitudes. The sense of the rotation of the magnetic surface current vector can be seen in Figure 5.4 which is in the anti-clockwise direction. This confirms the originality of the RHCP wave. It can also be noted that the presence of the vias on one side of the unit cells forces the E-field to produce null in that region and this very less intensive E-field can be seen present on the upper vertical edges of the patch w.r.t to its longitudinal axis (see Figure 5.4). So the major contribution of the radiation comes from the bottom half. So from the above explanation, it is clear that at the upper operating band, the ϕ-polarized component and the θ-polarized components are equal in magnitude and have quadrature phase difference, which gives rise to the generation of an RHCP wave pointing in a particular main beam direction as shown in Figure 5.5.
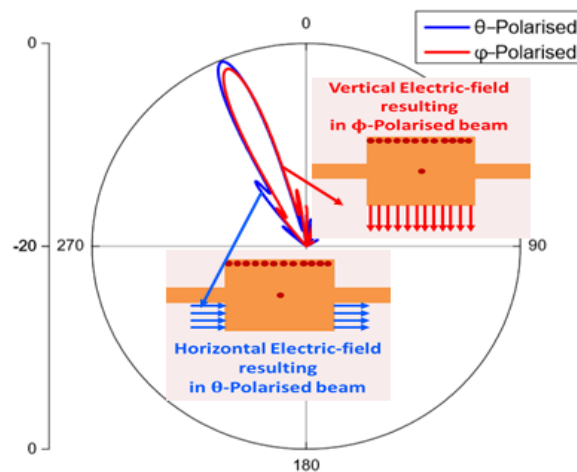
Figure 5.5: Simulated radiation pattern at 9 GHz of configuration-1 (consisting with 10 unit cells) at XZ plane.

5.4.2 Operating Principle of the Alternatingly Loaded Case

To better understand the radiation pattern behavior of the configuration-2 at the upper band, we plot the field distributions at 9 GHz in Figure 5.5. It can be observed that the alternatingly loaded short-circuits cause the vertical E-fields from the horizontal edges of the patches to orient in the opposite direction. This causes the magnetic surface current vector to rotate in an opposite sense between its consecutive unit cells as shown in

Figure 5.5. But no change is observed in the horizontal E-fields from the vertical edges of the patches. It results in exciting two orthogonal modes together in its consecutive unit cells. So they no longer satisfy the criteria for CP and the combined polarization becomes elliptical in nature. Since the horizontal component of E-field vector is responsible for generating the E_θ component and it does not change with the change of the position of the short-circuit, the radiation in the θ-direction does not have any extra phase shift and hence it still scans in the original backward direction, similar to the sequentially placed short-circuit one as explained in the previous case. But the change in the position of the short-circuits alter the vertical E-field vector which is responsible for generating E_ϕ component.
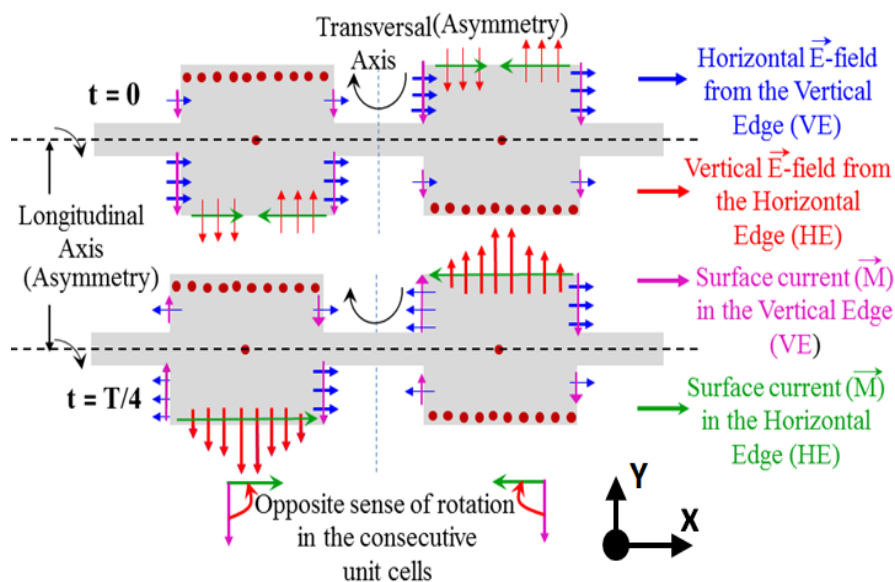
Figure 5.6: Graphical illustration of the vector field distributions at 9 GHz of configuration-2.

The radiation associated with it undergoes an extra phase shift as depicted in Figure 5.7 (a) and hence it scans from broadside to end-fire directions. Hence, the alternatingly placed configuration produces two beams with LP wave as shown in Figure 5.7(a). At the lower operating band, the sequentially placed configuration has forward radiation (FR). But alternatingly placed configuration has backward radiation (BR) as depicted in the radiation pattern at 6 GHz in Figure 5.7(b). This is due to the fact that the alternatingly loaded short-circuits contribute an extra π phase shift to the leaky modes

(from E_ϕ), thereby producing a horizontal phase delay causing the lower band to scan from backfire to broadside direction.
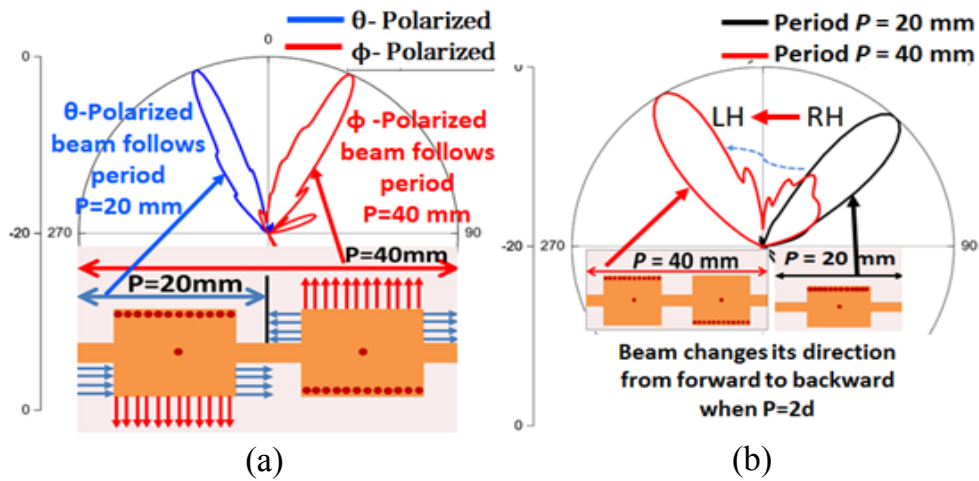
Figure 5.7: Simulated radiation pattern of configuration-2 at XZ plane (a) At 9 GHz (b) At 6 GHz

5.5 Results of Asymmetric HMSIW Leaky Wave Antennas

5.5.1 Results of Configuration-1

In this section, the simulated and measured results of the configuration-1 have been described. The fabricated prototype of configuration-1 is reported in Figure 5.8.
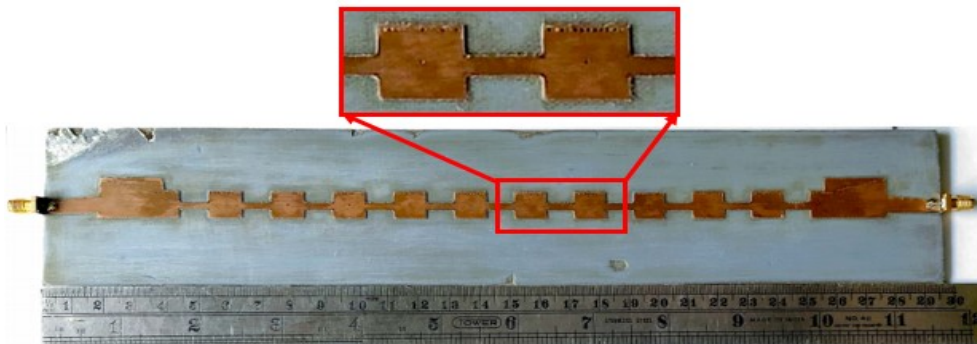
Figure 5.8: Fabricated prototype of configuration-1.

70

The S-parameters and the Bloch impedance over the frequency band of operation are shown in Figure 5.9 (a) and (b), respectively. It is observed from both simulated and measured results that the proposed antenna operates in two bands. The lower band is from 5.8 GHz to 6.9 GHz and the upper band is between 7.7 GHz and 10.1 GHz. As compared to the dispersion diagram, a 400 MHz shift can be observed at the upper operating band which may be attributed to the presence of microstrip transition at its input. Since the scattering parameters are calculated with respect to the port impedance, the transition at the port have a loading effect on the port impedance, which may slightly shift the frequency band. It can be noted that the central via-hole provides an additional shunt inductance between the top conductor and the ground plane, which helps to improve the matching at the lower operating band. It can also be seen from Figure 5.9(a) that, with the considered number of unit cells, the transmission coefficient is observed considerably low between its two ports, indicating that most of the power gets radiated before it reaches the other end of the port. Figure 5.9(b) also reports the normalized leakage constant calculated using (Jackson and Oliner (2008)).
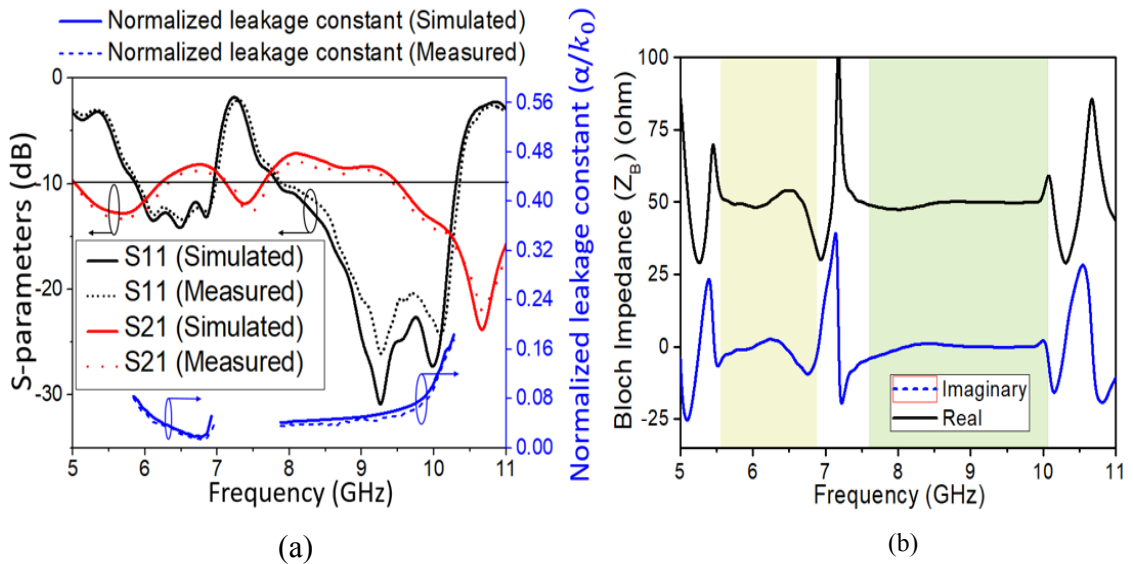
Figure 5.9: (a) S-parameters and Normalized leakage constant of configuration-1 (b) Bloch Impedance variation over frequency of configuration-1.

In the lower portion of the RH band and in the upper portion of the LH band, the leakage rate is observed high. It can be noticed from Figure 5.9(b) that, at both RH and LH bands, the real part of the Bloch impedance is matched with the characteristic
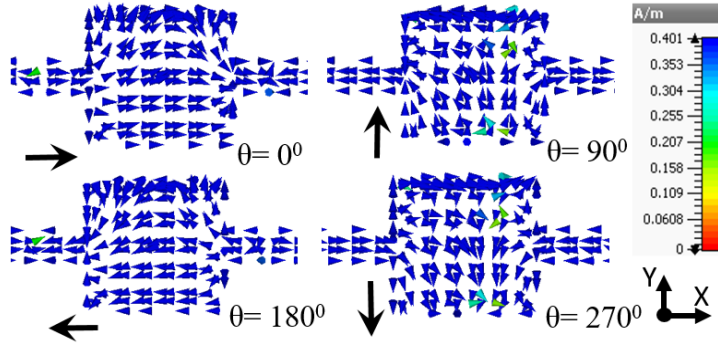
Figure 5.10: Surface current distribution at upper band (9 GHz) of configuration-1.

impedance of the transmission line and the reactive part around zero indicates a good impedance matching over the broad frequency regime of the antenna.

The simulated surface current distribution at the upper band is presented in Figure 5.10 and it has been verified with the analysis presented in section 5.4.1. From this, it can be observed that the surface current vector rotates in the counter clock-wise direction at different time instants at 9 GHz, thereby generating an RHCP electromagnetic radiation from the antenna.

The simulated radiation pattern of the configuration-1 in the XZ plane at both operating bands are reported in Fig. 5.11. In the lower operating band, antenna scans LP beam in the forward direction from 33^0 to 69^0, and in the upper operating band, the antenna scans RHCP beam from endfire to broadside direction between -33^0 and -17^0. The cross-pol level is observed below -12 dB.

The variation of the axial ratio over the beam scanning angle and over the frequency is reported in Figure 5.12(a) and (b), respectively. Figure 5.12 (a) shows the axial ratio within the 3 dB beamwidth region of the main beam pointing angle. It signifies that, at each angle within the 3 dB beamwidth region, the antenna maintains an axial ratio 3 dB, indicating that a good quality of CP radiation is achieved. Figure 5.12(b) reports the 3 dB axial ratio bandwidth (usable) from 8.5 GHz to 9.5 GHz (with 3-dB fractional bandwidth of 11%). The good quality of CP radiation is achieved by optimizing the longitudinal asymmetry of the unit cells. It can be noted that if the asymmetry is increased by shifting the short-circuit vias towards the longitudinal axis,

72

(a)

(b)
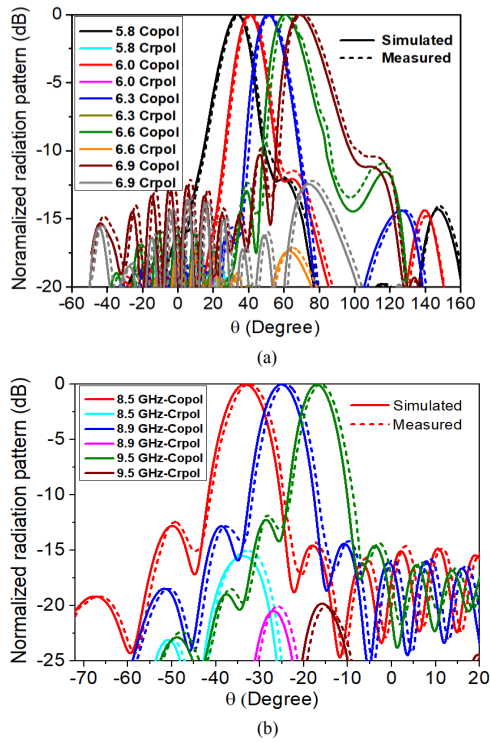
Figure 5.11: Normalized RHCP radiation pattern of configuration-1 in the XZ plane (a) At Lower band (b) At Upper band.
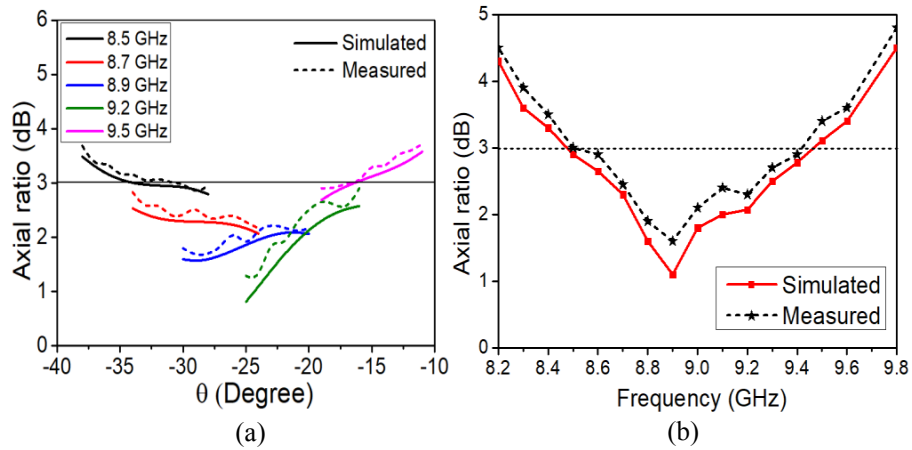
Figure 5.12: Configuration-1 (a) Axial ratio variation over the beam scanning angle (b) Variation of axial ratio over frequency.

the quality of the CP radiation can further be improved, but it affects the impedance matching performance at the lower operating band. So, the antenna configuration-1 is optimized for good quality of CP radiation as well as for good impedance matching over all frequency regimes.
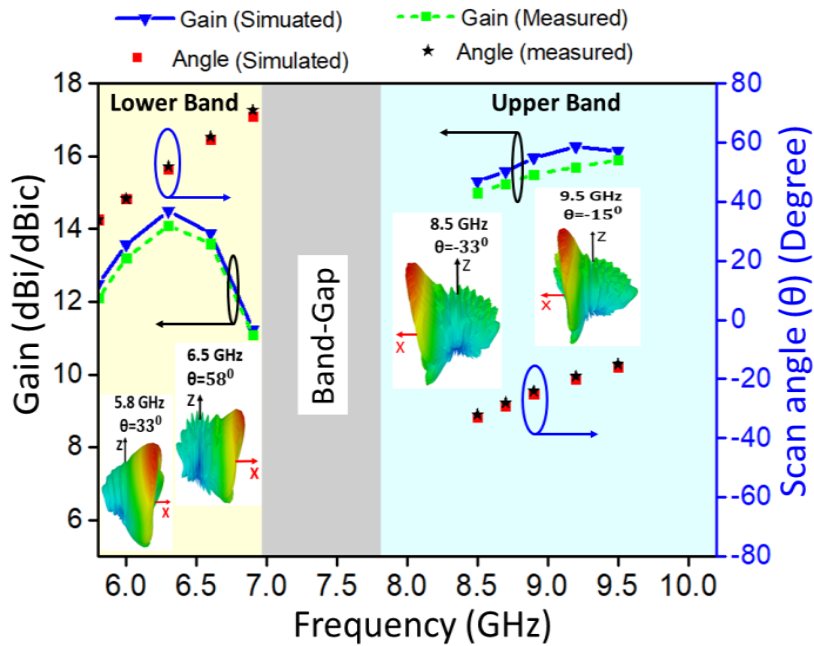
Figure 5.13: Simulated and measured Gain and Scan angle over the frequency of configuration-1.

The simulated gain and the scan angle of the configuration-1 is reported in Figure 5.13. The peak gain in the lower operating band and in the upper operating band are observed around 14 dBi and 16 dBic, respectively. Fig. 5.13 also reports the angle of radiation with respect to frequency. As the antenna scans from broadside to the endfire direction in the lower operating band, especially towards its upper portion, the gain of the antenna drops to 12 dBi. In the upper operating band, the gain of the antenna shows slight variation and remains almost constant around 16 dBi. In the lower band, radiation efficiency is between 94 % and 70% from 5.8 GHz to 6.9 GHz, and in the upper band, radiation efficiency is between 92% and 96% from 8.5 GHz to 9.5 GHz. In the lower band, radiation efficiency falls towards upper portion of the lower band and it is constant in the upper band.

5.5.2   Results of Configuration-2

In this section, the simulated and measured results of configuration-2 has been described. The fabricated prototype is reported in Figure 5.14. The simulated and measured
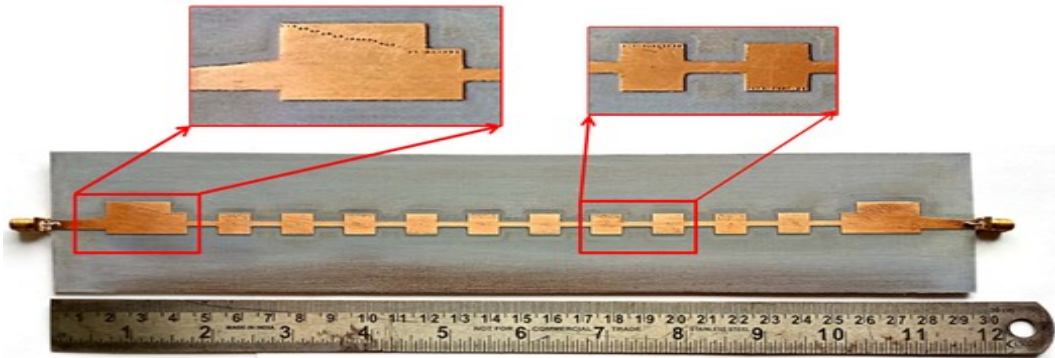
Figure 5.14: Fabricated prototype of configuration-2.
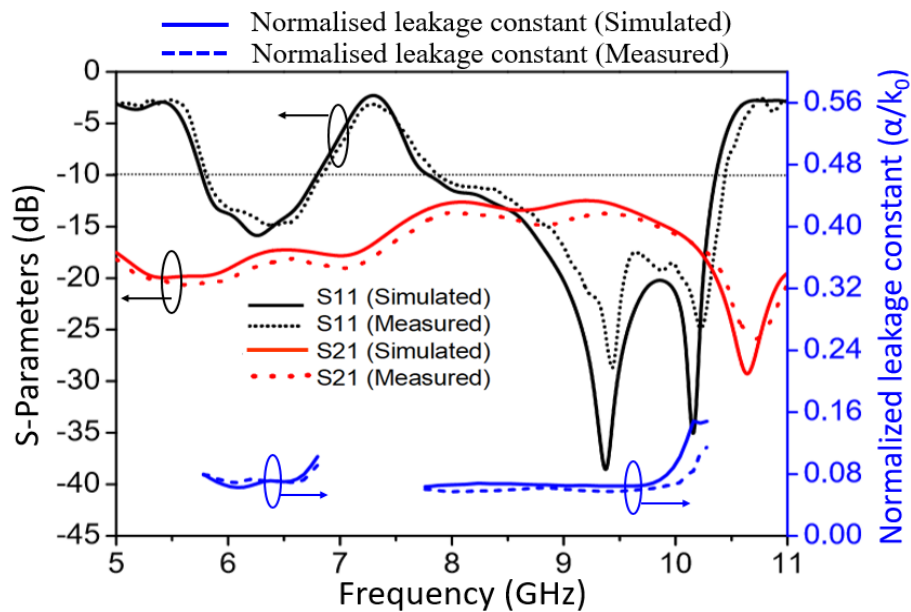
Figure 5.15: Fabricated prototype of configuration-2.

scattering parameters of configuration-2 and the normalized leakage constants are shown in Figure 5.15. It is observed that the proposed antenna operates in two bands as well. The lower band ranges between 5.8 GHz and 6.8 GHz and the upper band operates between 7.7 GHz and 10.2 GHz. The simulated and measured scattering parameters are found in a good agreement. A 400 MHz of the shift in bandwidth is observed between the results obtained from the dispersion diagram (Figure. 5.2(b)) and the scattering parameters. This shift may be attributed to the microstrip transition at the port. Since the scattering parameters are calculated with respect to the port impedance, the transition at the port have a loading effect on the port impedance, which may slightly shift the

75

frequency band. The transmission coefficient of the antenna is noticed below -13 dB, which signifies that most of the input power can contribute to the leaky wave radiation. The normalized leakage constant, as shown in Figure 5.15, is observed very low all over the frequency regime, indicating that a good radiation efficiency can be obtained from this leaky-wave structure. It can be noted that, similar to configuration-1, the real part of the Bloch impedance in this new design is observed around 50 ohms and the reactive part of the Bloch impedance is around zero, indicating that the antenna can be matched easily with the characteristic impedance of the transmission line over a broad bandwidth. In the lower operating band, the transmitted power is observed -5 dB lower than that of the configuration-1, indicating that the input mismatch loss at the input of the configuration-2 is negligibly small.
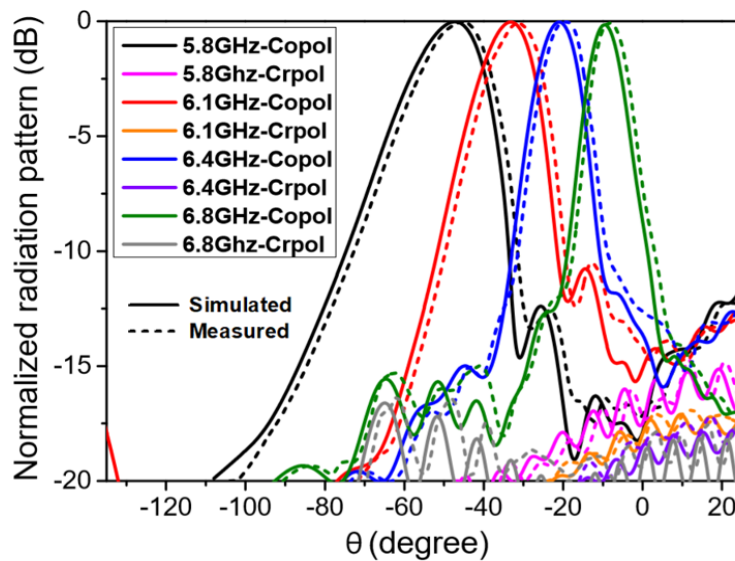
Figure 5.16: Normalized radiation pattern of lower band of configuration-2 at XZ plane.

The simulated and measured radiation patterns of the configuration-2 at the XZ plane in the lower operating band is reported in Figure 5.16. It can be observed from this figure that the antenna in the lower operating band scans in the backward direction from -48^0 to -10^0, as explained in section 5.2. The cross-pol radiation is observed below -15 dB. From Figure 5.16, it is also observed that $\theta = -21^0$ at 6.4 GHz is approximately equal to the angle $\theta = -23^0$ at 6.4 GHz, as obtained from (equation 5.7). It validates the working principle of the proposed antenna as explained in the

section 5.2. Figure 5.17 represents the simulated and measured radiation patterns of the configuration-2 at the XZ plane in the upper operating band. It can be seen from Figure 5.19 that the antenna radiates two beams, in which one beam is θ-polarized and the other is ϕ-polarized.
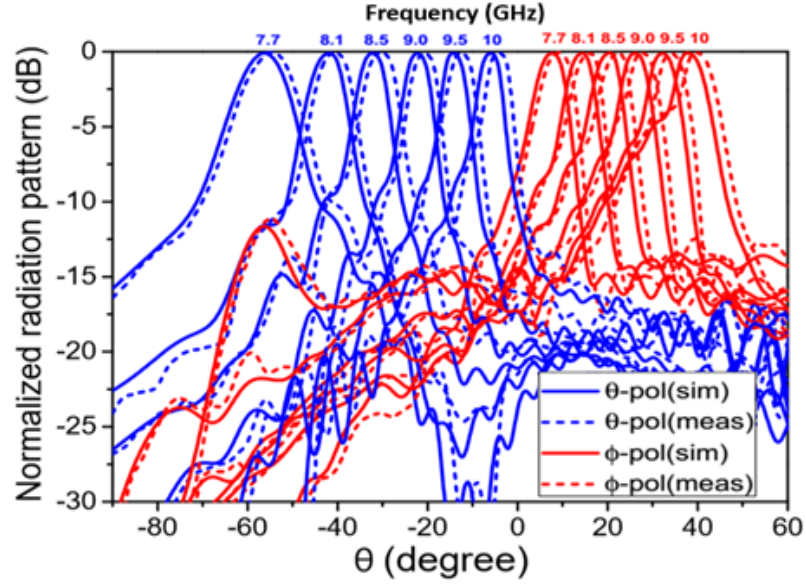
Figure 5.17: Normalized radaition pattern at upper band of configuration-2 at XZ plane.

From Figure 5.17 it can be noted that the θ-polarized beam does not alter its scanning nature with the position of the short-circuits. The θ-polarized beam scans from backfire to broadside direction from -56^0 to -6^0 and the ϕ-polarised beam scans from broadside to endfire direction from 8^0 to 40^0. It is also observed that $\theta = 23^0$ from Figure 5.17 is approximately equal to the $\theta = 26^0$ at 8.5 GHz obtained from the dispersion analysis equation (5.7). It verifies the dispersion analysis in Figure 5.2(b). In both bands the cross polarizations are observed below -12 dB. To further verify the dual-beam behavior, the antenna surface current vector of the unit cell at 9 GHz is presented in Figure 5.18. It can be observed that the surface current vector rotates like configuration-1. But the ϕ-polarized beam undergoes an extra π phase shift due to the change in the mutually opposite direction of the adjacent unit cells, which indicates that the unit cell supports LHCP like wave radiation and the adjacent unit cell excites RHCP like wave radiation. As a result, the polarization becomes elliptic in two symmetrical side beams that can independently scan in their respective directions.

77
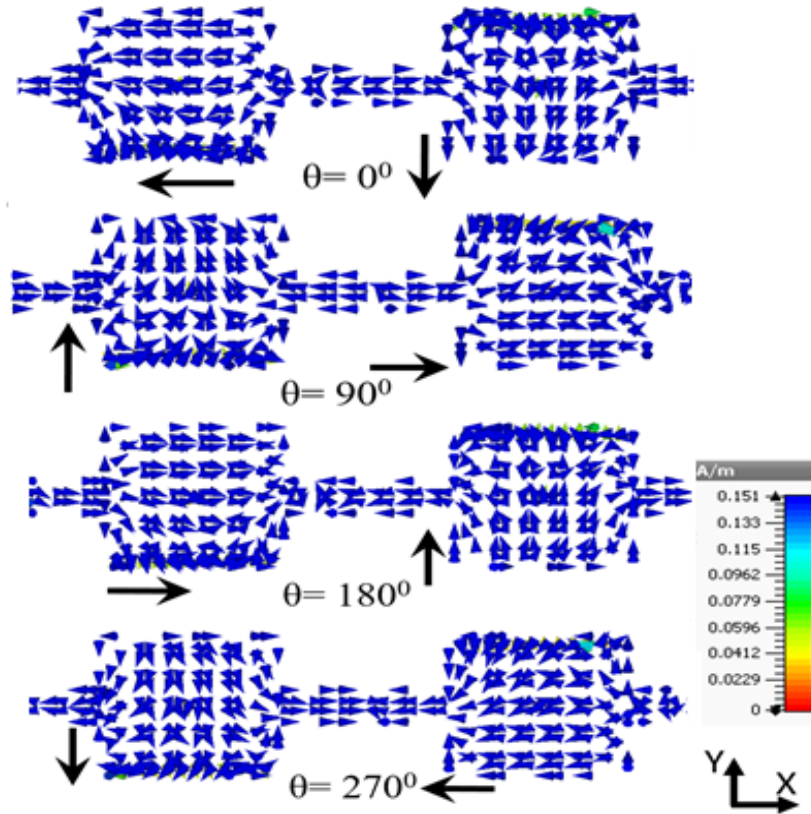
Figure 5.18: Surface current vector distribution of configuration-2 at 9 GHz.

The simulated and measured gains of configuration-2 are shown in Figure 5.19 at both lower and upper operating bands. The peak gain is observed around 11 dBi at 6.4 GHz. Since the power in the upper operating band distributes between the two orthogonally polarized beams, the average gain is observed lower than that of the configuration-1. The measured peak gain for θ-polarized radiation is obtained around 10.3 dBi at 9 GHz, and the measured peak gain for the ϕ-polarized radiation is observed to be 10 dBi. It can be also be seen from Figure5.19 that, towards the right edge of the upper operating band (> 9.5 GHz), the dominant radiation is ϕ-polarized, and hence the gain of the θ-polarized beam drastically falls below 9 dBi. It produces over 10 dBi gain within the frequency band between 8.5 GHz and 9.5 GHz. It can be noted that, if the number of the unit cells is increased, the antenna gain can also be increased by an amount of 2 dB to 3 dB. This increment is observed more in the upper band as compared to the lower operating band.

Finally, the performance of the proposed LWA configurations are compared in Table
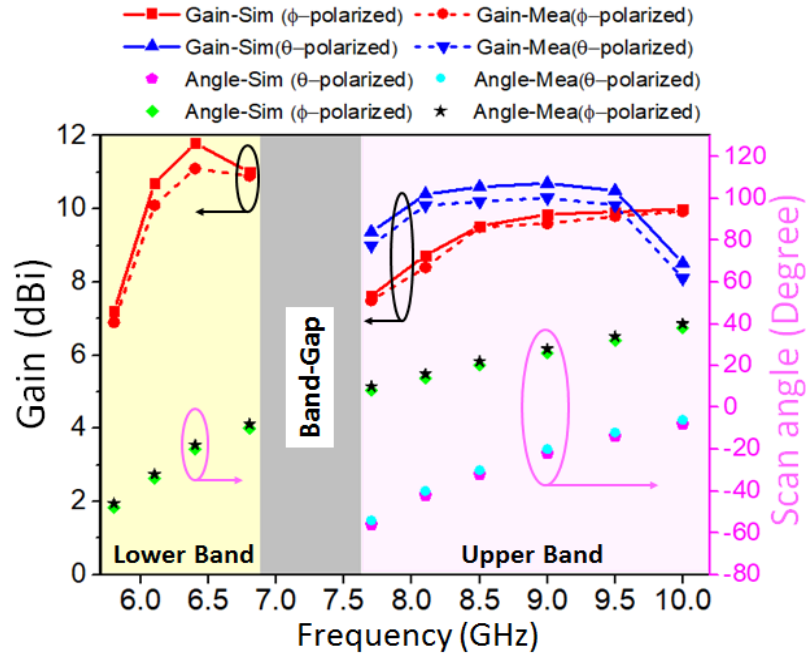
Figure 5.19: Simulated and measured Gain and Scan angle of configuration-2

5.3 with some of the already existing dual-beam LWAs. Unlike [Karmokar and Esselle (2015)], [Li and Wang (2018)] the proposed LWAs can exhibit dual-polarized behavior. In [Zhang et al. (2019)], a dual-polarized LWA was proposed but its gain and efficiency were low and the antenna scan is limited in the upper and bottom half-space due to the slots etched on the top and the bottom conductor, respectively. It is not capable of scanning in the first and the second quadrant like all other LWAs do. The proposed LWA antenna configuration-1 scans in the upper half-space with the LP band in the forward quadrant and CP band in the backward quadrant. The configuration-1 peak gain is 16 dB and average radiation efficiency is 90% is high in both the bands when compared to other works reported in Table 5.3.

Similarly, configuration-2 is also compared with the previously reported works. The works [Ma and Jiang (2015)],[Ma et al. (2016)], [Rahimi and Kishk (2018)] reported in Table 5.3 produces dual-beams. But these dual-beams exhibit the same polarization (single linear polarized beams i.e. either θ-polarized or ϕ-polarized). But our proposed LWA antenna configuration-2 produces dual-beams with different polarization (one beam is θ-polarized and another beam ϕ-polarized, dual linear) in the upper band.

Table 5.3: Comparison between the existing dual-beam works and the proposed LWAs

Ref.	Fabrication Technology	Geometry	Frequency (GHz) (Scan BW)	Scan Angle (degree)	Peak Gain (dBi /dBic)	Avg radiation efficiency (%)	Remarks
Ma and Jiang (2015)	Microstrip	Triple periodic super-cell	4.3-7.3	First beam:-58 to -10 Second beam: +18 to +54	-	-	Both beams are Single and Linear Polarization
Ma et al. (2016)	Microstrip +SIW	Series SIW vias	6.92-8.72	First beam: -75 to -38 Second beam: +75 to +38	12.7, 12.7	88	Both the beams are Single and Linear Polarization
Ma et al. (2016)	Dielectric Grating	Super-cell	57-63	First beam:-33 to -22 Second beam: +23 to +28	22.8 25	-	Both the beams are Single and Linear Polarization
Rahimi and Kishk (2018)	Printed Ridge Gap Technology	SIW-Gap Waveguide	59-67	First beam:-70 to -40 Second beam: +12 to +28	17.4 15.5	85	Both the beams are Single and Linear Polarization
Al-Bassam et al. (2017)	Microstrip	Double-asymmetric	23.7-24.	Both beams pointing to the same angle	9.5	80	1st beam is θ-polarized 2nd beam is ϕ-polarized
Karmokar and Esselle (2015)	SIW Half-Microstrip+ slots	U Shaped slot	5.24–6.37 7.9-9.02	+30 to +65 -46 to -10	12, 15	81	Linear Polarization Linear Polarization
Li and Wang (2018)	Microstrip +SIW	Uniform slots	5.3-8.4 35-41.5	-64 to 0 +11 to 70	16.3, 16	70, 60	Linear, Linear Polarization
Zhang et al. (2019)	SIW	Slots on both top and bottom face	9.0-10.7 13.4-16.2	+107 to +167 (upper space) -41 to -114 (lower space)	10 11	-	Linear, Circular Polarization
Rudramuni et al. (2020)	HMSIW +CRLH	Spiral slots on top face	4.86 – 6.4 7.4-9.6	+19 to +69 -17 to -32	13.5 13.5	-	Linear,Circular Polarization
[Proposed Work]	HMSIW Configuration-1	HMSIW +Mi-crostrip	5.8-6.9 7.7-10.1	+33 to +69 -33 to -17	14.5 16.3	5, 89	Linear, Circular Polarization
[Proposed Work]	HMSIW Configuration-2	Alternate HMSIW +Mi-crostrip	5.8-6.8 7.7-10	-48 to -10 θ-beam: -56 to-6 ϕ-beam: +8 to +40	11 10.2 10	90 92	Linear Polarization (Simulatanoues radiation of θ and ϕ)

The LWA antenna reported in [Al-Bassam et al. (2017)] exhibits dual-polarized beams. But they use two excitation ports to produce the dual-polarized beams (one port is to produce θ-polarized beam and another port is used to produce ϕ-polarized beam) and also these two polarized beams radiate in the same direction. Comparing with them, the proposed LWA configuration-2 produces dual-beams with different polarization using only one excitation port. It can be also be seen that the two beams radiate in different directions. Also, the reported works in [Ma and Jiang (2015)],[Rahimi and Kishk (2018)],[Al-Bassam et al. (2017)] are limited to the single-band but our proposed work configuration-2 is capable of producing two bands. The lower band produces the LP beam and the upper band produces dual-polarized beams (configuration-2) or circularly polarized beam (configuration-1). Apart from these improvements, the proposed configurations demonstrate higher gain and higher radiation efficiency with relatively less number of unit cells, as compared with the other reported works in Table 5.3.

5.6 Summary

In this chapter, two configurations of novel dual-band HMSIW LWA are presented. The first proposed antenna radiates LP waves in the lower band and CP waves in the upper band when the unit cells are cascaded sequentially. The second antenna, where the sidewall via of the HMSIW unit cells are connected alternatingly, provides simultaneous dual-beams with different polarization in the upper operational band in addition to the LP beam in the lower operational band. This antenna could be effectively used for multi-objective tracking applications and for enhancing the channel capacity of automotive and satellite-based wireless communication systems. Since both antenna configurations had dual frequency bands with different pointing directions in scanning, it can also be useful for vehicular applications to track different objects in its nearby locations.

CHAPTER 6

CONCLUSION AND FUTURE WORK

LWA possess a unique properties such as narrow-beam, high directvity, wide bandwidth and beam direction can be steered with change in excitation frequency. Hence, they are widely used in sensor systems such as automotive radar, satellite links and beam scanning applications etc. This research aims at the design and development of LWA for novel functionalities such as wide angle beam scanning, dual-band, dual-polarized features using efficient Goubau and HMSIW transmission lines. Also, asymmetry is investigated in HMSIW to obtain dual-beams. The designed LWA models are capable of providing

- Efficient wide-angle beam scanning and radiation towards endfire direction based on Goubau line.

- Dual-band dual-polarized LWA with forward and backward beam scanning for circular polarization flexible antenna application .

- Dual-band LWA for circular polarization and simultaneous dual-beam scanning functionalities.

6.1 Contributions

The thesis contribution can be summarized into sections based on the designed antennas and their functionalities.

6.1.1 Wide-angle beam scanning Goubau LWA

In the first design, Goubau line LWA with a wide-angle beam scanning is discussed. In contrast to the conventional Goubau line leaky wave with a small scanning angle range,

this work employed a periodically bending Goubau line, which not only brings in a periodic perturbation for leaky wave radiation, but also enhances the scanning range due to the increased delay for each line element. The simulation and experimental results show that the proposed LWA provides 155^0 with 90% radiation efficiency and 7–10 dBi radiation gain from backfire to endfire through broadside as frequency changes. The proposed antenna features good radiation performance and has a compact and low profile configuration.

6.1.2 Goubau line based endfire antenna

A simple and low profile planar Goubau line based endfire antenna. Endfire radiation is achieved by modifying the Goubau line into inverted periodic arrangement of V-shaped unit cells. The proposed antenna radiates toward end-fire direction between 7.8 and 8.3 GHz. The maximum gain of the antenna is obtained around 7.2 dBi. The average efficiency is observed 70% over the entire operating bandwidth. Proposed endfire antenna has a single metallic layer with simple configuration which is easy to fabricate and also easy to integrate with other electronics circuits.

6.1.3 Dual-band dual-polarized HMSIW LWA

A dual-band dual-polarized LWA with polarization diversity is developed using HM-SIW based technology. By etching simple spiral type slots on the HMSIW cavity, a novel dual-band dual-polarized LWA is obtained. The proposed antenna resonates at 5.6 and 8.5 GHz. Moreover, the antenna radiates the LP wave in the lower band and CP wave in the upper operating band. Also, in the upper operating band between 8.7 and 9.3 GHz, the proposed overall antenna exhibits both RHCP as well as the LHCP in the near main beam direction. The -10 dB impedance bandwidth of the proposed antenna at the lower and the higher operating bands are 27% (4.86-6.4 GHz) and 25% (7.4-9.6 GHz), respectively. In the higher band, the 3-dB axial ratio bandwidth of 6.6% (8.7-9.3 GHz) is achieved. The main beam of the antenna can be steered from 19^0 to 69^0 in the

forward direction in the lower operating band. In the higher operating band, the antenna can steer the CP beam between -17^0 and -32^0. In both the lower bands, the realized peak gain is observed around 13.3 dBi, whereas in the higher band, the realized peak gain is observed around 14 dBi.

6.1.4 Asymmetric HMSIW LWA for simultaneous dual-beam scanning

Two configurations of novel dual-band HMSIW LWAs are designed. The first proposed antenna radiates LP waves in the lower band and CP waves in the upper band when the unit cells are cascaded sequentially. The second antenna, where the sidewall via of the HMSIW unit cells are connected alternatingly, provides simultaneous dual-beams with different polarization in the upper operational band in addition to the LP beam in the lower operational band. The unit cells of two antennas are analyzed in terms of their dispersion behaviors.

6.2 Future Work

In the present communication system, circularly polarized antennas are widely preferred due its advantages. The proposed wide-angle beam scanning LWA is linearly polarized, it can be further extended to design circularly polarized wide-angle beam scanning Goubau line LWA. Terahertz technology is rapidly growing due to its large bandwidth. Terahertz frequency range is from 300 GHz to 3 THz. It is used for body scanner at airport, sensing and for short-range high data rate communications. Goubau line is also widely studied at THz range to design filters and couplers etc. The proposed Goubau line LWAs can be further studied at THz frequency range.

Theory of asymmetry to obtain simultaneous dual-beams can be further investigated in metallic waveguide and Microstrip LWAs. In the proposed dual-beam HMSIW LWA, each beam scans in only one quadrant either in backward quadrant or in forward quad-

rant, this can further studied to obtain wide-angle beam scanning dual-beam LWA as an extension of this work. Also, Cross-polarization levels in the proposed dual-band HMSIW LWAs is low, it can be further improved to get high cross-pol level. Application of asymmetry and double periodic unit cells are studied to obtain multi-beams with different polarization.

The shortage of bandwidth due to the rapid increase of mobile applications at low frequencies leading to exploration of millimeter wave communication. Millimeter waves can support higher data rate due to higher bandwidth. Also, millimeter wave human body scanners are getting popular nowadays. It has the ability to scan with high precision and cause less harm to human body. There is limited research on millimeter wave LWAs. Therefore, the proposed LWAs can be further extended to millimeter wave frequency range for scanning applications.

REFERENCES

Akalin, T., A. Treizebre, and B. Bocquet (2006), "Single-wire transmission lines at terahertz frequencies." *IEEE Transactions on Microwave Theory and Techniques*, 54, 2762–2767.

Al-Bassam, A., S. Otto, D. Heberling, and C. Caloz (2017), "Broadside dual-channel orthogonal-polarization radiation using a double-asymmetric periodic leaky-wave antenna." *IEEE Transactions on Antennas and Propagation*, 65, 2855–2864.

Brillouin, L. (1946), *Wave Propagation in Periodic Structures*. New York.

Caloz, C. and T. Itoh (2003), "Novel microwave devices and structures based on the transmission line approach of meta-materials." *IEEE MTT-S International Microwave Symposium Digest, 2003*, 1, 195–198 vol.1.

Chen, P., W. Hong, Z. Kuai, and J. Xu (2009), "A substrate integrated waveguide circular polarized slot radiator and its linear array." *IEEE Antennas and Wireless Propagation Letters*, 8, 120–123.

Cheng, Y. J., W. Hong, and K. Wu (2010), "Millimeter-wave half mode substrate integrated waveguide frequency scanning antenna with quadri-polarization." *IEEE Transactions on Antennas and Propagation*, 58, 1848–1855.

Chiba, J. (1977), "Experimental studies of the losses and radiations due to bends in the goubau line." *IEEE Transactions on Microwave Theory and Techniques*, 25, 94–100.

Collin, R. E. (1991), *Field theory of guided waves*. IEEE Press.

Cumming, W. (1955), "A nonresonant endfire array for vhf and uhf." *IRE Transactions on Antennas and Propagation*, 3, 52–58.

Dong, Y. and T. Itoh (2011), "Composite right/left-handed substrate integrated waveguide and half mode substrate integrated waveguide leaky-wave structures." *IEEE Transactions on Antennas and Propagation*, 59, 767–775.

Feng, Wenjie, Yanhao Feng, Lin-Sheng Wu, Yongrong Shi, Xin Yu Zhou, and Wenquan Che (2020), "A novel leaky wave endfire filtering antenna based on spoof surface plasmon polaritons." *IEEE Transactions on Plasma Science*, 48, 3061–3066.

Fuscaldo, W., D. R. Jackson, and A. Galli (2017), "Beamwidth properties of endfire 1-d leaky-wave antennas." *IEEE Transactions on Antennas and Propagation*, 65, 6120–6125.

Goubau, G. (1951), "Single-conductor surface-wave transmission lines." *Proceedings of the IRE*, 39, 619–624.

Goubau, G. (1956), "Open wire lines." *IRE Transactions on Microwave Theory and Techniques*, 4, 197–200.

Goubau, Georg (1950), "Surface waves and their application to transmission lines." *Journal of Applied Physics*, 21, 1119–1128.

Greiser, J. and P. Mayes (1964), "The bent backfire zigzag–a vertically- polarized frequency-independent antenna." *IEEE Transactions on Antennas and Propagation*, 12, 281–290.

Guglielmi, M. and G. Boccalone (1991), "A novel theory for dielectric-inset waveguide leaky-wave antennas." *IEEE Transactions on Antennas and Propagation*, 39, 497–504.

Haghighi, S. S., A. Heidari, and M. Movahhedi (2015), "A three-band substrate integrated waveguide leaky-wave antenna based on composite right/left-handed structure." *IEEE Transactions on Antennas and Propagation*, 63, 4578–4582.

Hansen, W. W. (1940), "Radiating electromagnetic waveguide." No. 2,402,.U.S. Patent, 1940.

Hansen, W. W. and J. R. Woodyard (1938), "A new principle in directional antenna design." *Proceedings of the Institute of Radio Engineers*, 26, 333–345.

Hines, J. N. and J. R. Upson (1957), "A wide aperture tapered-depth scanning antenna." *Ohio State Univ. Res. Found*, 667.

Hong, W., B. Liu, Y. Wang, Q. Lai, H. Tang, X. X. Yin, Y. D. Dong, Y. Zhang, and K. Wu (2006), "Half mode substrate integrated waveguide: A new guided wave structure for microwave and millimeter wave application." *2006 Joint 31st International Conference on Infrared Millimeter Waves and 14th International Conference on Teraherz Electronics*, 219–219.

Horestani, A. K., W. Withayachumnankul, A. Chahadih, A. Ghaddar, M. Zehar, D. Abbott, C. Fumeaux, and T. Akalin (2013), "Metamaterial-inspired bandpass filters for terahertz surface waves on goubau lines." *IEEE Transactions on Terahertz Science and Technology*, 3, 851–858.

Itoh, T. and B. Adelseck (1980), "Trapped image guide leaky-wave antennas for millimeter-wave applications." *1980 Antennas and Propagation Society International Symposium*, 18, 19–22.

Jackson, D. and A. Oliner (2008), *Modern Antenna Handbook*. John Wiley and Sons.

Jie, L., Q. Cui, and F. Lin (2019), "Reconfigurable hmsiw quadrature coupler." *IEEE Microwave and Wireless Components Letters*, 29, 648–651.

Kandwal, A., Q. Zhang, X. Tang, L. W. Liu, and G. Zhang (2018), "Low-profile spoof surface plasmon polaritons traveling-wave antenna for near-endfire radiation." *IEEE Antennas and Wireless Propagation Letters*, 17, 184–187.

Karmokar, D. K. and K. P. Esselle (2015), "Periodic u-slot-loaded dual-band half-width microstrip leaky-wave antennas for forward and backward beam scanning." *IEEE Transactions on Antennas and Propagation*, 63, 5372–5381.

Karmokar, D. K., K. P. Esselle, and T. S. Bird (2016), "Wideband microstrip leaky-wave antennas with two symmetrical side beams for simultaneous dual-beam scanning." *IEEE Transactions on Antennas and Propagation*, 64, 1262–1269.

Karmokar, D. K., Y. J. Guo, P. Qin, K. P. Esselle, and T. S. Bird (2017), "Forward and backward beam-scanning tri-band leaky-wave antenna." *IEEE Antennas and Wireless Propagation Letters*, 16, 1891–1894.

Kianinejad, A., Z. N. Chen, and C. Qiu (2017), "A single-layered spoof-plasmon-mode leaky wave antenna with consistent gain." *IEEE Transactions on Antennas and Propagation*, 65, 681–687.

Li, Y. and J. Wang (2018), "Dual-band leaky-wave antenna based on dual- mode composite microstrip line for microwave and millimeter-wave applications." *IEEE Transactions on Antennas and Propagation*, 66, 1660–1668.

Li, Y., Q. Xue, E. K. Yung, and Y. Long (2010), "The periodic half-width microstrip leaky-wave antenna with a backward to forward scanning capability." *IEEE Transactions on Antennas and Propagation*, 58, 963–966.

Liu, J., D. R. Jackson, Y. Li, C. Zhang, and Y. Long (2014), "Investigations of siw leaky-wave antenna for endfire-radiation with narrow beam and sidelobe suppression." *IEEE Transactions on Antennas and Propagation*, 62, 4489–4497.

Liu, J., D. R. Jackson, and Y. Long (2012a), "Substrate integrated waveguide (siw) leaky-wave antenna with transverse slots." *IEEE Transactions on Antennas and Propagation*, 60, 20–29.

Liu, J., X. Tang, Y. Li, and Y. Long (2012b), "Substrate integrated waveguide leaky-wave antenna with h-shaped slots." *IEEE Transactions on Antennas and Propagation*, 60, 3962–3967.

Liu, P., H. Feng, Y. Li, and Z. Zhang (2018), "Low-profile endfire leaky-wave antenna with air media." *IEEE Transactions on Antennas and Propagation*, 66, 1086–1092.

L.Tang, X., Q. Zhang, A. Kandwal, and S. Hu (2017), "Continuous beam steering through broadside using asymmetrically modulated goubau line leaky-wave antennas." *Scientific Reports*, 7, 11685.

Luxey, C. and J. M. Laheurte (1997), "Simple design of dual-beam leaky-wave antennas in microstrips." *IEE Microwave Antennas and Propogation*, 144, 397–402.

Ma, Z. L. and L. J. Jiang (2015), "One-dimensional triple periodic dual-beam microstrip leaky-wave antenna." *IEEE Antennas and Wireless Propagation Letters*, 14, 390–393.

Ma, Z. L., L. J. Jiang, S. Gupta, and W. E. I. Sha (2015), "Dispersion characteristics analysis of one dimensional multiple periodic structures and their applications to antennas." *IEEE Transactions on Antennas and Propagation*, 63, 113–121.

Ma, Z. L., K. B. Ng, C. H. Chan, and L. J. Jiang (2016), "A novel supercell-based dielectric grating dual-beam leaky-wave antenna for 60-ghz applications." *IEEE Transactions on Antennas and Propagation*, 64, 5521–5526.

Metzler, T. (1981), "Microstrip series arrays." *IEEE Transactions on Antennas and Propagation*, 29, 174–178.

Nguyen-Trong, N. and C. Fumeaux (2018), "Half-mode substrate-integrated waveguides and their applications for antenna technology: A review of the possibilities for antenna design." *IEEE Antennas and Propagation Magazine*, 60, 20–31.

Otto, S., A. Al-Bassam, A. Rennings, K. Solbach, and C. Caloz (2014a), "Transversal asymmetry in periodic leaky-wave antennas for bloch impedance and radiation efficiency equalization through broadside." *IEEE Transactions on Antennas and Propagation*, 62, 5037–5054.

Otto, S., Z. Chen, A. Al-Bassam, A. Rennings, K. Solbach, and C. Caloz (2014b), "Circular polarization of periodic leaky-wave antennas with axial asymmetry: Theoretical proof and experimental demonstration." *IEEE Transactions on Antennas and Propagation*, 62, 1817–1829.

Pourghorban Saghati, Ali, Mir Mojtaba Mirsalehi, and Mohammad Hassan Neshati (2014), "A hmsiw circularly polarized leaky-wave antenna with backward, broadside, and forward radiation." *IEEE Antennas and Wireless Propagation Letters*, 13, 451–454.

Rahimi, M. R. and A. A. Kishk (2018), "Dual-beam leaky-wave antenna based on substrate integrated printed ridge gap waveguide." *2018 18th International Symposium on Antenna Technology and Applied Electromagnetics (ANTEM)*, 1–2.

Rahmani, M. H. and D. Deslandes (2017), "Backward to forward scanning periodic leaky-wave antenna with wide scanning range." *IEEE Transactions on Antennas and Propagation*, 65, 3326–3335.

Rotman, W. and A. Oliner (1959), "Asymmetrical trough waveguide antennas." *IRE Transactions on Antennas and Propagation*, 7, 153–162.

Rudramuni, K., K. Kandasamy, Q. Zhang, X. Tang, A. Kandwal, P. K. T. Rajanna, and H. Liu (2018), "Goubau-line leaky-wave antenna for wide-angle beam scanning from backfire to endfire." *IEEE Antennas and Wireless Propagation Letters*, 17, 1571–1574.

Rudramuni, Karthik, Basudev Majumder, and Krishnamoorthy Kandasamy (2020), "Dual-band dual-polarized leaky-wave structure with forward and backward beam scanning for circular polarization-flexible antenna application." *Microwave and Optical Technology Letters*, 62, 2075–2084.

Sarkar, Anirban, Moitreya Adhikary, Abhishek Sharma, Animesh Biswas, Mohammed Jaleel Akhtar, and Zhirun Hu (2018), "Composite right/left-handed based compact and high gain leaky-wave antenna using complementary spiral resonator on hmsiw for ku band applications." *IET Microwaves, Antennas & Propagation*, 12, 1310–1315.

Sarkar, Anirban, Abhishek Sharma, Animesh Biswas, and M. Jaleel Akhtar (2019), "Emsiw-based compact high gain wide full space scanning lwa with improved broadside radiation profile." *IEEE Transactions on Antennas and Propagation*, 67, 5652–5657.

Sengupta, D. (1958), "The radiation characteristics of a zig-zag antenna." *IRE Transactions on Antennas and Propagation*, 6, 191–194.

Simorangkir, R. B. V. B. and Y. Lee (2015), "A planar dual-band periodic leaky-wave antenna based on a mu-negative (mng) transmission line." *IEEE Transactions on Antennas and Propagation*, 63, 2370–2374.

Sánchez-Escuderos, D., M. Ferrando-Bataller, J. I. Herranz, and M. Cabedo-Fabrés (2013), "Periodic leaky-wave antenna on planar goubau line at millimeter-wave frequencies." *IEEE Antennas and Wireless Propagation Letters*, 12, 1006–1009.

Sánchez-Escuderos, D., M. Ferrando-Bataller, J. I. Herranz, and V. M. Rodrigo-Peñarrocha (2016), "Low-loss circularly polarized periodic leaky-wave antenna." *IEEE Antennas and Wireless Propagation Letters*, 15, 614–617.

Suntives, A. and S. V. Hum (2012), "A fixed-frequency beam-steerable half-mode substrate integrated waveguide leaky-wave a'ntenna." *IEEE Transactions on Antennas and Propagation*, 60, 2540–2544.

Tang, X., Q. Zhang, Y. Chen, and H. Liu (2019), "Single-layer fixed-frequency beam-scanning goubau-line antenna using switched pin diodes." *IEEE Microwave and Wireless Components Letters*, 29, 430–432.

Treizebre, A., T. Akalin, and B. Bocquet (2005), "Planar excitation of goubau transmission lines for thz biomems." *IEEE Microwave and Wireless Components Letters*, 15, 886–888.

Vaughn, B. J., D. Peroulis, and A. Fisher (2018), "Mid-range wireless power transfer based on goubau lines." *2018 IEEE/MTT-S International Microwave Symposium - IMS*, 968–971.

Volakis, John L. (1991), *Antenna Engineering Handbook*. IEEE Press.

Wang, Y., W. Hong, Y. Dong, B. Liu, H. J. Tang, J. Chen, X. Yin, and K. Wu (2007), "Half mode substrate integrated waveguide (hmsiw) bandpass filter." *IEEE Microwave and Wireless Components Letters*, 17, 265–267.

Xu, J., W. Hong, H. Tang, Z. Kuai, and K. Wu (2008), "Half-mode substrate integrated waveguide (hmsiw) leaky-wave antenna for millimeter-wave applications." *IEEE Antennas and Wireless Propagation Letters*, 7, 85–88.

Yin, J. Y., D. Bao, J. Ren, H. C. Zhang, B. C. Pan, Y. Fan, and T. J. Cui (2017), "Endfire radiations of spoof surface plasmon polaritons." *IEEE Antennas and Wireless Propagation Letters*, 16, 597–600.

Zehar, M., G. Moreno, A. Chahadih, I. Turer, A. Ghaddar, and T. Akalin (2013), "Low loss terahertz planar goubau line on high resistivity silicon substrate." *2013 13th Mediterranean Microwave Symposium (MMS)*, 1–3.

Zhang, Q., Q. Zhang, H. Liu, and C. H. Chan (2019), "Dual-band and dual-polarized leaky-wave antenna based on slotted siw." *IEEE Antennas and Wireless Propagation Letters*, 18, 507–511.

Zhou, Y., Y. M. Huang, H. Jin, S. Ding, D. Xu, L. Silvestri, M. Bozzi, and L. Perregrini (2018), "Slow-wave half-mode substrate integrated waveguide 3-db wilkinson power divider/combiner incorporating nonperiodic patterning." *IEEE Microwave and Wireless Components Letters*, 28, 765–767.

LIST OF PAPERS BASED ON THESIS

Peer reviewed International Journals

1. K.Rudramuni, K.Kandasamy, Q.Zhang, B. Majumder, Puneeth Kumar,"Dual-Band Asymmetric Leaky Wave Antennas for Circular Polarization and Simultaneous Dual Beam Scanning" in IEEE Transactions on Antennas and Propagation.

2. K.Rudramuni, K.Kandasamy, Q.Zhang, A. Kandiwala, P. Kumar, "Goubau-Line Leaky-Wave Antenna for Wide-Angle Beam Scanning From Backfire to Endfire," in IEEE Antennas and Wireless Propagation Letters, vol. 17, no. 8, pp. 1571-1574, Aug. 2018.

3. K.Rudramuni, K.Kandasamy, Q.Zhang, B. Majumder, Puneeth Kumar,"Planar Goubau-Line Based Endfire Antenna" in International journal of RF and Microwave computer-aided engineering, vol 29, 2018.

4. K. Rudramuni, B. Majumder, K. Kandasamy,"Dualband dualpolarized leakywave structure with forward and backward beam scanning for circular polarizationflexible antenna application" in Microwave and Optical Technology Letters, vol. 62, pp. 2075-2084, 2020.

International Conferences

1. Karthik Rudramuni, Puneeth Kumar T R, Krishnamoorthy K, Basudev Majumder and Qingfeng Zhang Zhang, "Planar Goubau Line Based Endfire Antenna", 2018 IEEE-INAE Workshop on Electromagnetics (IIWE), December 06 to 08, 2018, Trivandrum, India. (Conference Travel grant awarded)

2. Karthik Rudramuni, Krishnamoorthy K and Basudev Majumder, "Periodic Spiral-Slot-Loaded Dual-Band Dual Polarized Half-Width Microstrip Leaky-Wave Antennas with Forward and Backward Beam Scanning Properties", 2018 IEEE-INAE Workshop on Electromagnetics (IIWE), December 06 to 08, 2018, Trivandrum, India. (Satish Dhawan Best paper Award)

CURRICULUM VITAE

Name	Karthik R
Address	Katavanahalli
	Nerlagunte,Challakre,Chitradurga -577536
	Karnataka, India
E-mail	karthik.r.muni@gmail.com
Qualification	• M.Tech | RF and Microwave Engineering | VTU University Karnataka
	• B.E | Electronics and Communication Engineering | VTU University Karnataka